[redacted]

RESEARCH MEMORANDUM

for the

Bureau of Aeronautics, Department of the Navy

STATIC LONGITUDINAL AND LATERAL STABILITY AND CONTROL CHARACTERISTICS OF AN 0.065-SCALE MODEL OF THE CHANCE VOUGHT REGULUS II MISSILE AT MACH NUMBERS OF 1.41, 1.61, AND 2.01

TED NO. NACA AD 398

By Ross B. Robinson, Cornelius Driver,
and M. Leroy Spearman

Langley Aeronautical Laboratory
Langley Field, Va.

NATIONAL ADVISORY COMMITTEE
FOR AERONAUTICS
WASHINGTON
June 6, 1955

NACA RM SL55E31

NATIONAL ADVISORY COMMITTEE FOR AERONAUTICS

RESEARCH MEMORANDUM

for the

Bureau of Aeronautics, Department of the Navy

STATIC LONGITUDINAL AND LATERAL STABILITY AND CONTROL CHARACTERISTICS OF AN 0.065-SCALE MODEL OF THE CHANCE VOUGHT REGULUS II MISSILE AT MACH NUMBERS OF 1.41, 1.61, AND 2.01

TED NO. NACA AD 398

By Ross B. Robinson, Cornelius Driver,
and M. Leroy Spearman

SUMMARY

An investigation has been conducted in the Langley 4- by 4-foot supersonic pressure tunnel to determine the static longitudinal and lateral stability and control characteristics of an 0.065-scale model of the Chance Vought Regulus II missile. The tests were made at Mach numbers of 1.41, 1.61, and 2.01 and Reynolds numbers, based on the mean geometric chord, of 1.86×10^6, 1.79×10^6, and 1.54×10^6, respectively.

INTRODUCTION

At the request of the Bureau of Aeronautics, Department of the Navy, an investigation of the aerodynamic characteristics of the Chance Vought Regulus II missile (XRSSM-N-9) at supersonic speeds has been undertaken by the National Advisory Committee for Aeronautics.

This missile is a jet-propelled surface-to-surface type having a wing with 43.5° of sweep of the quarter-chord line, an aspect ratio of 2.75, taper ratio of 0.6, and modified circular-arc airfoil sections with a thickness of 4 percent chord.

The present paper contains the results obtained at Mach numbers of 1.41, 1.61, and 2.01 in the Langley 4- by 4-foot supersonic pressure tunnel.

COEFFICIENTS AND SYMBOLS

The results of the tests are presented as standard NACA coefficients of forces and moments. The data are referred to the stability-axes system (fig. 1) with the reference center-of-moments on the longitudinal center line of the basic body of revolution at a longitudinal station corresponding to the leading edge of the wing mean geometric chord (fig. 2).

The coefficients and symbols are defined as follows:

C_L lift coefficient, $\frac{-Z}{qS}$

C_N normal-force coefficient, $\frac{\text{Normal force}}{qS}$

C_X longitudinal-force coefficient, $\frac{X}{qS}$

C_C chord-force coefficient, $\frac{\text{Chord force}}{qS}$

C_D drag coefficient, $\frac{\text{Drag}}{qS}$

C_Y lateral-force coefficient, $\frac{Y}{qS}$

C_l rolling-moment coefficient, $\frac{L}{qSb}$

C_m pitching-moment coefficient, $\frac{M'}{qS\bar{c}}$

C_n yawing-moment coefficient, $\frac{N}{qSb}$

$C_{h_{e_L}}$ elevon hinge-moment coefficient, $\frac{H}{2qM_e}$

[redacted]

X	force along X-axis
Y	force along Y-axis
Z	force along Z-axis
L	moment about X-axis
M'	moment about Y-axis
N	moment about Z-axis
H	elevon hinge moment about hinge axis
q	free-stream dynamic pressure
M	Mach number
S	wing area including body intercept, 88.47 sq in.
M_e	moment-area of elevon
b	wing span, 15.63 in.
$\bar{c}$	wing mean geometric chord, 5.78 in.
n_p	neutral-point location, percent $\bar{c}$
α	angle of attack of fuselage center line, deg
β	angle of sideslip of fuselage center line, deg
δ_e	elevon deflection normal to the hinge line, deg
δ_r	rudder deflection, deg
L/D	lift-drag ratio, $\frac{C_L}{-C_X}$
ΔC_X	rise in longitudinal-force coefficient with lift above minimum longitudinal force
C_{m_0}	pitching-moment coefficient at zero lift
m/m_o	mass flow ratio

[redacted]

$C_{L_\alpha} = \frac{\partial C_L}{\partial \alpha}$

$C_{m_{C_L}} = \frac{\partial C_m}{\partial C_L}$

$C_{h_\alpha} = \frac{\partial C_h}{\partial \alpha}$

$C_{h_{\delta_e}} = \frac{\partial C_h}{\partial \delta_e}$

$C_{m_{\delta_e}} = \frac{\partial C_m}{\partial \delta_e}$

$C_{Y_\beta} = \frac{\partial C_Y}{\partial \beta}$

$C_{l_\beta} = \frac{\partial C_l}{\partial \beta}$

$C_{n_\beta} = \frac{\partial C_n}{\partial \beta}$

$C_{n_{\delta_r}} = \frac{\partial C_n}{\partial \delta_r}$

$\beta_{\delta_r} = \frac{\partial \beta}{\partial \delta_r}$

$C_{l_{\delta_e}} = \frac{\partial C_l}{\partial \delta_e}$, where δ_e is the differential deflection of the elevons in deg

Subscripts:

trim	measured for $C_m = 0$
R	right
L	left

MODEL AND APPARATUS

A three-view drawing of the model and details of various components are presented in figures 2 and 3. The geometric characteristics of the model are presented in table I. Photographs of two of the configurations are shown in figure 4.

The model was equipped with a wing having 43.5° of sweep of the quarter-chord line, aspect ratio 2.75, taper ratio 0.6, and modified circular-arc airfoil sections with a thickness of 4 percent chord (see table I). The wing was mounted 0.26 inch above the fuselage center line and had zero incidence and dihedral.

Elevons of the plain trailing-edge flap type provided both longitudinal and lateral control (fig. 2). The model had a swept vertical tail and movable rudder (fig. 2). Deflections of all control surfaces were set manually.

Coordinates of the basic fuselage are presented in table II. A simulated static-pressure probe was attached to the nose of the fuselage (see fig. 4). A scoop inlet equipped with a boundary-layer diverter (fig. 3) was incorporated into the fuselage to simulate the internal-flow conditions of the missile. The inlet air flow, which could be throttled manually to provide variable mass-flow ratios, was discharged out the rear of the fuselage around the sting. The limited travel of the throttling mechanism could not produce a zero internal-flow condition. A solid fairing (figs. 3 and 4) was used for all the "closed inlet" configurations to permit investigations of the model with no internal air flow. The wing and vertical tail were removable in order to permit investigation of various combinations of components.

Force and moment measurements were made through the use of an experimental, all welded, six-component strain-gage balance furnished by NACA. This experimental balance is characterized by an extremely small size but with an attendant increase in balance deflections and interactions. Space limitation was the primary consideration in its selection. The left elevon was equipped with a strain-gage beam furnished by the contractor to facilitate the measurement of elevon hinge moments.

The following pressure measurements were made:

(1) the static pressure in the balance chamber inside the model

(2) the static pressure on the rim base area of the fuselage

(3) the total and static pressures of the exit air flow with open inlet by means of a total-pressure rake fastened to the sting at the base of the model.

Since the model was mounted on a 5° bent sting, it was possible to test through an angle-of-attack range at angles of sideslip of 0° and about ±5° and through an angle-of-sideslip range at angles of attack of 0° and about ±5°.

TEST CONDITIONS AND PROCEDURE

The conditions for the tests were:

Mach number	1.41	1.61	2.01
Reynolds number, based on $\bar{c}$	1.86×10^6	1.79×10^6	1.54×10^6
Stagnation pressure, lb/sq in.	13	13	13
Stagnation temperature, °F	100	100	100
Stagnation dewpoint, °F	<-25	<-25	<-25
Mach number variation	±0.01	±0.01	±0.015
Flow angle in horizontal or vertical plane, deg	±0.1	±0.1	±0.1

At each Mach number the effects of mass-flow ratio on lift, longitudinal force, and pitching moment were determined for a limited number of throttle settings for $\alpha = \beta = 0°$. From these results a throttle setting was selected to give the desired mass flow for the remaining tests.

Tests were made through an angle-of-attack range from about -12° to about 8° for zero angle of sideslip and through an angle-of-sideslip range of about -10° to about 4° for zero angle of attack. Additional tests were made through the angle-of-attack range at $\beta \approx 5°$ for $M = 1.41$ and 1.61 at $\beta \approx -5°$ for $M = 2.01$.

CORRECTIONS AND ACCURACY

The angles of attack and sideslip were corrected for the deflection of the balance and sting under load. The nominal values for elevon deflection presented in this report are not corrected for deflection due to load. Approximate values of elevon deflection under load are presented in the following table:

[redacted]

Mach number	$\partial\delta_{e_L}/\partial C_{h_e}$, deg	
	Left elevon	Right elevon
1.41	5	4
1.61	6	5
2.01	6	5

Although the variation of rudder deflection was not known, it was assumed to be small (within $\pm 0.1^\circ$) since the surface was rigidly fixed in the desired position by bead of solder along the leading edge of the rudder.

Base-pressure measurements were made and the longitudinal-force coefficients of all configurations were adjusted to free-stream static pressure at the base. For all configurations with the open inlet, the internal pressure in the model balance chamber was measured and corrections for a buoyant force on the balance were applied to the results. The internal drag was determined from the change in momentum from free-stream conditions to measured conditions at the duct exit. Base drag, buoyant force, and internal drag have been subtracted from the total longitudinal-force measurements so that a net external longitudinal-force coefficient was obtained. Mass-flow ratios were about 0.85, 0.95, and 0.92 for the stability and control tests at Mach numbers of 1.41, 1.61, and 2.01, respectively. The magnitude of the base, internal, and buoyant longitudinal-force coefficients at $\alpha = 0^\circ$ for the three Mach numbers is indicated by the following table:

	M = 2.01	M = 1.61	M = 1.41
Base C_X	0.0001	0.0001	-0.0012
Internal C_X	-0.0050	-0.0034	-0.0032
Bouyant C_X	0.0125	0.0116	0.0092

The estimated errors in the individual measured quantities are as follows:

[redacted]

	M = 1.41	M = 1.61	M = 2.01
C_L, C_N	±0.002	±0.002	±0.003
C_C, C_X, C_D	±0.001	±0.001	±0.002
C_m	±0.005	±0.005	±0.005
C_l	±0.0001	±0.0001	±0.0002
C_n	±0.0001	±0.0001	±0.0002
C_Y	±0.0014	±0.0014	±0.0016
α, deg	±0.1	±0.1	±0.1
β, deg	±0.1	±0.1	±0.1
δ_r and δ_e (corrected for deflection of elevon under load), deg	±0.1	±0.1	±0.1
M	±0.01	±0.01	±0.015

PRESENTATION OF RESULTS

The results are presented as follows:

RESULTS

The basic results are presented without analysis in order to expedite issuance. However, some general observations relative to the results might be made.

One result of significance is the large negative value of pitching-moment coefficient at zero lift C_{m_0} with zero control deflection that apparently is caused by the air inlet (see fig. 9). The occurrence of these large negative values of C_{m_0} necessitate large control deflections for trim with a resultant increase in drag and reduction in maneuverability. Means of reducing the negative C_{m_0} would be of considerable importance.

Another result of interest concerns the directional stability C_{n_β} which decreases quite rapidly with both increasing Mach number and angle of attack until regions of instability are reached (see figs. 19 and 23). The low initial value of C_{n_β} appears to be a result of the large unstable moment of the wing-body combination. Although it may be possible to control the missile directionally with these low values of stability, it would appear that the low C_{n_β} together with a rather large variation of pitching moment with sideslip (see fig. 19(a), for example) might lead to cross-coupled motions that may be difficult to control. Further study of these effects would, of course, be desirable.

Langley Aeronautical Laboratory,
National Advisory Committee for Aeronautics,
Langley Field, Va., May 18, 1955.

Ross B. Robinson
Aeronautical Research Scientist

Cornelius Driver
Cornelius Driver
Aeronautical Research Scientist

for M. Leroy Spearman
Aeronautical Research Scientist

Approved:

L. J. Turner Jr.
for John V. Becker
Chief of Compressibility Research Division

mgk

TABLE I.- GEOMETRIC CHARACTERISTICS OF MODEL

Wing:	
Total area, including fuselage intercept, sq in.	88.47
Span, in.	15.63
Root chord, in.	7.08
Tip chord, in.	4.27
Length of mean geometric chord, $\bar{c}$, in.	5.78
Aspect ratio	2.75
Taper ratio	0.60
Sweep angle of $\bar{c}/4$ line, deg	43.5
[1]Airfoil section, streamwise:	
Maximum thickness, percent chord	4.0
Location of maximum thickness, percent chord	53.7
Trailing edge thickness, percent chord	0.04
Dihedral, deg	0
Incidence, deg	0
Elevons:	
Area behind hinge line, each, sq in.	4.61
Moment of area, each, cu in.	2.49
Span, in.	3.42
Sweep of hinge line, deg	37.3
Vertical tail:	
Span (to model center line), in.	5.07
Area (to model center line), sq in.	23.08
Tip chord (theoretical), in.	2.35
Root chord, in.	7.16
Length of tail mean geometric chord, in.	5.28
Aspect ratio	1.12
Taper ratio (theoretical tip)	0.33
Rudder area, sq in.	2.35
Airfoil section	Same as wing
Fuselage:	
Length (without probe), in.	44.15
Maximum diameter, in.	3.25
Maximum cross-sectional area, sq in.	11.10
Base inner diameter, in.	2.01
Sting diameter, in.	1.25
Area of rim of base, sq in.	0.45
Annular area of base for internal flow, sq in.	1.94
Maximum length-diameter ratio	13.6
Total base area (annular + rim + sting), sq in.	3.62

[1]Symmetric airfoil section defined by

$$\frac{t}{c} = 0.122496 - 0.015168\,\frac{x}{C} - \left(0.028768\left(\frac{x}{C}\right)^2 - 0.033096\,\frac{x}{C} + 0.0150052\right)^{1/2}$$

[redacted]

TABLE II.- COORDINATES OF THE BASIC FUSELAGE

[x is distance from nose in in.; r is radius in in.]

x	r
0.000	0.000
.038	.018
.075	.033
.150	.061
.225	.085
.300	.107
.450	.148
.601	.184
.751	.218
.901	.250
1.502	.362
2.252	.486
3.003	.596
3.754	.698
4.505	.792
6.006	.964
7.508	1.117
9.009	1.255
10.511	1.376
12.012	1.478
13.514	1.567
15.015	1.625
34.761	1.625
37.765	1.586
40.086	1.493
41.850	1.345
42.850	1.245
43.850	1.115
44.150	1.065

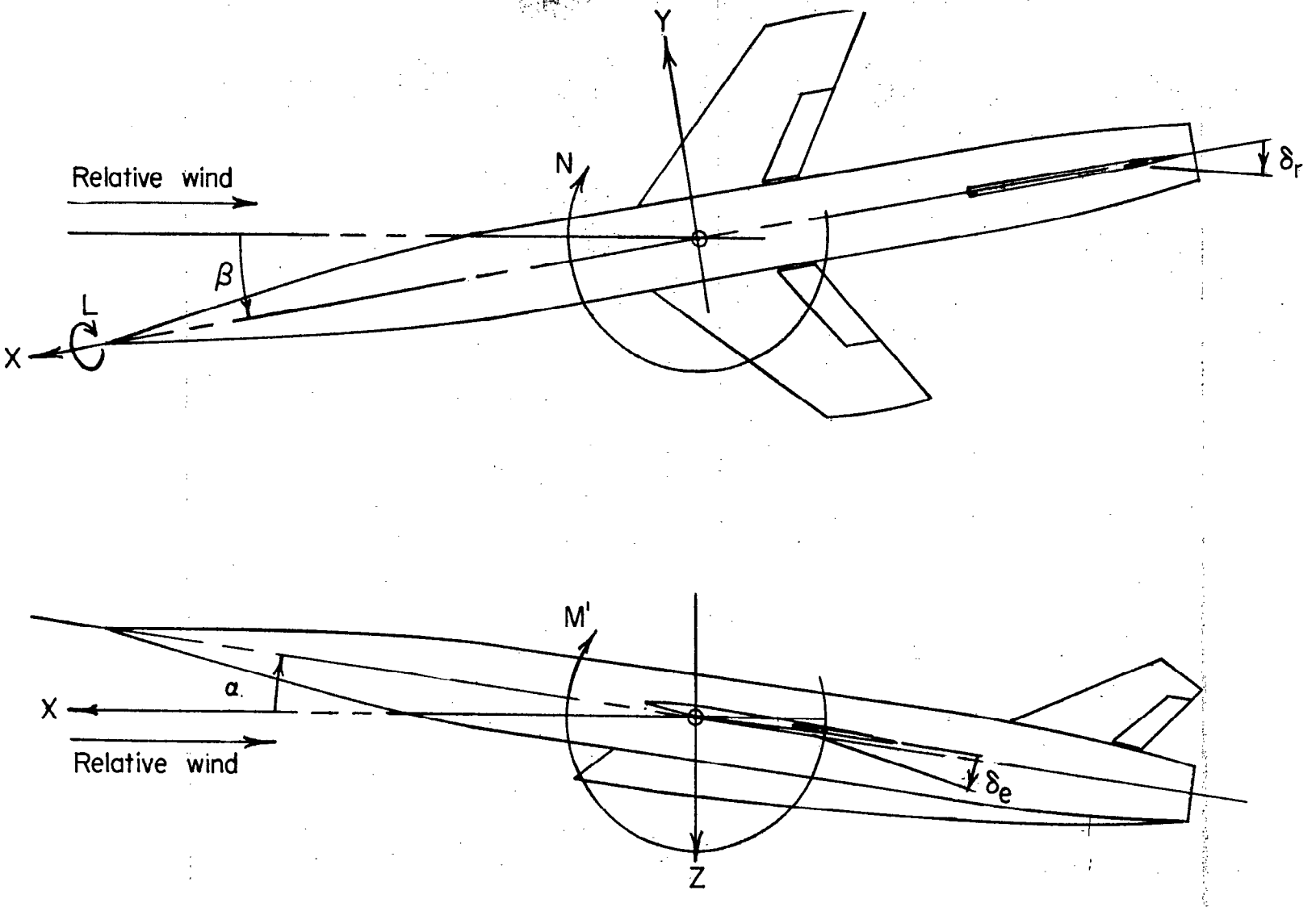

Figure 1.- System of stability axes. Arrows indicate positive values.

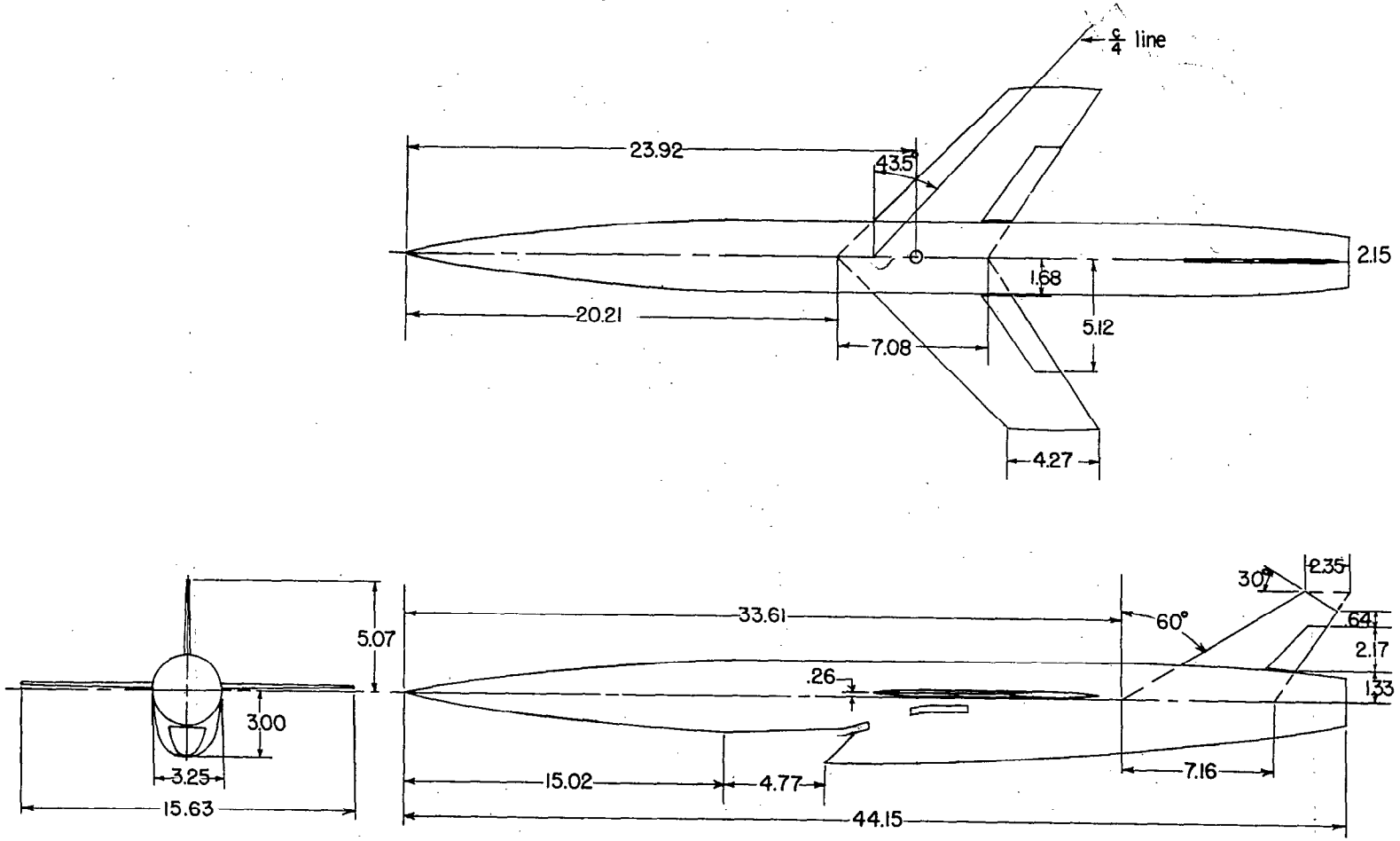

(a) Three-view drawing of model.

Figure 2.- Details of model.

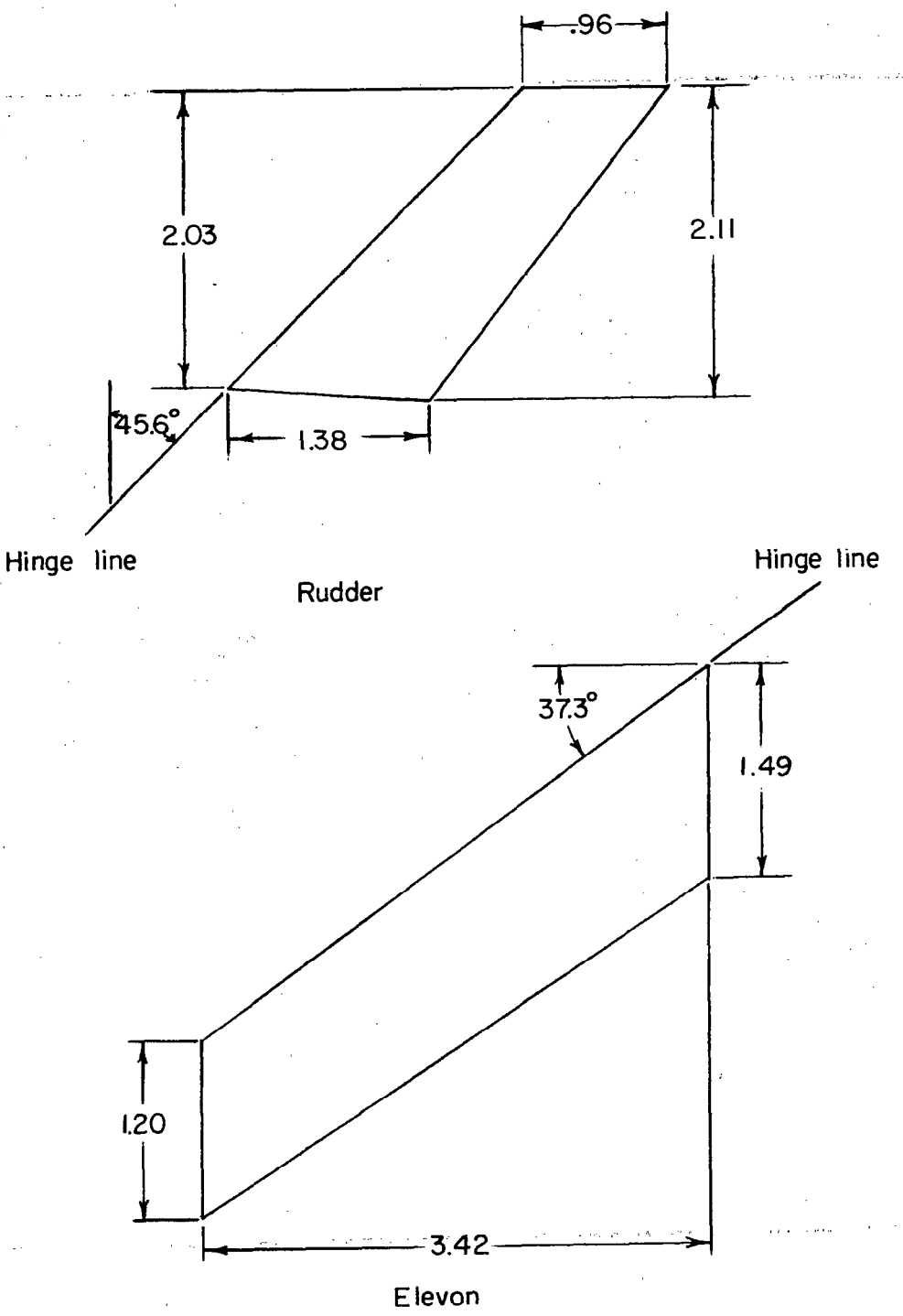

(b) Details of rudder and elevon.

Figure 2.- Concluded.

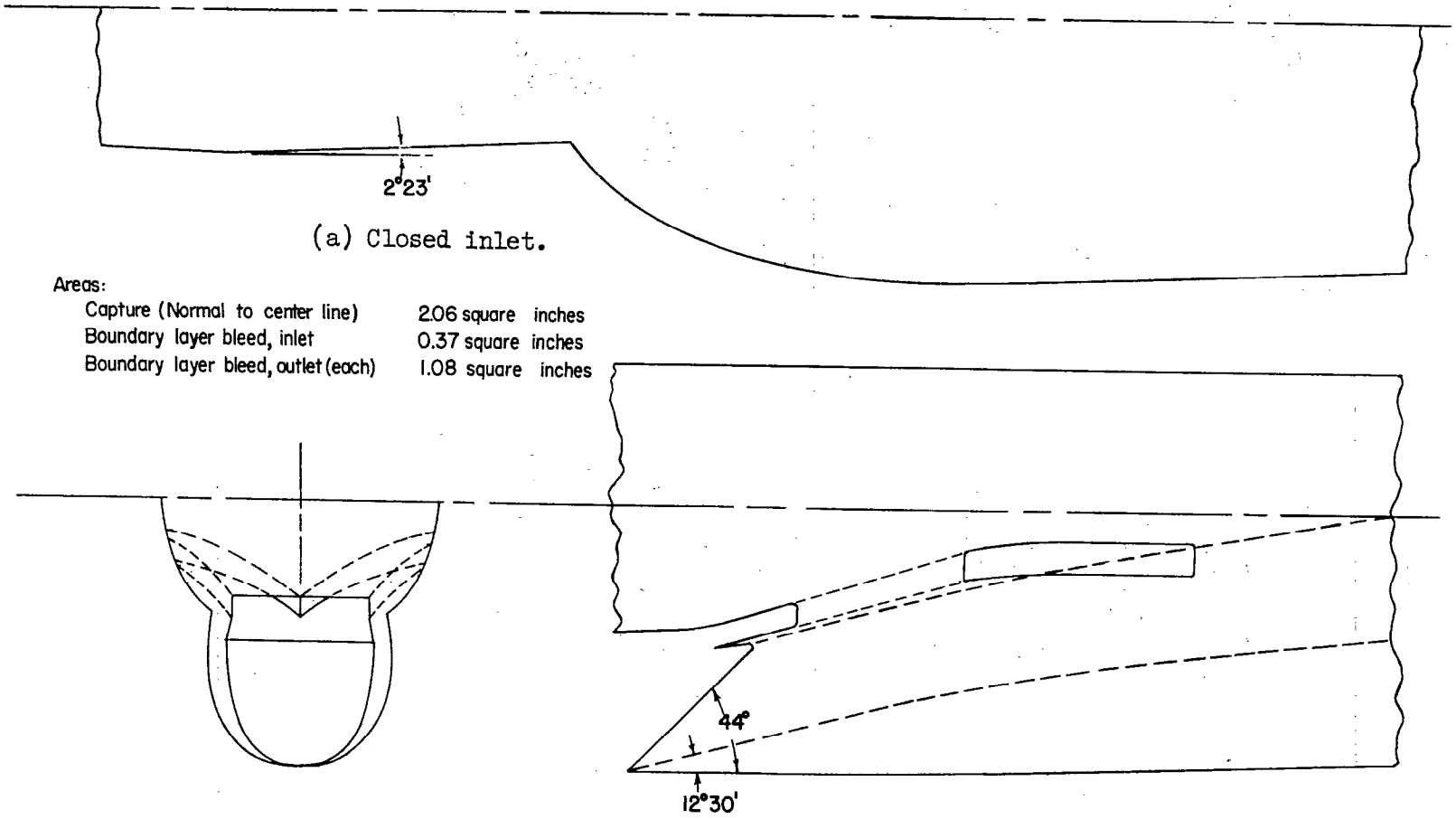

(a) Closed inlet.

(b) Open inlet.

Figure 3.- Inlet details, open and faired closed.

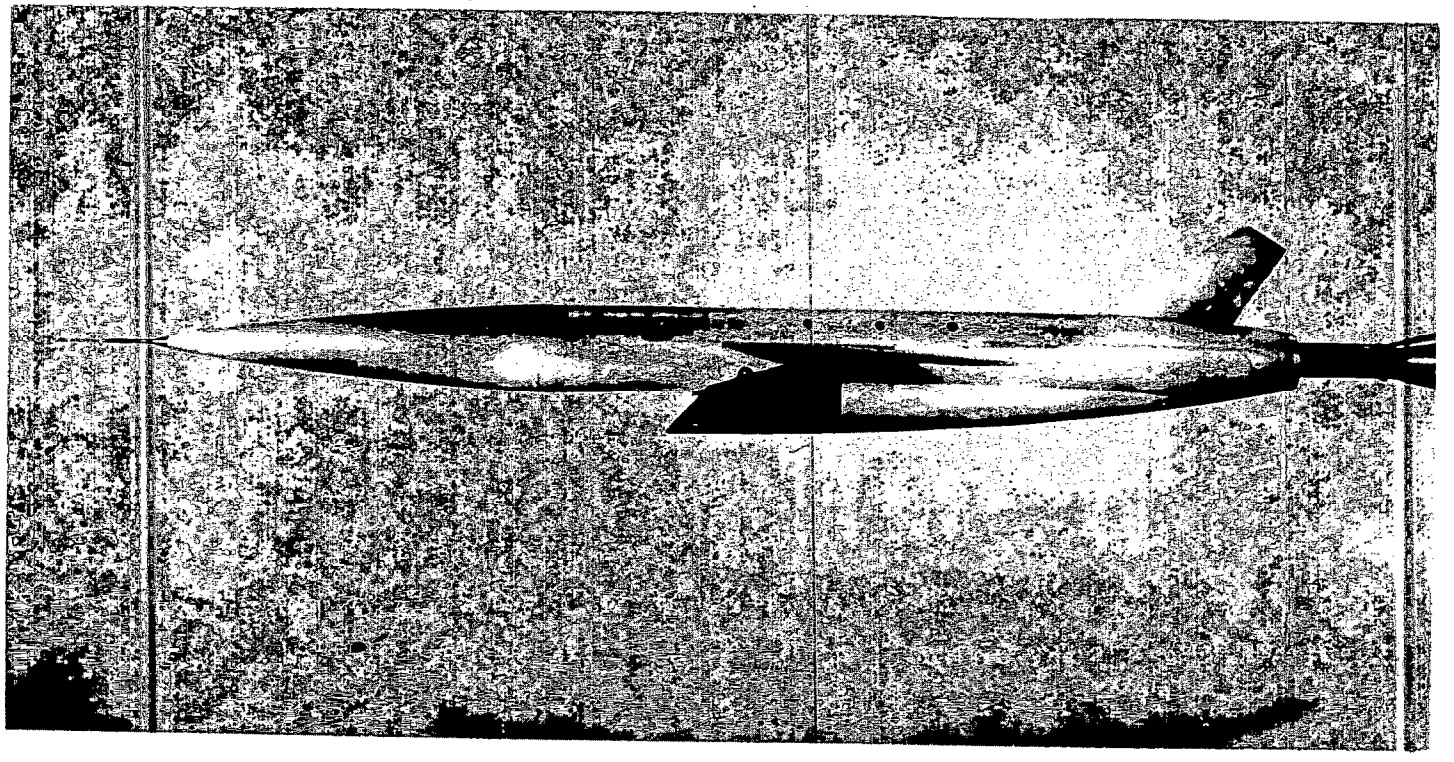

(a) Inlet open. L-85138

Figure 4.- Photographs of open- and closed-inlet configurations.

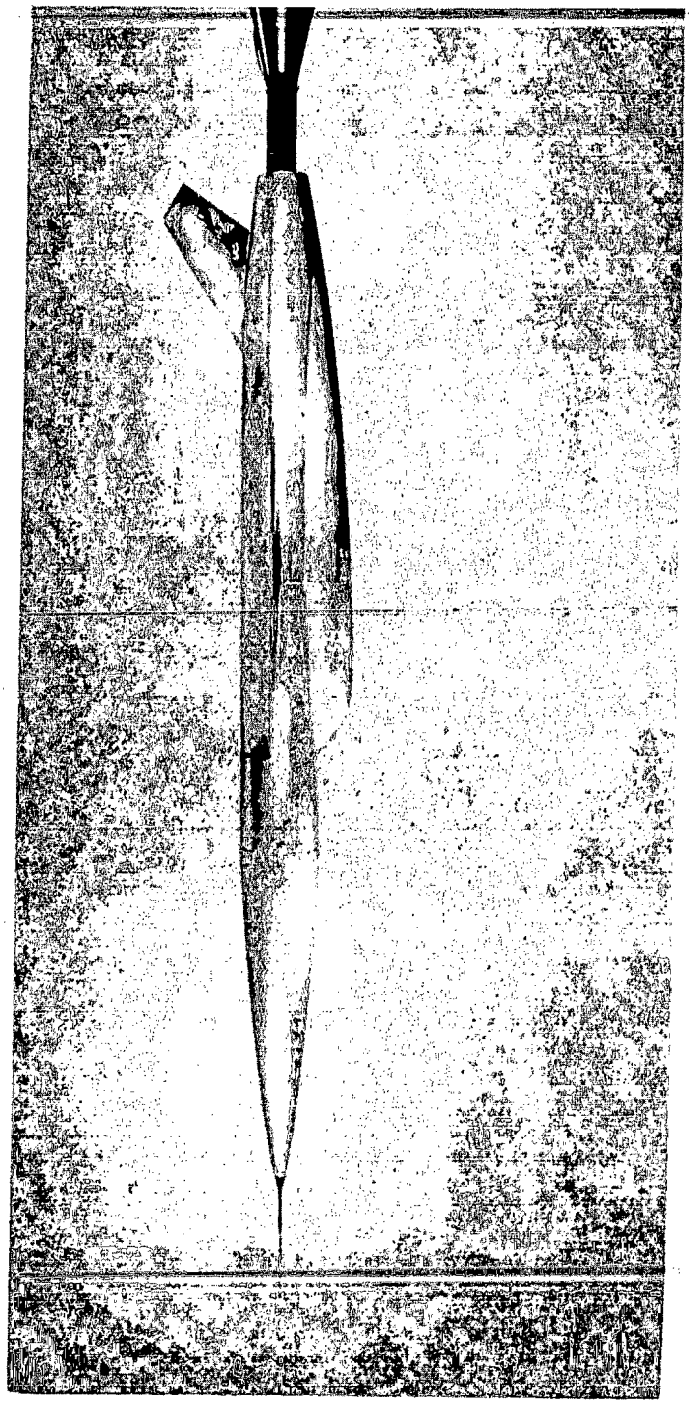

L-85137

(b) Inlet closed.

Figure 4.- Continued.

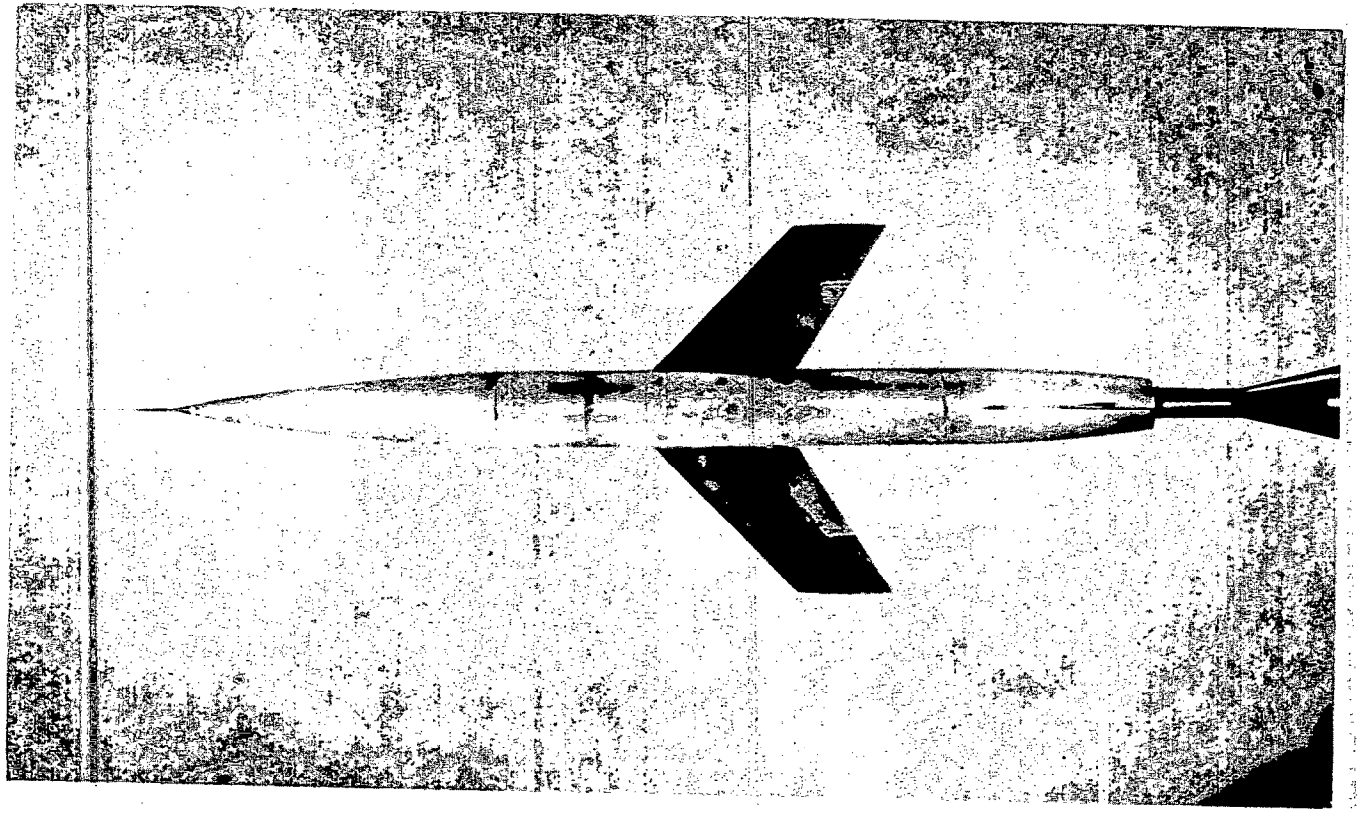

(c) Top view. L-85136

Figure 4.- Concluded.

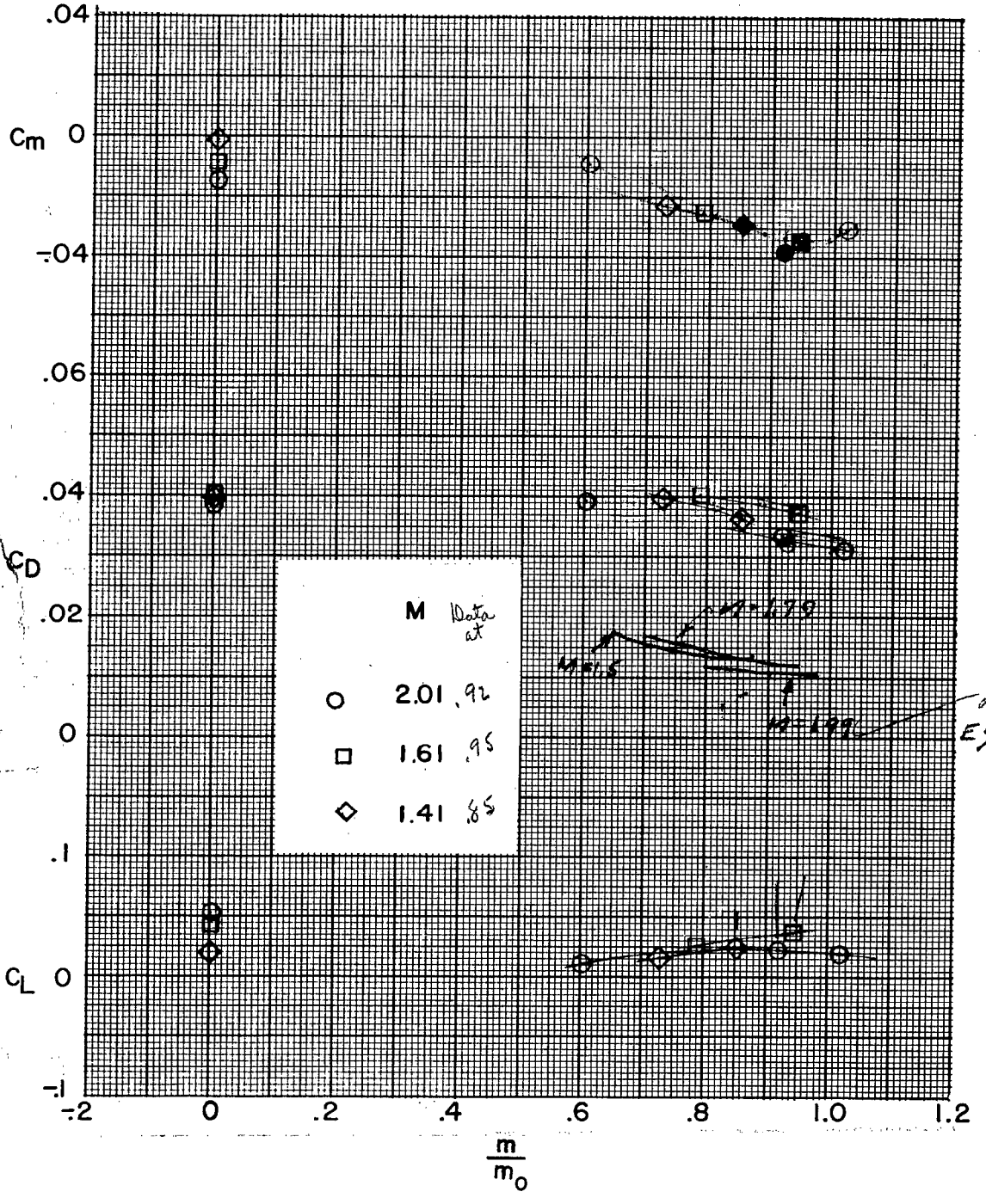

Figure 5.- Effects of mass flow on the aerodynamic characteristics in pitch at several Mach numbers. $\alpha \approx \beta \approx 0^{\circ}$. $m/m_o = 0$ is for faired closed inlet.

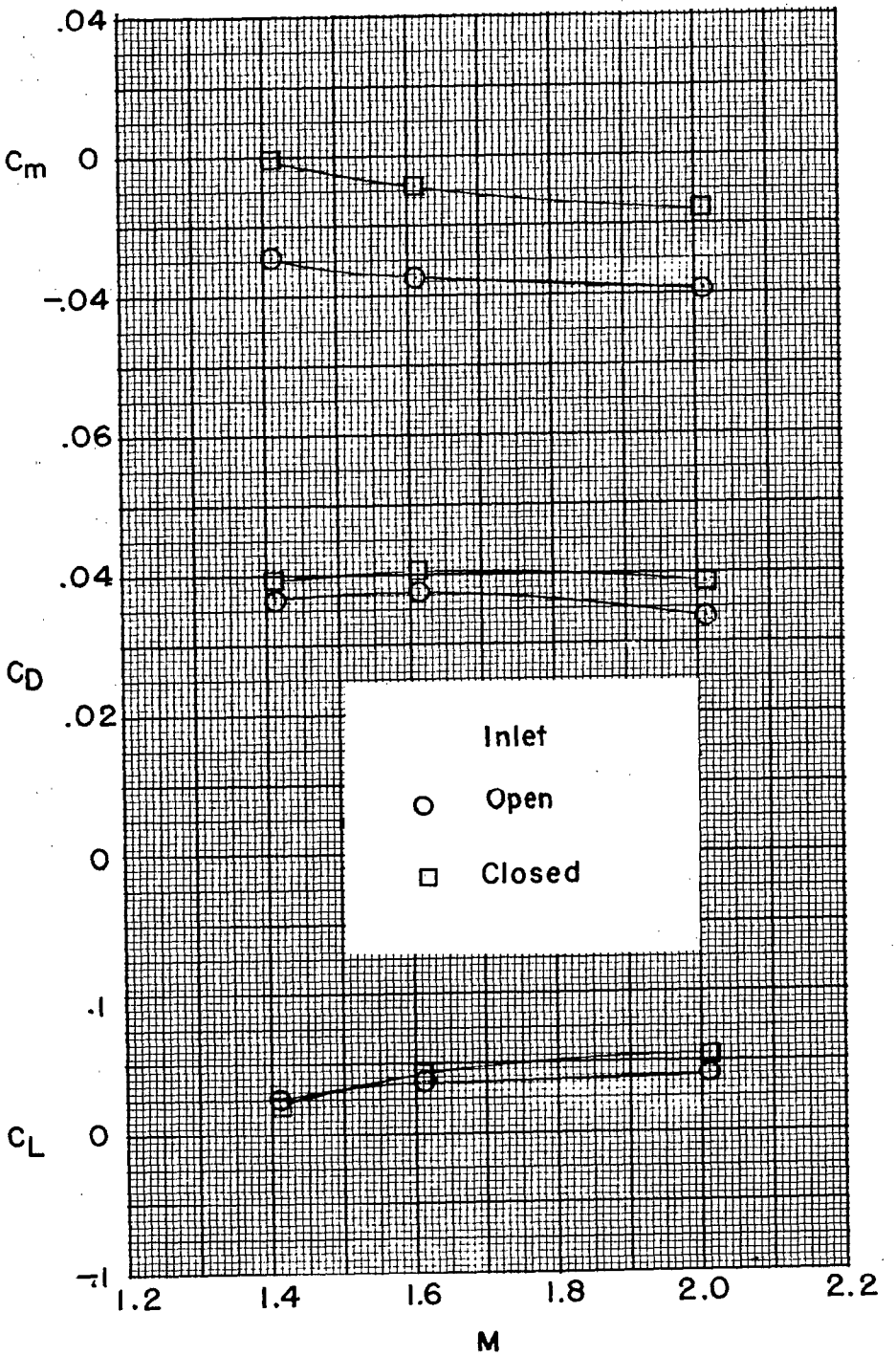

Figure 6.- Effects of internal flow on the variation of the aerodynamic characteristics in pitch with Mach number. $\alpha \approx \beta \approx 0^{\circ}$.

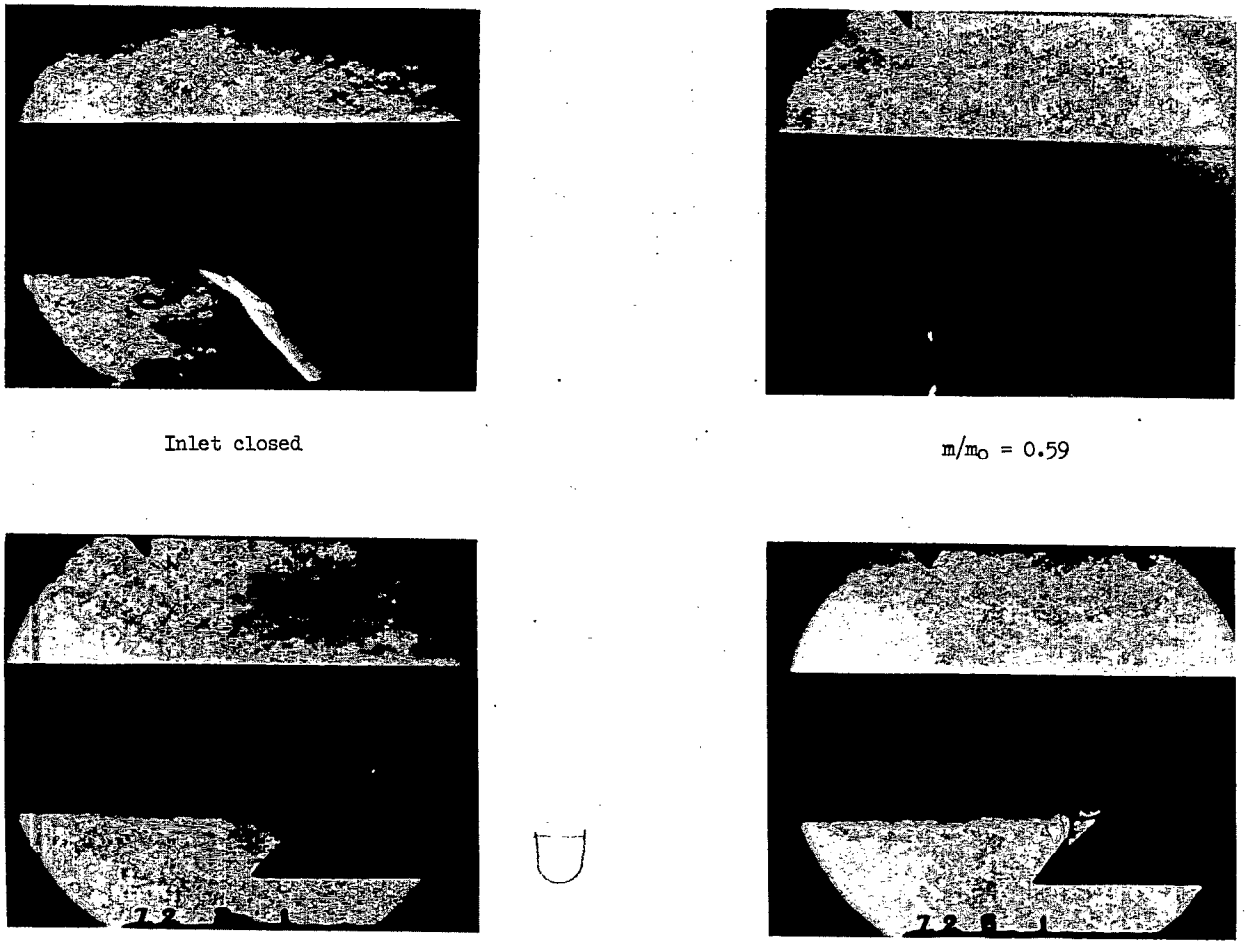

(a) M = 2.01.

L-87965

Figure 7.- Schlieren photographs of various inlet configurations. $\alpha = 0^o$ except as noted.

(b) M = 1.61.

Figure 7.- Continued.

L-87966

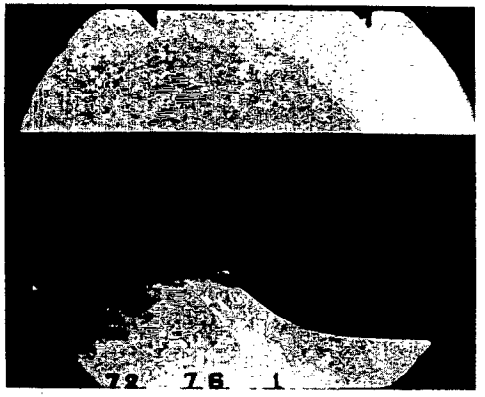

Inlet closed

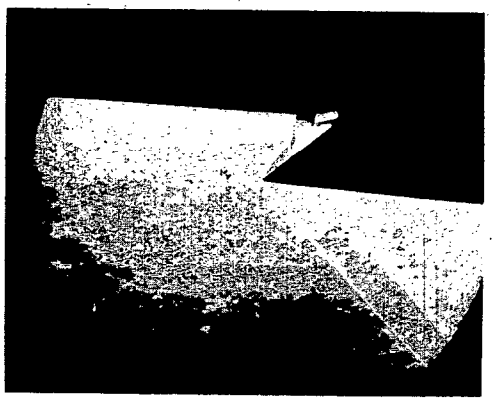

$\alpha \approx 5^{\circ}$

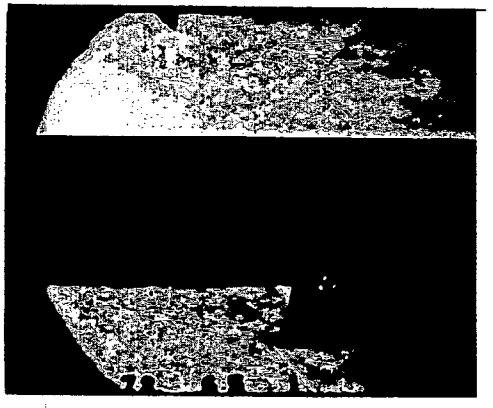

$m/m_o = 0.85$

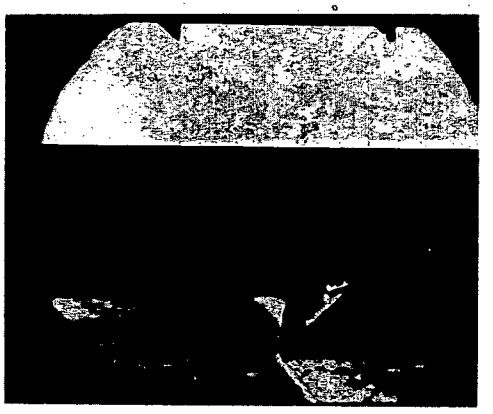

$m/m_o = 0.73$

(c) M = 1.41.

L-87967

Figure 7.- Concluded.

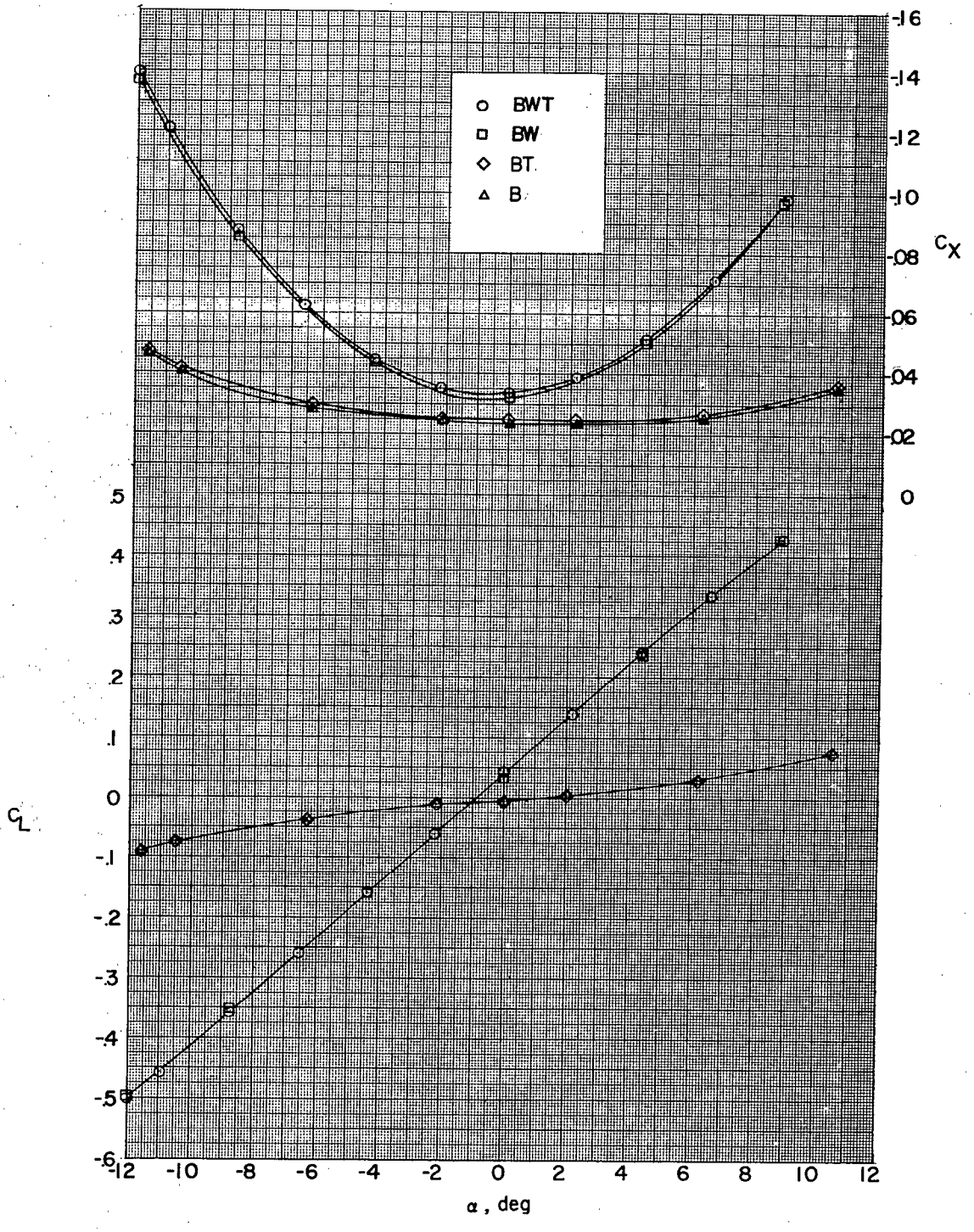

Figure 8.- Aerodynamic characteristics in pitch for various component parts. M = 2.01.

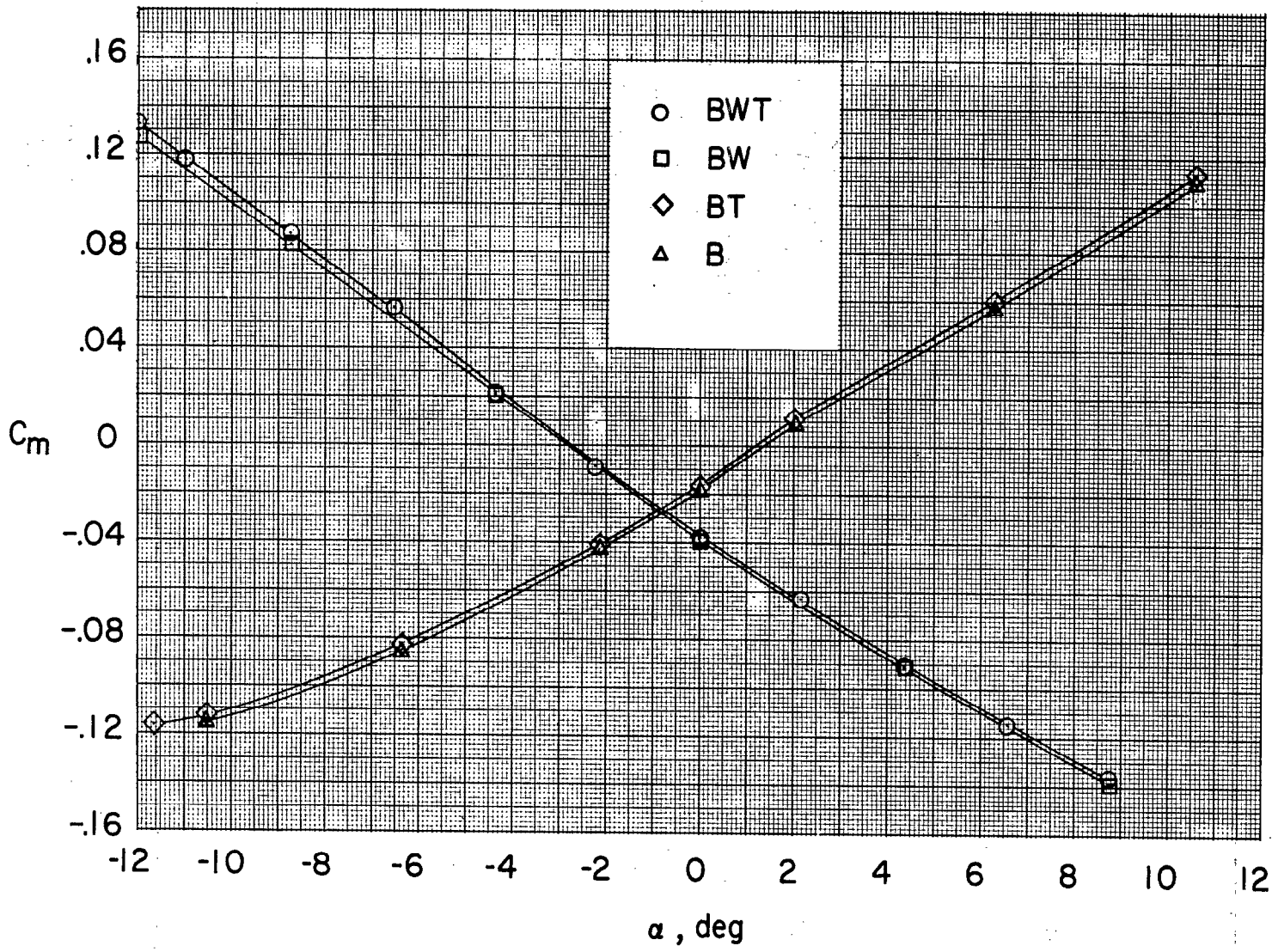

Figure 8.- Concluded.

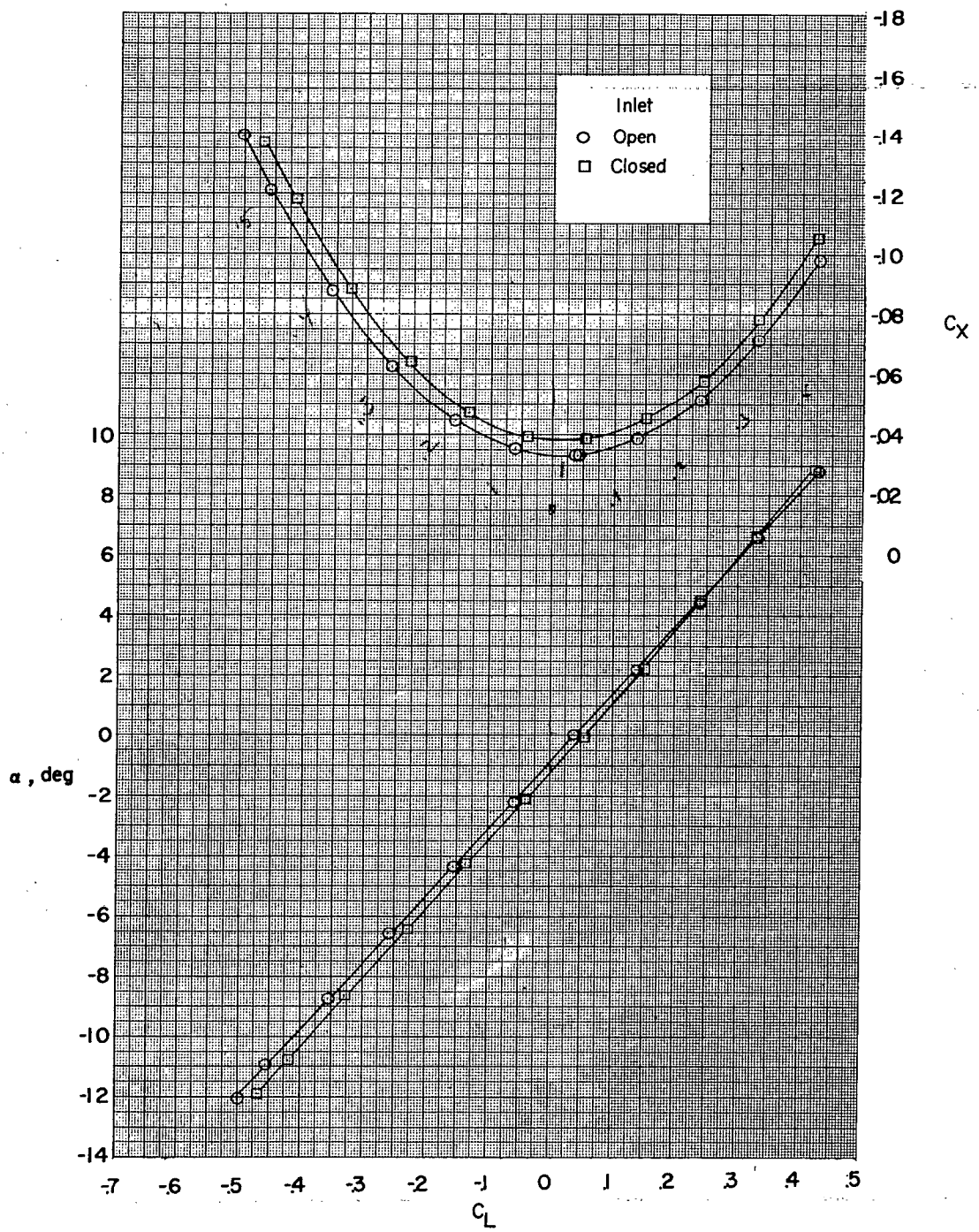

(a) M = 2.01.

Figure 9.- Effect of internal flow on aerodynamic characteristics in pitch. $\delta_{e_L} = \delta_{e_R} = 0^\circ$; $\beta \approx 0^\circ$. Inlet closed means faired closed.

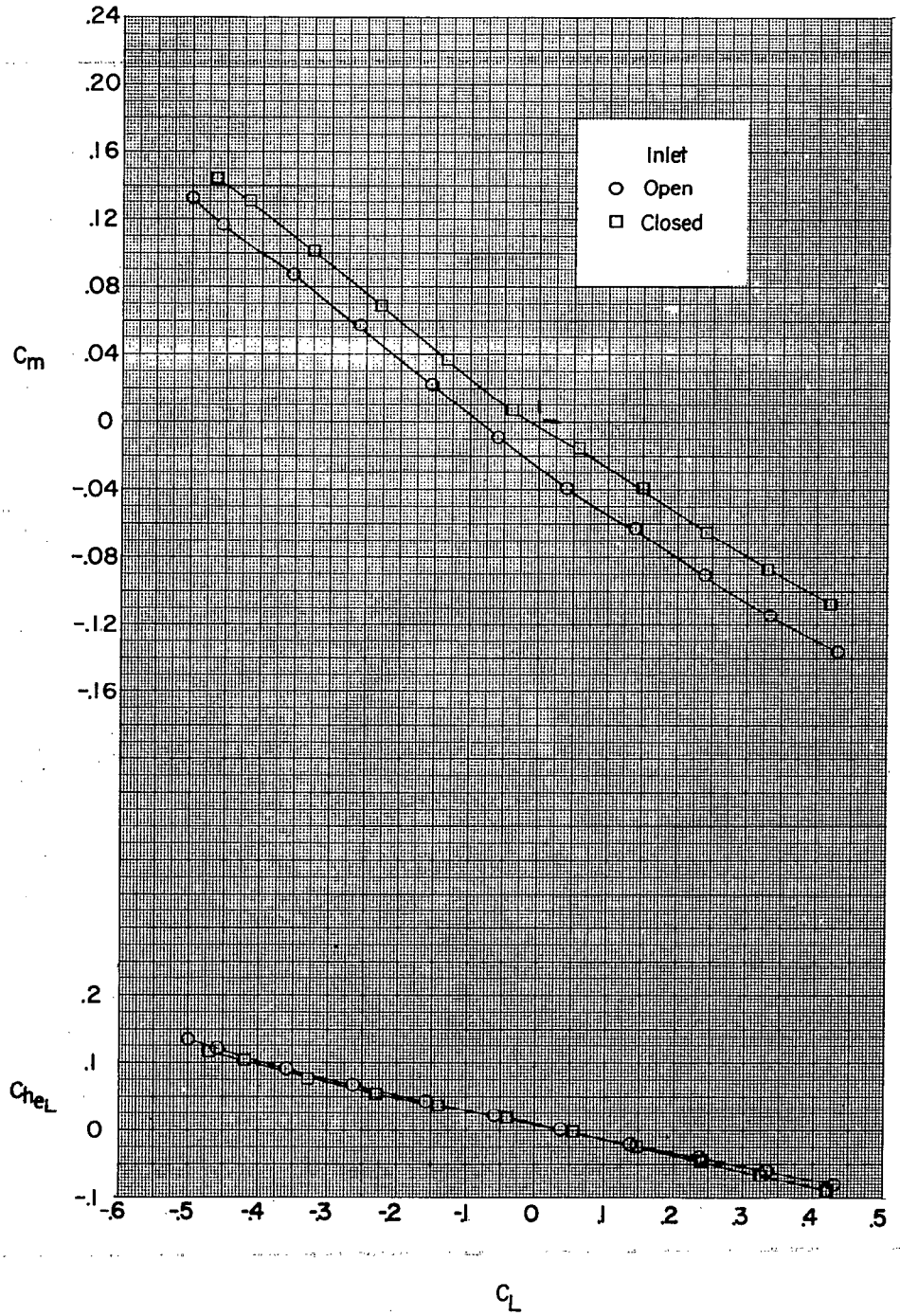

(a) Concluded.

Figure 9.- Continued.

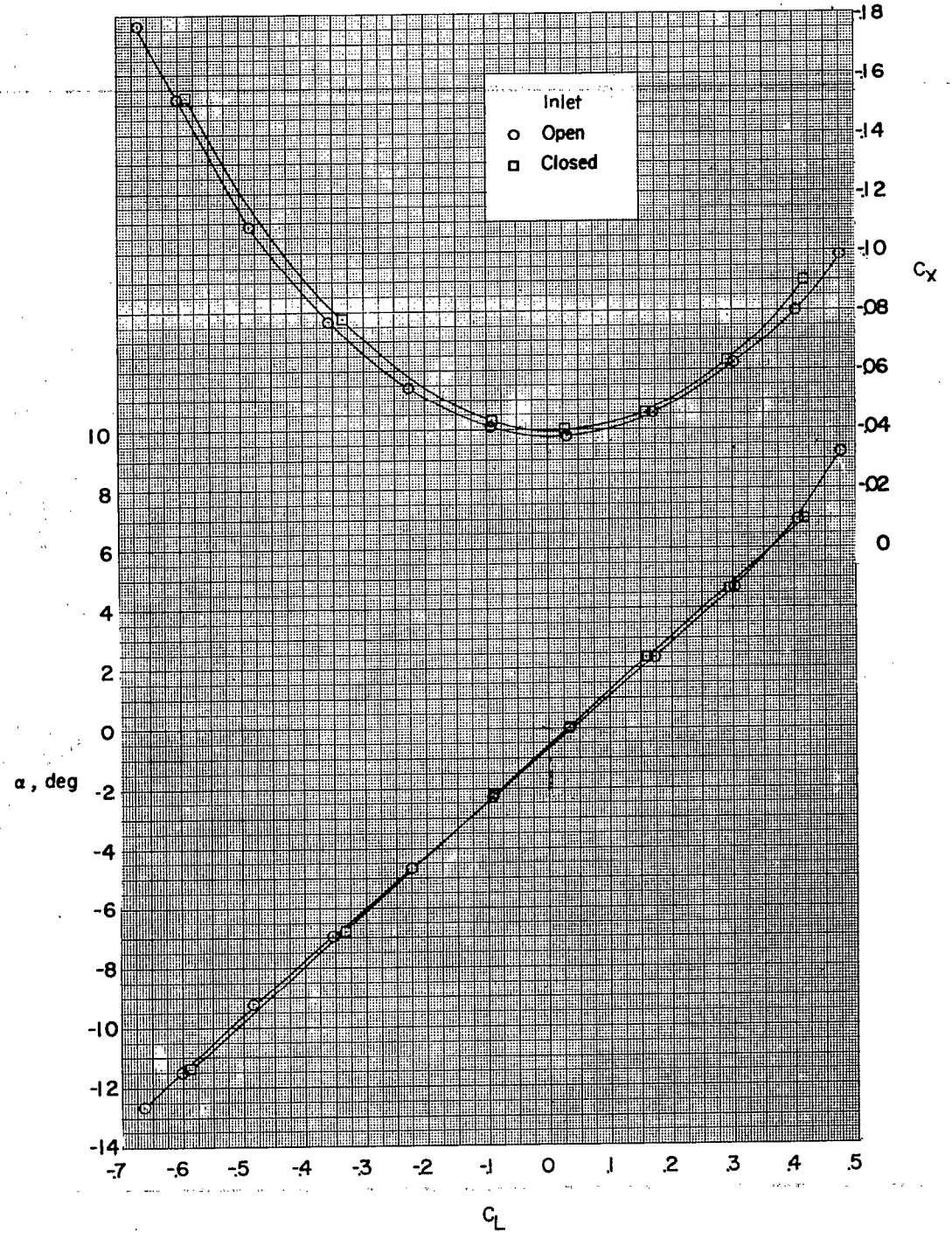

(b) M = 1.41.

Figure 9.- Continued.

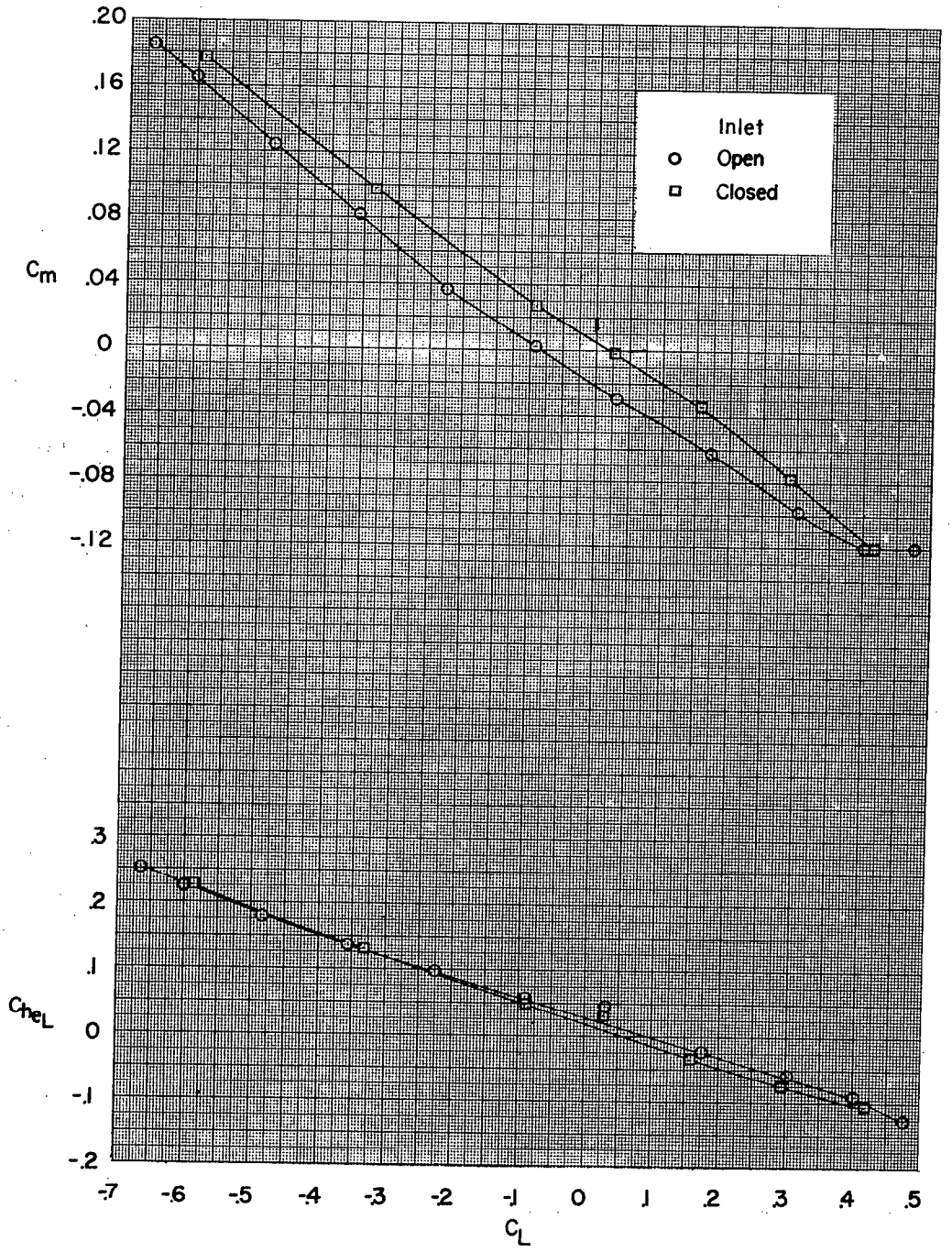

(b) Concluded.

Figure 9.- Concluded.

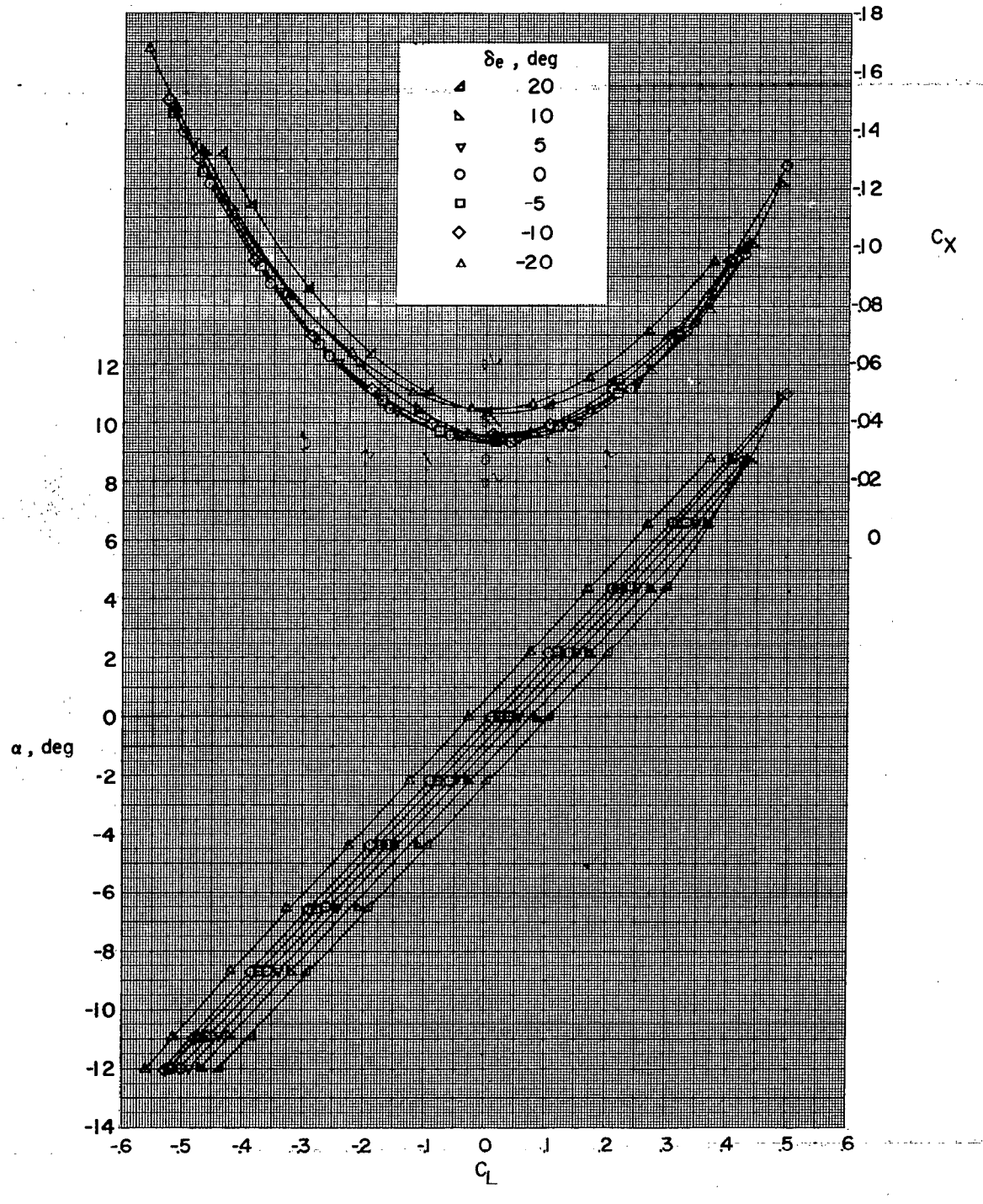

(a) M = 2.01; inlet open.

Figure 10.- Effect of elevon deflection on the aerodynamic characteristics in pitch. $\beta \approx 0^\circ$; $\delta_{e_L} = \delta_{e_R}$.

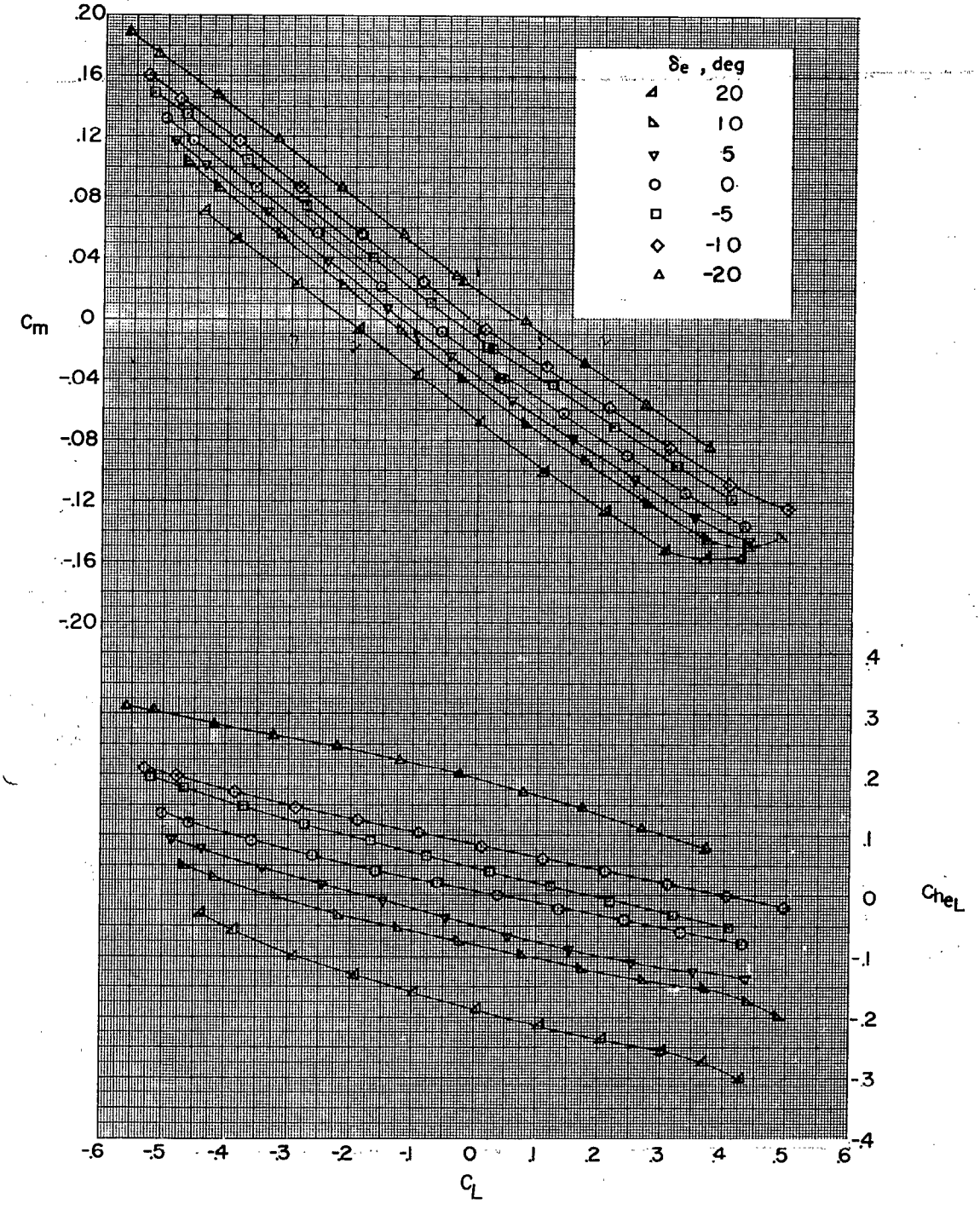

(a) Concluded.

Figure 10.- Continued.

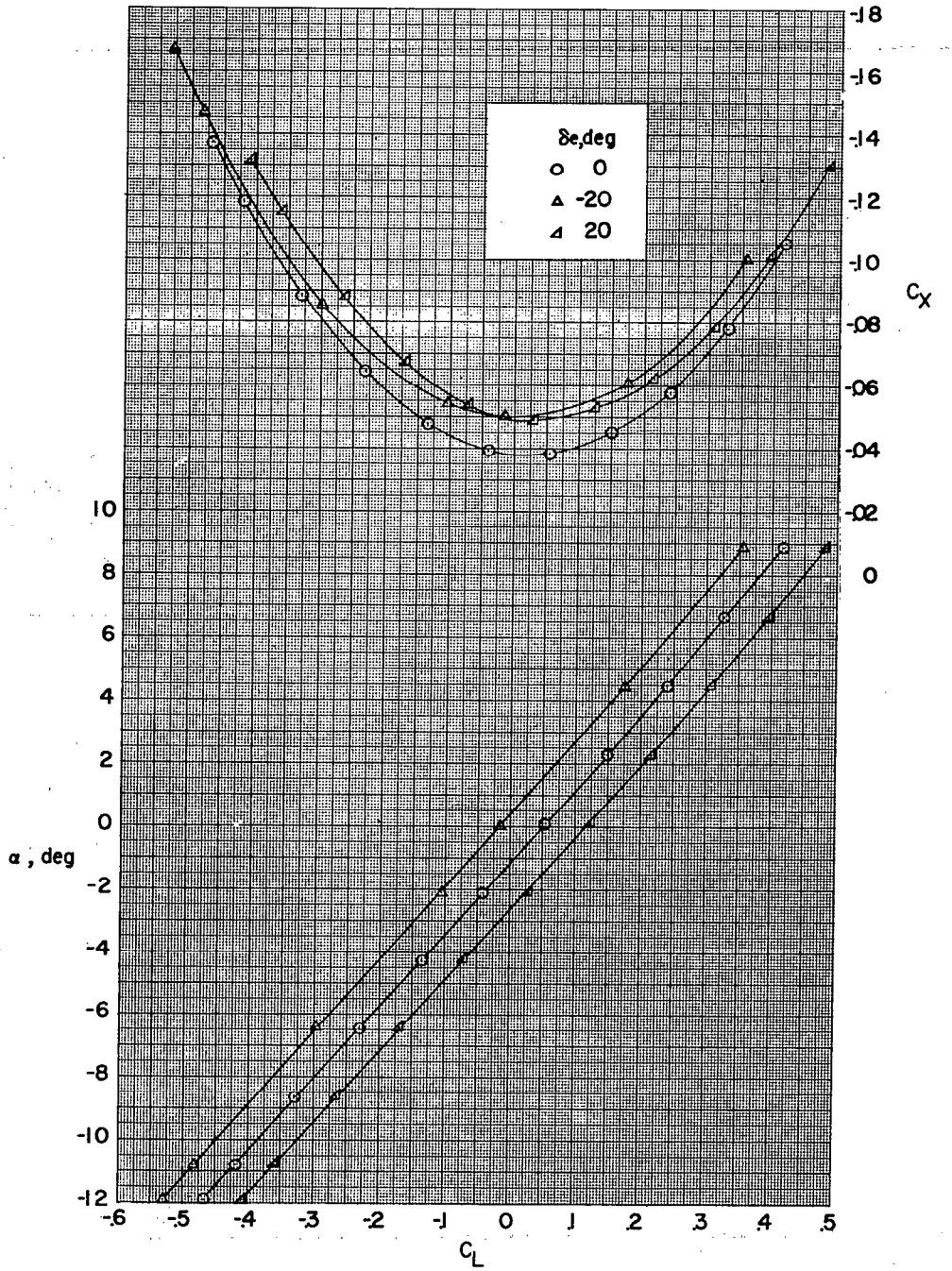

(b) M = 2.01; inlet faired closed.

Figure 10.- Continued.

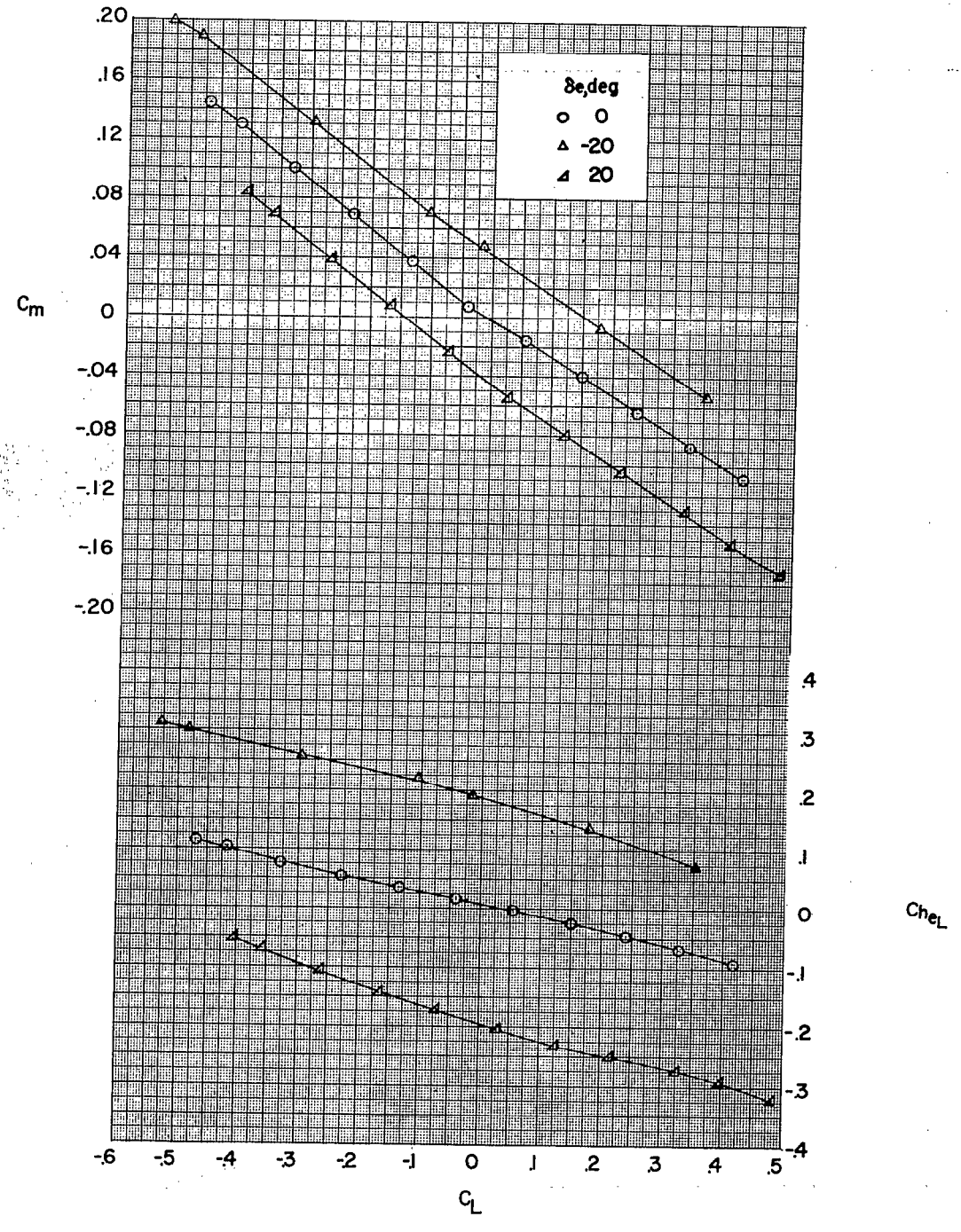

(b) Concluded.

Figure 10.- Continued.

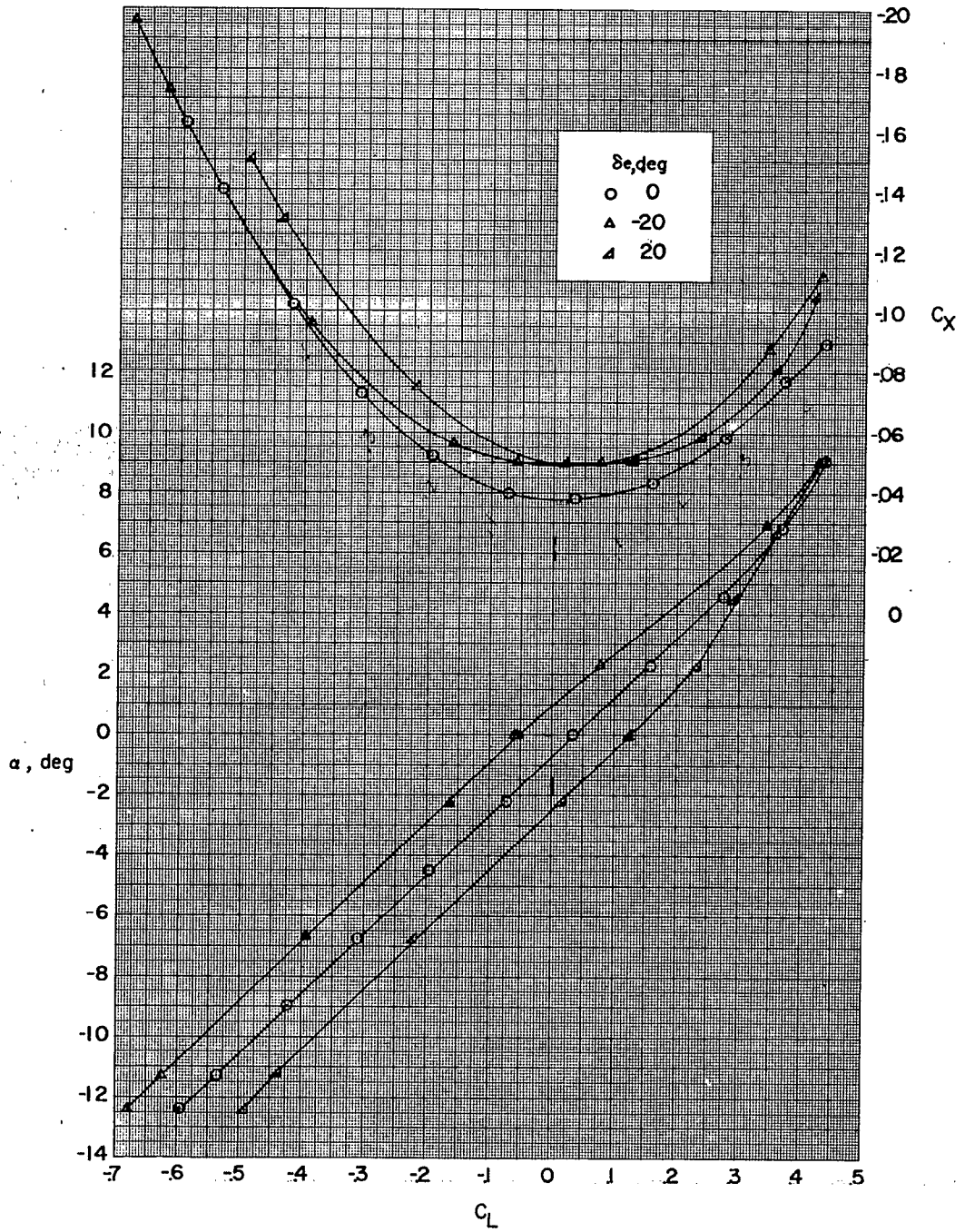

(c) M = 1.61; inlet open.

Figure 10.- Continued.

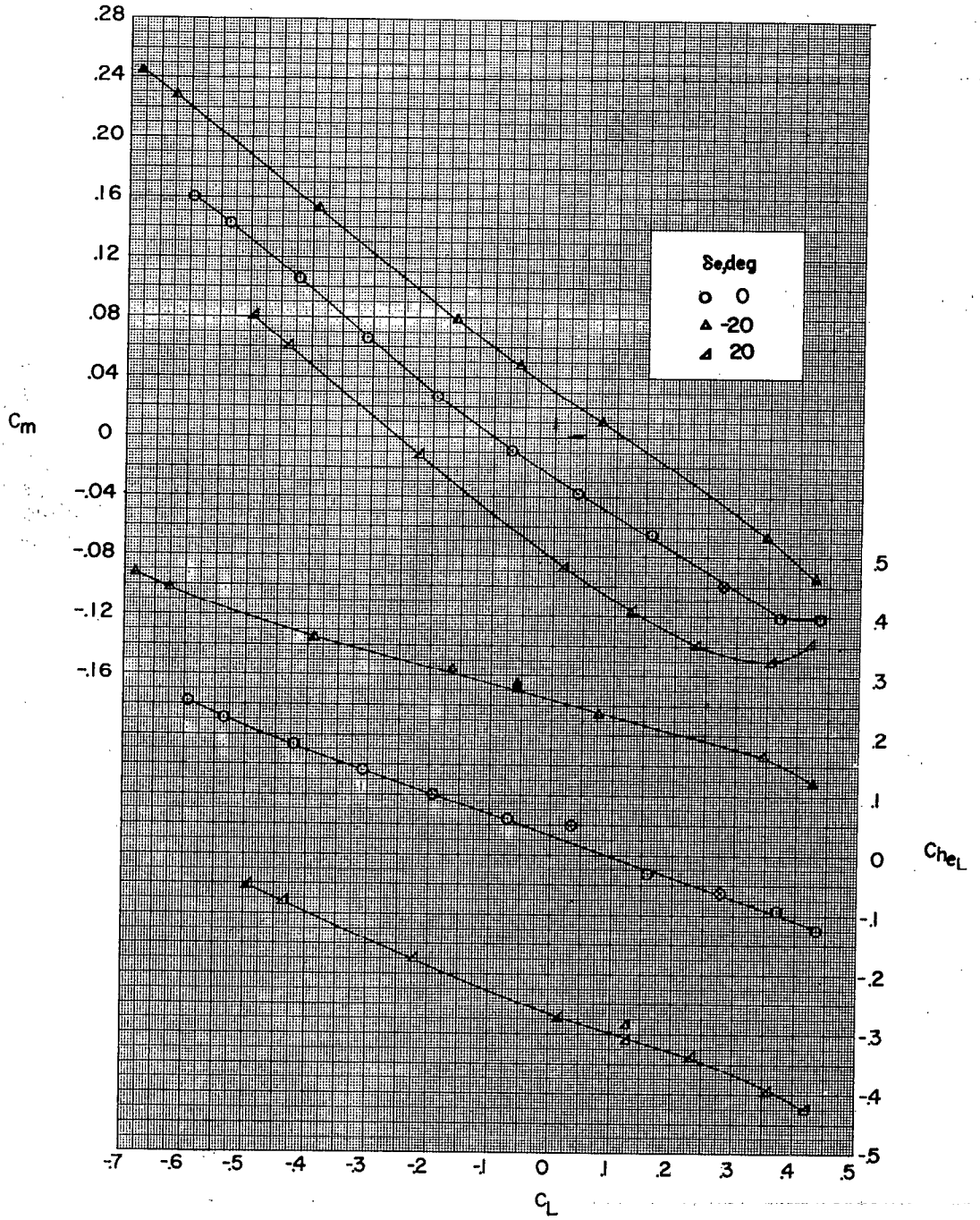

(c) Concluded.

Figure 10.- Continued.

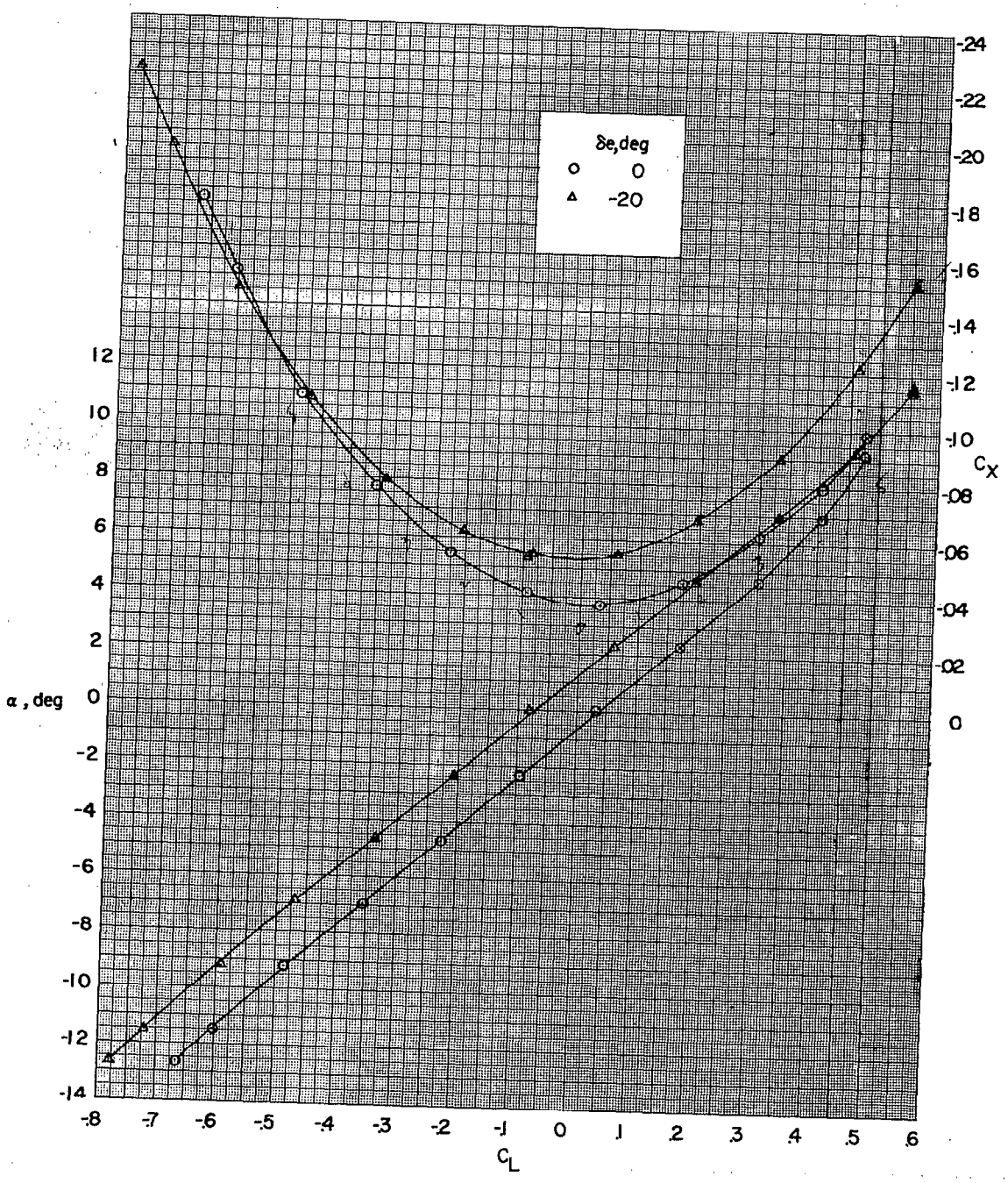

(d) M = 1.41; inlet open.

Figure 10.- Continued.

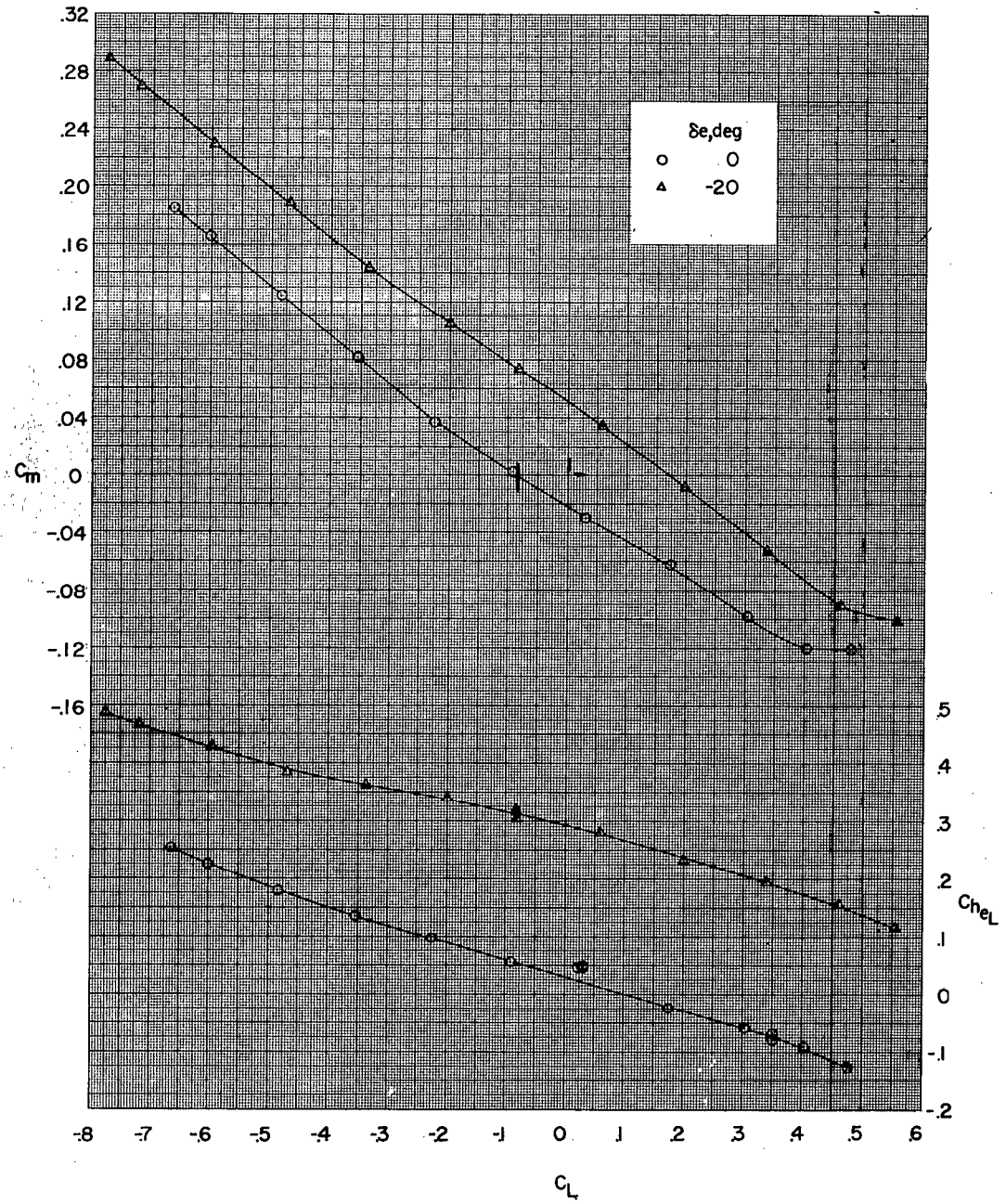

(d) Concluded.

Figure 10.- Concluded.

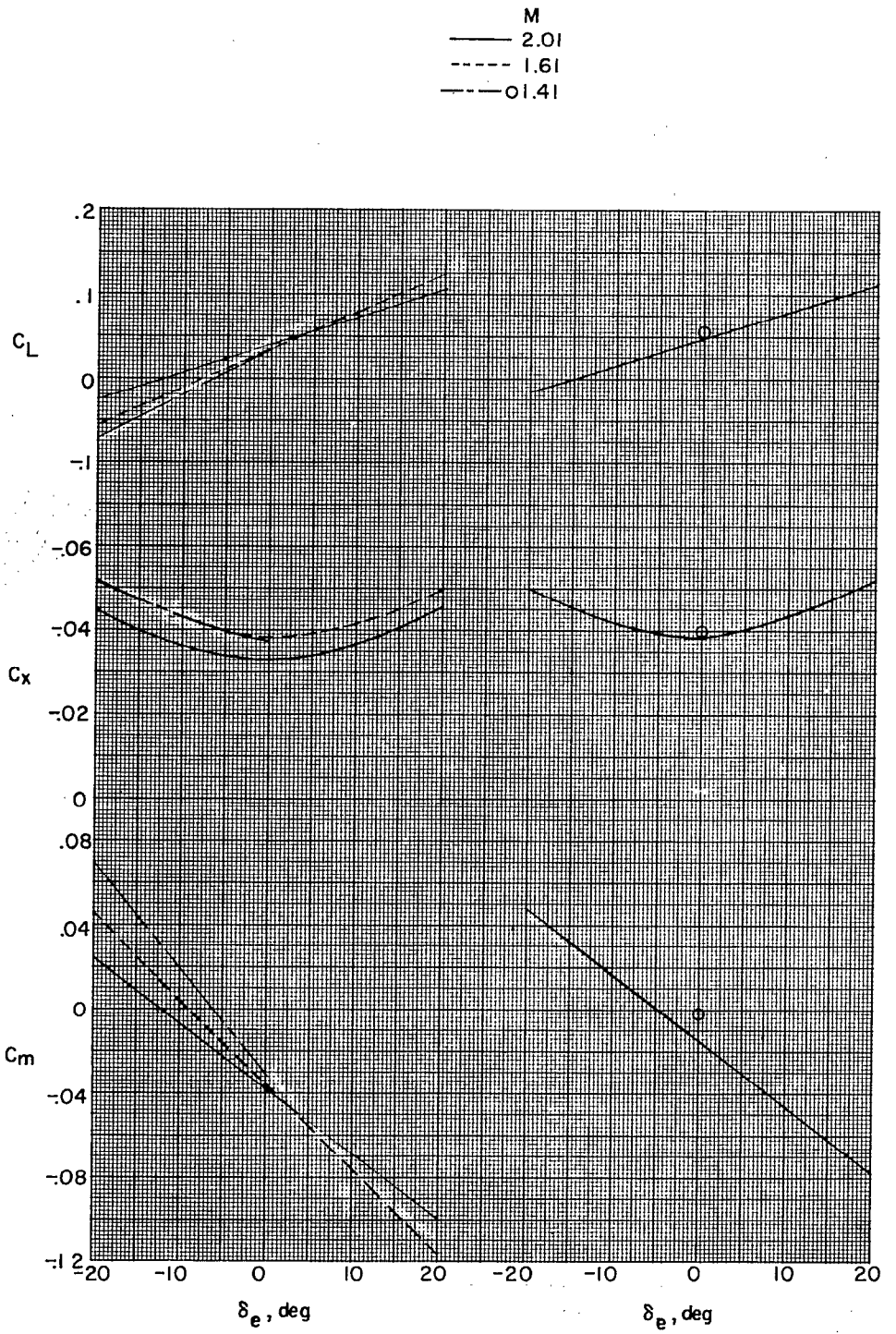

(a) Inlet open. (b) Inlet closed.

Figure 11.- Pitch control characteristics. $\alpha \approx \beta \approx 0^\circ$.

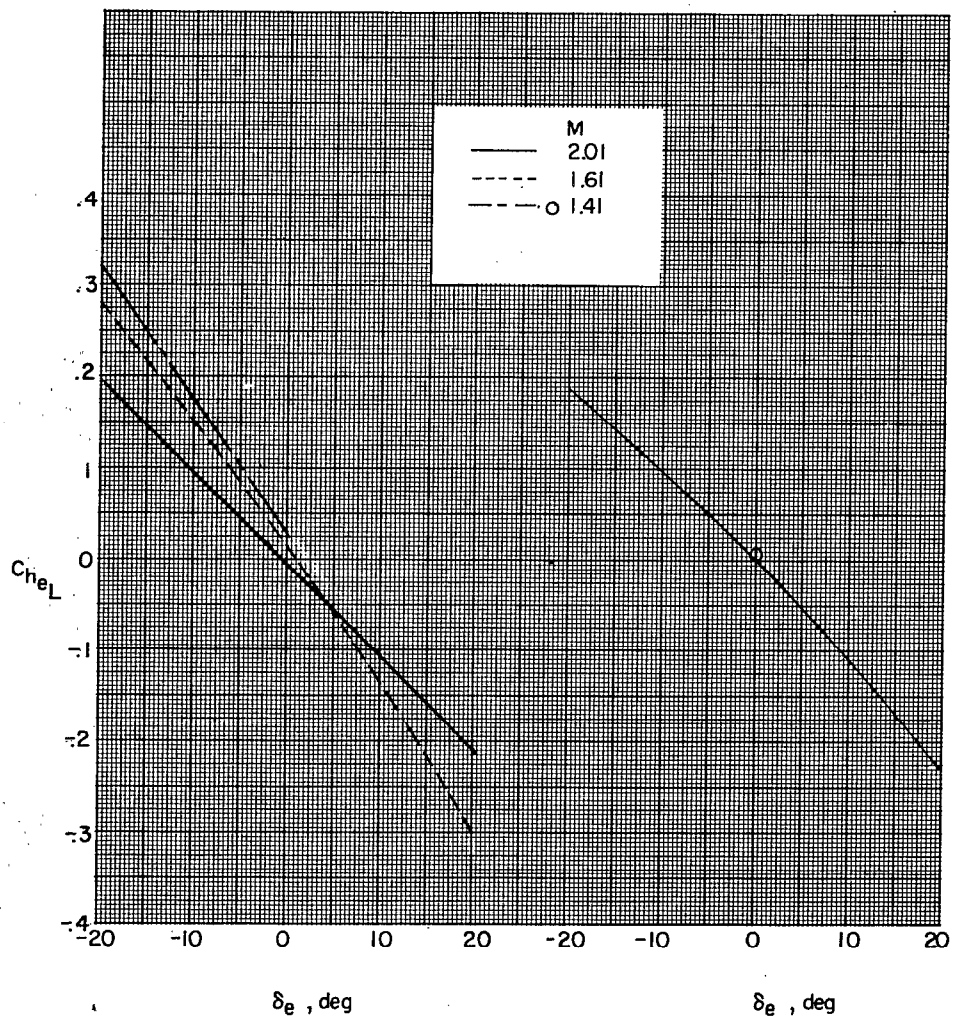

(a) Concluded.

(b) Concluded.

Figure 11.- Concluded.

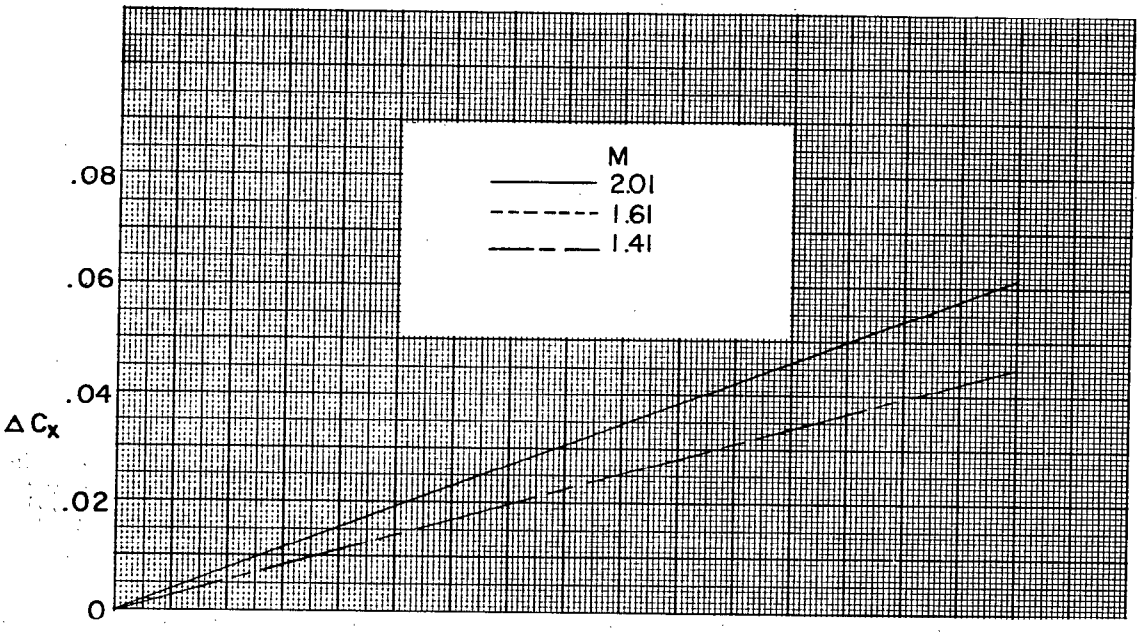

(a) Inlet faired closed.

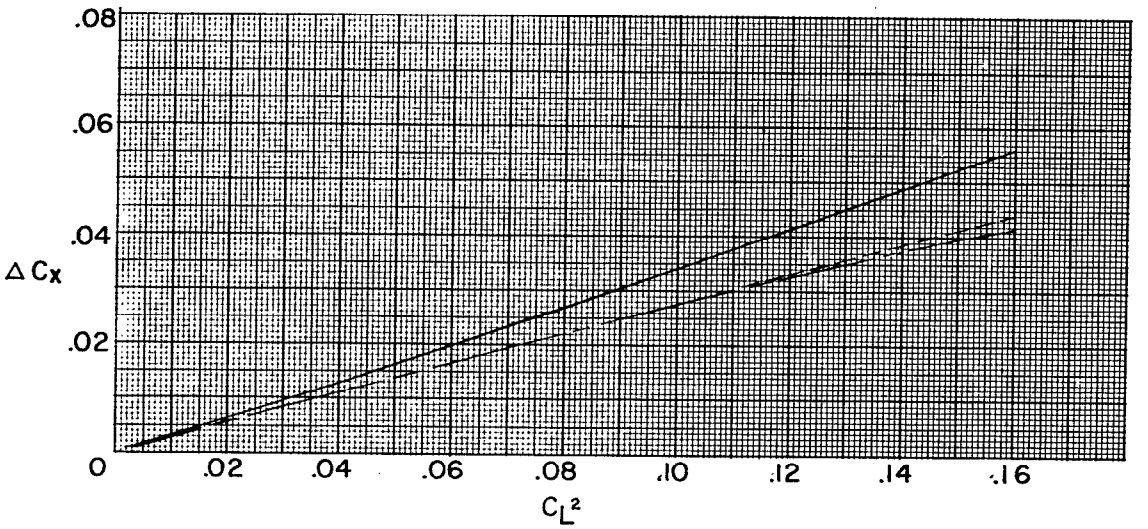

(b) Inlet open.

Figure 12.- Drag due to lift.

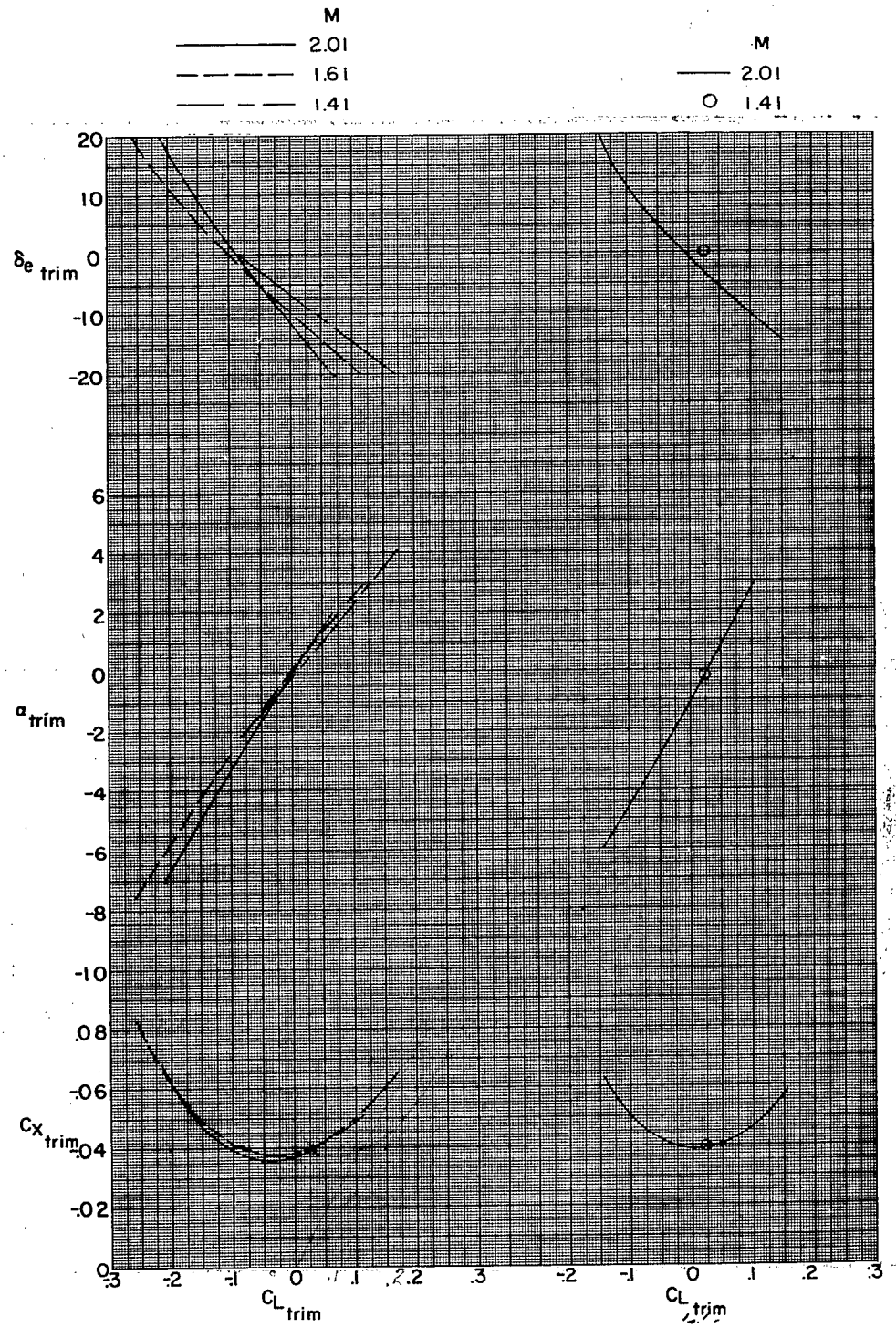

(a) Inlet open. (b) Inlet closed.

Figure 13.- Longitudinal characteristics for trim.

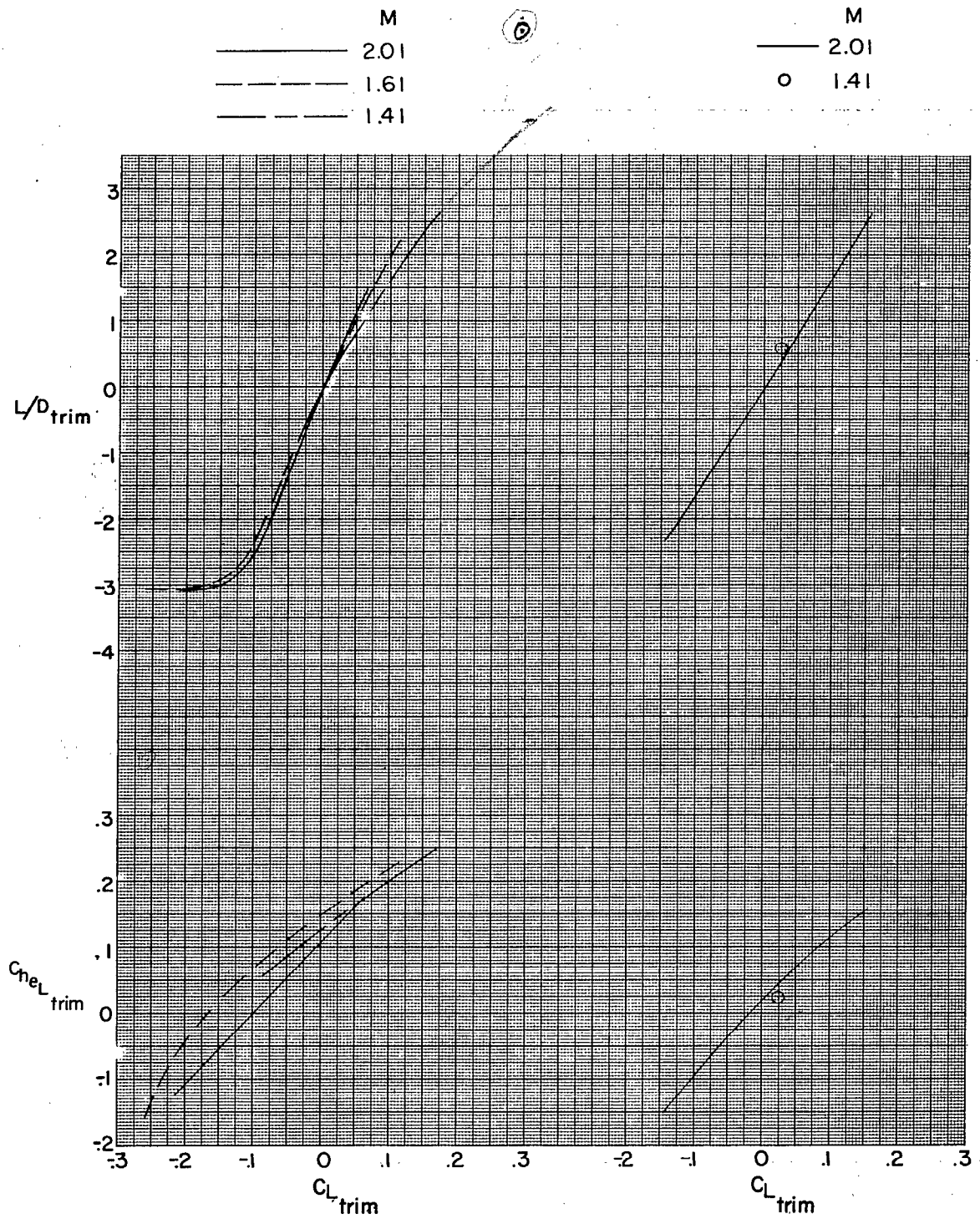

(a) Concluded. (b) Concluded.

Figure 13.- Concluded.

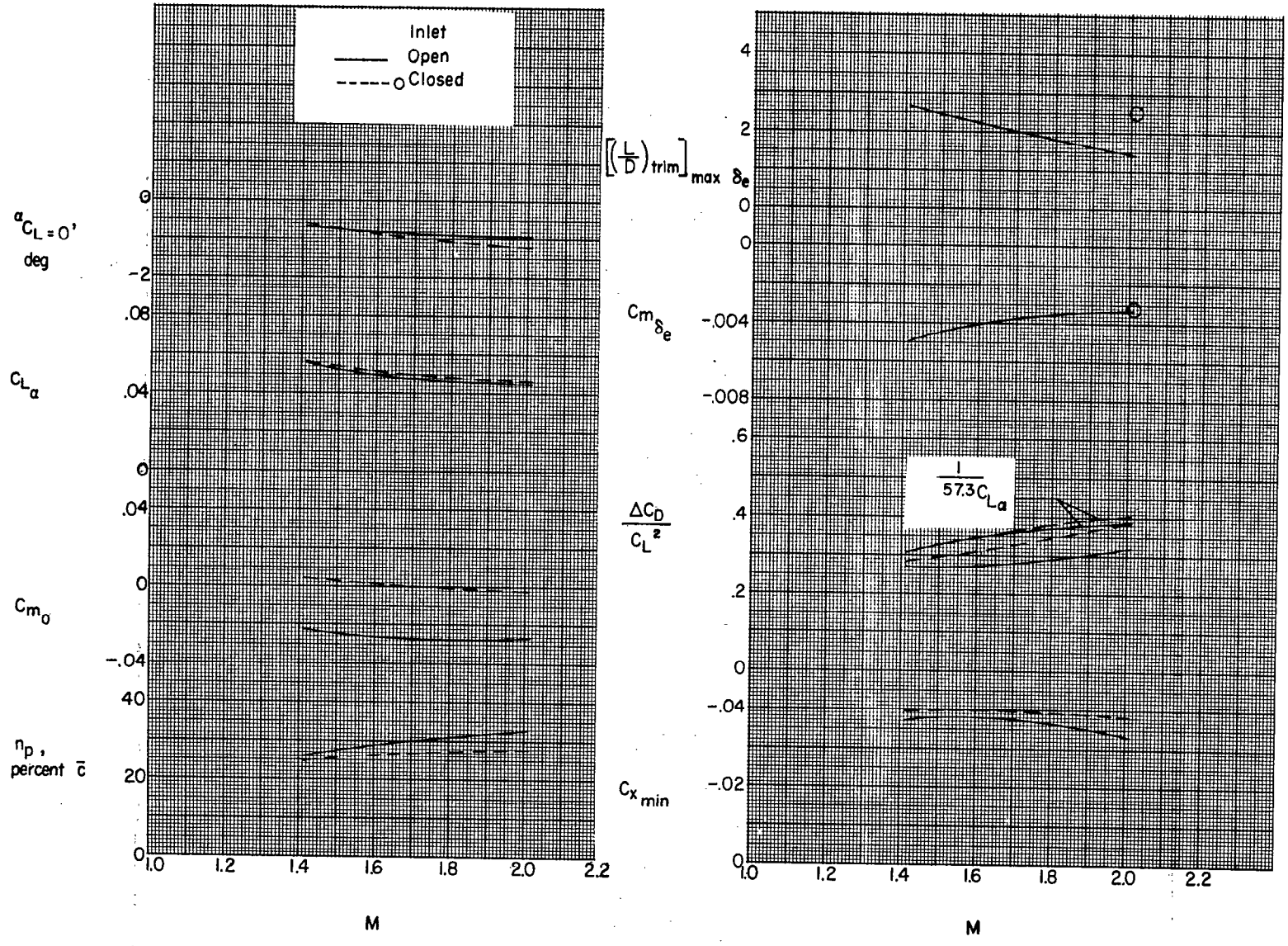

Figure 14.- Summary of longitudinal parameters.

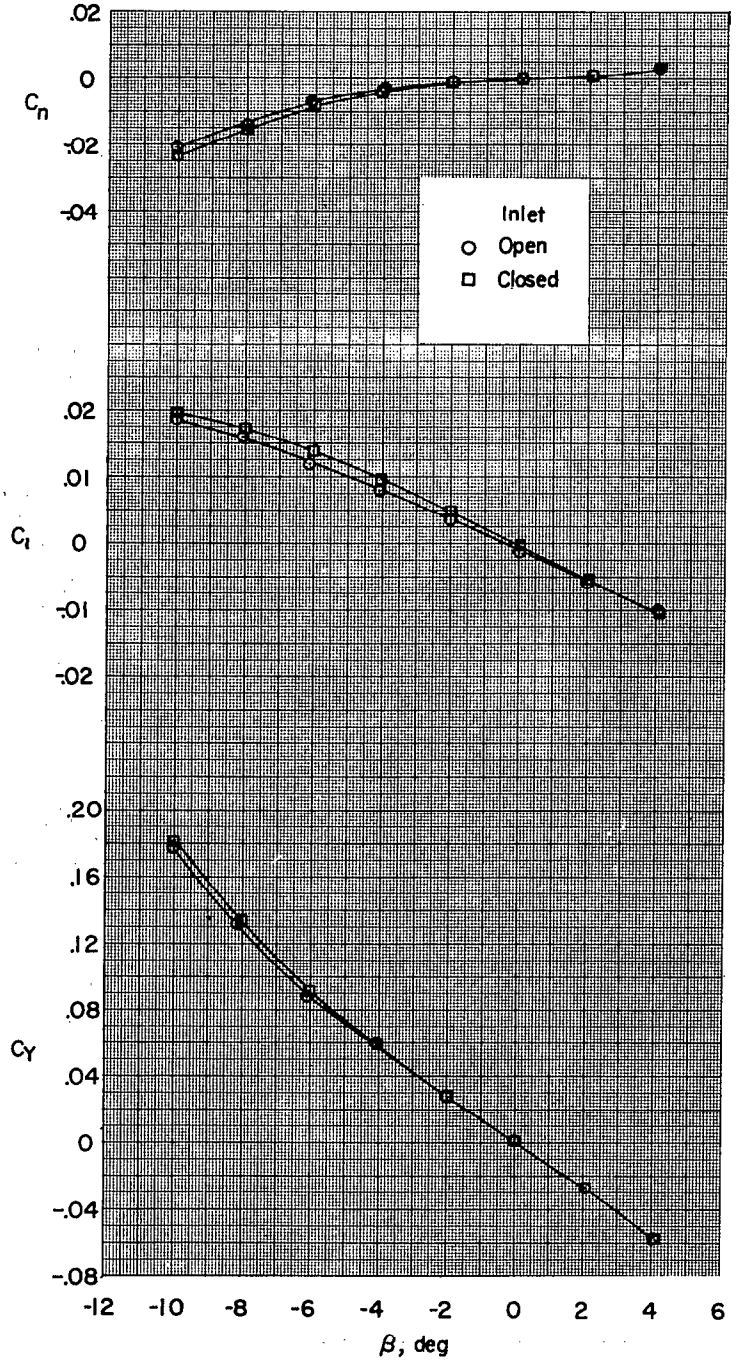

(a) M = 2.01; $\alpha = 0^{\circ}$.

Figure 15.- Effect of internal flow on aerodynamic characteristics in sideslip. Closed inlet means faired closed.

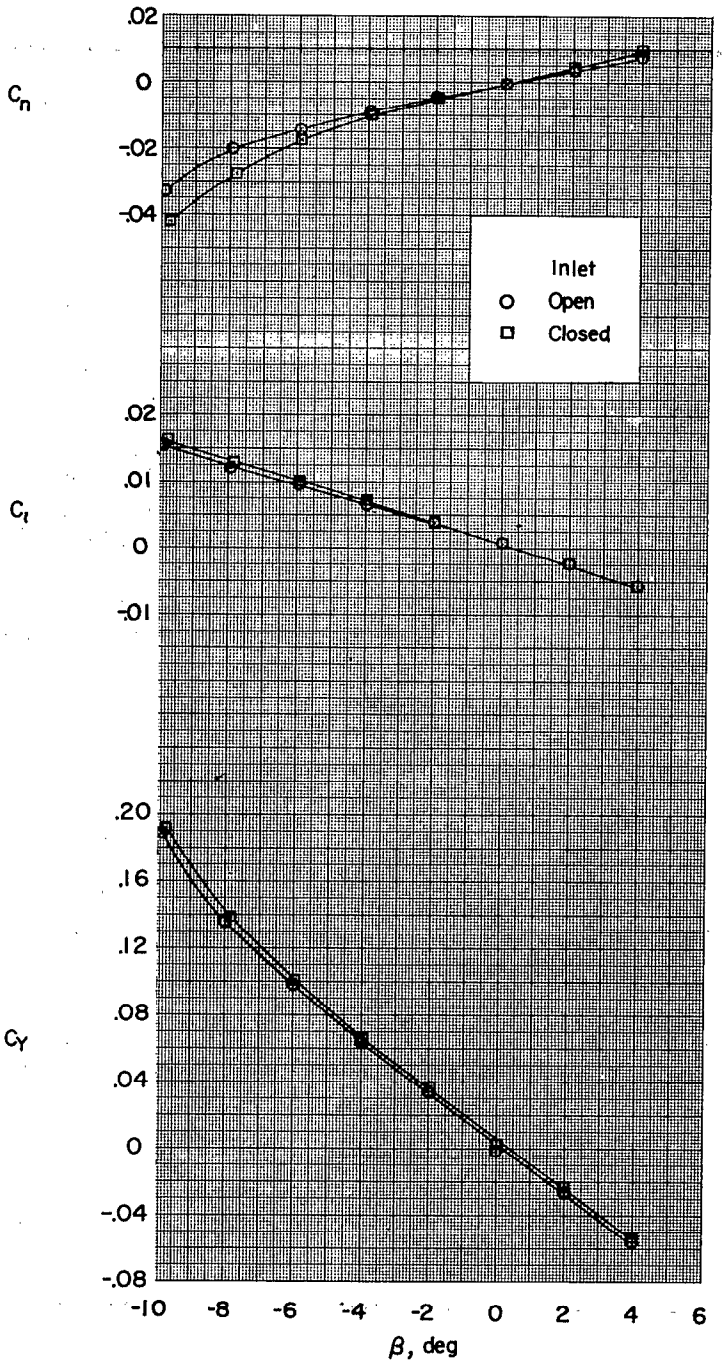

(b) M = 2.01; $\alpha = -5^\circ$.

Figure 15.- Continued.

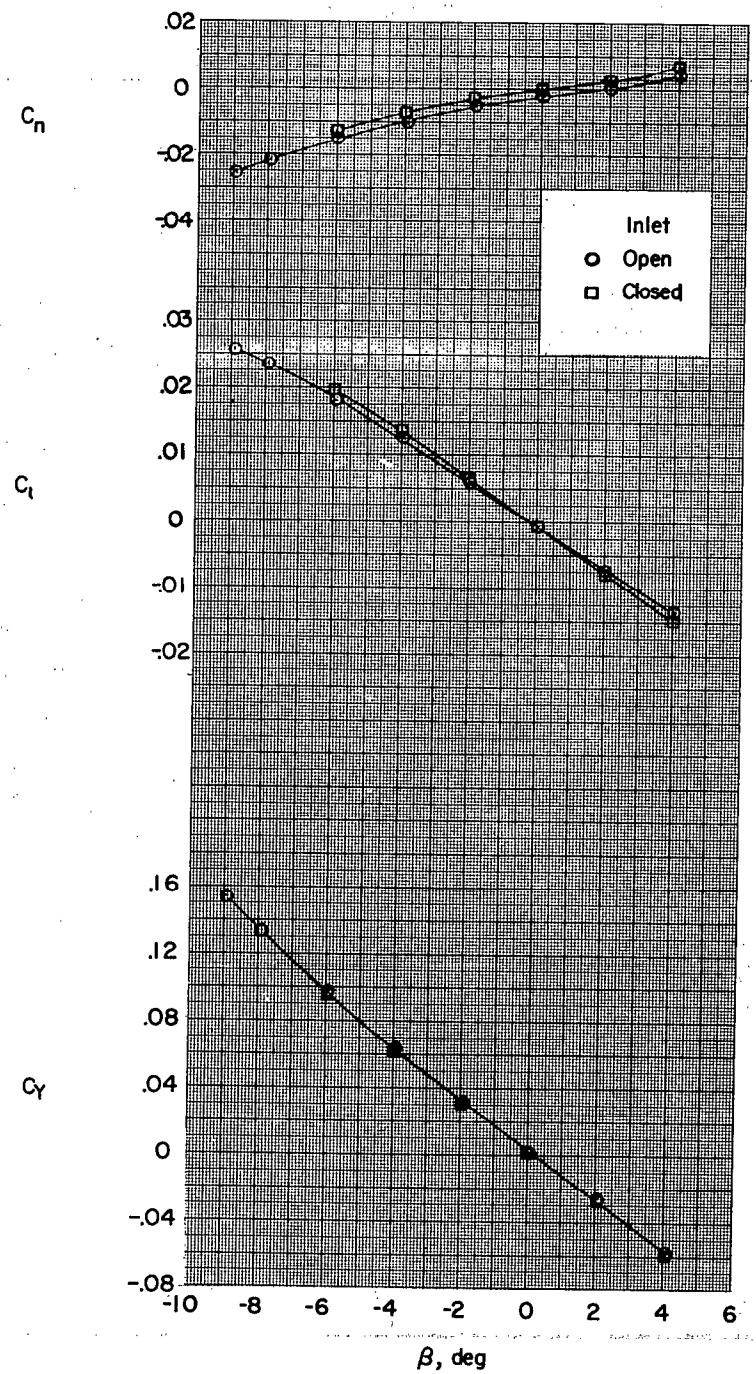

(c) M = 1.61; $\alpha = 0^\circ$.

Figure 15.- Continued.

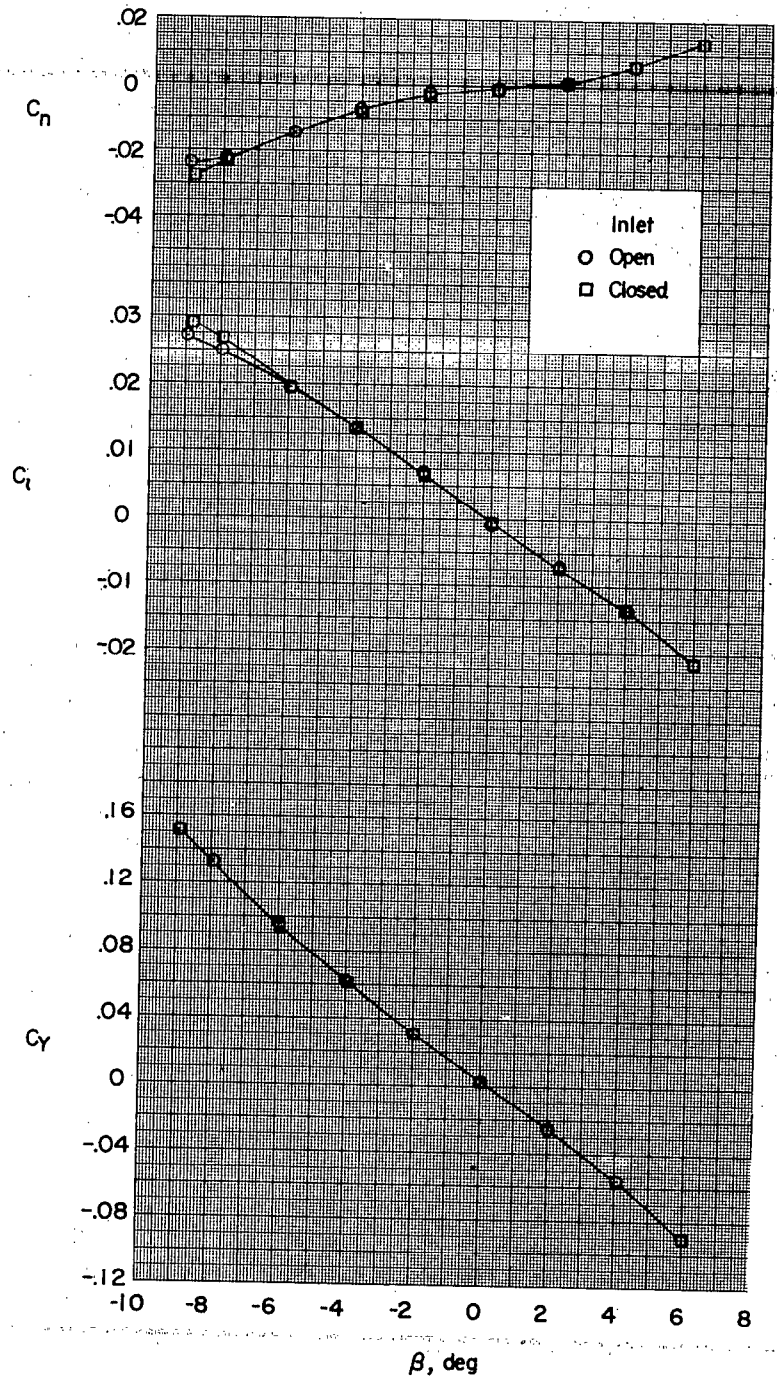

(d) $M = 1.41$; $\alpha = 0^\circ$.

Figure 15.- Concluded.

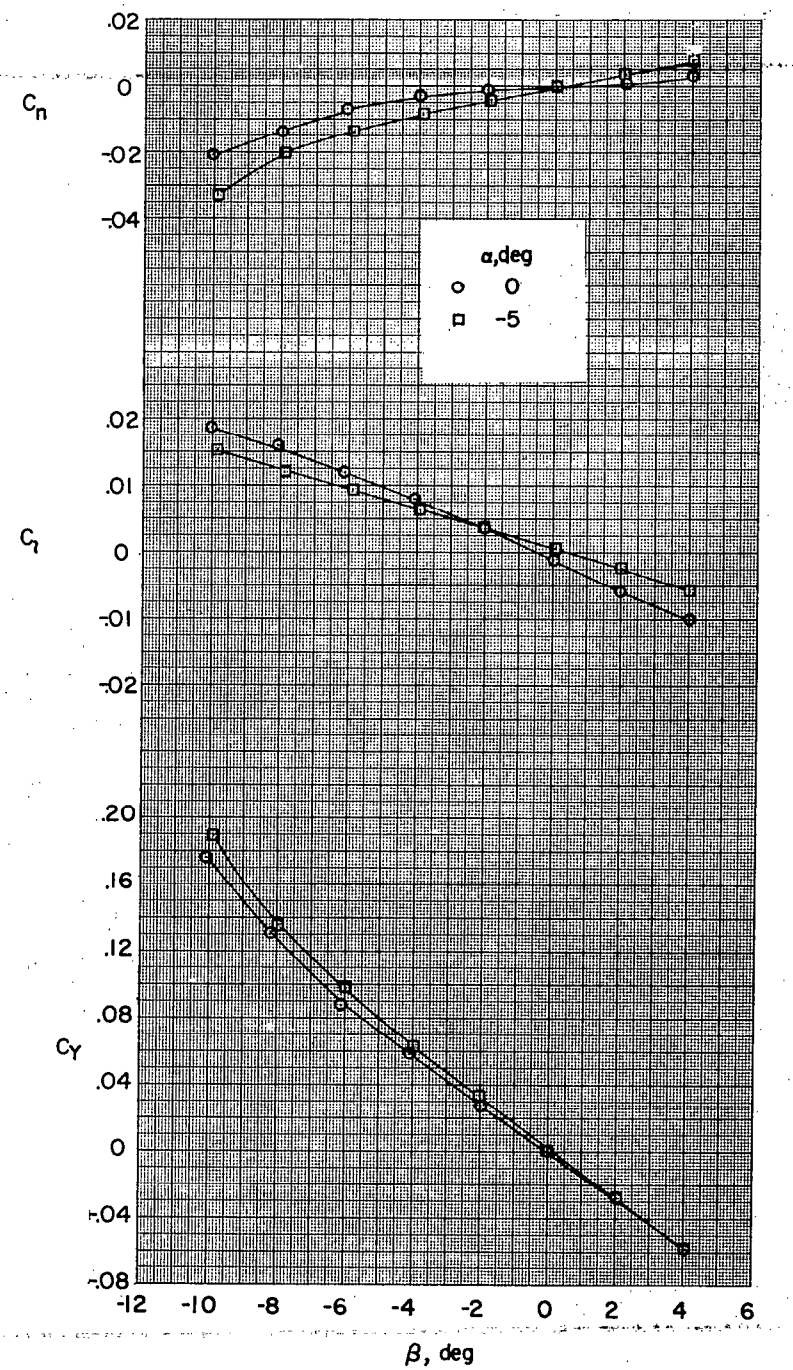

(a) M = 2.01; inlet open.

Figure 16.- Effect of angle of attack on aerodynamic characteristice in sideslip.

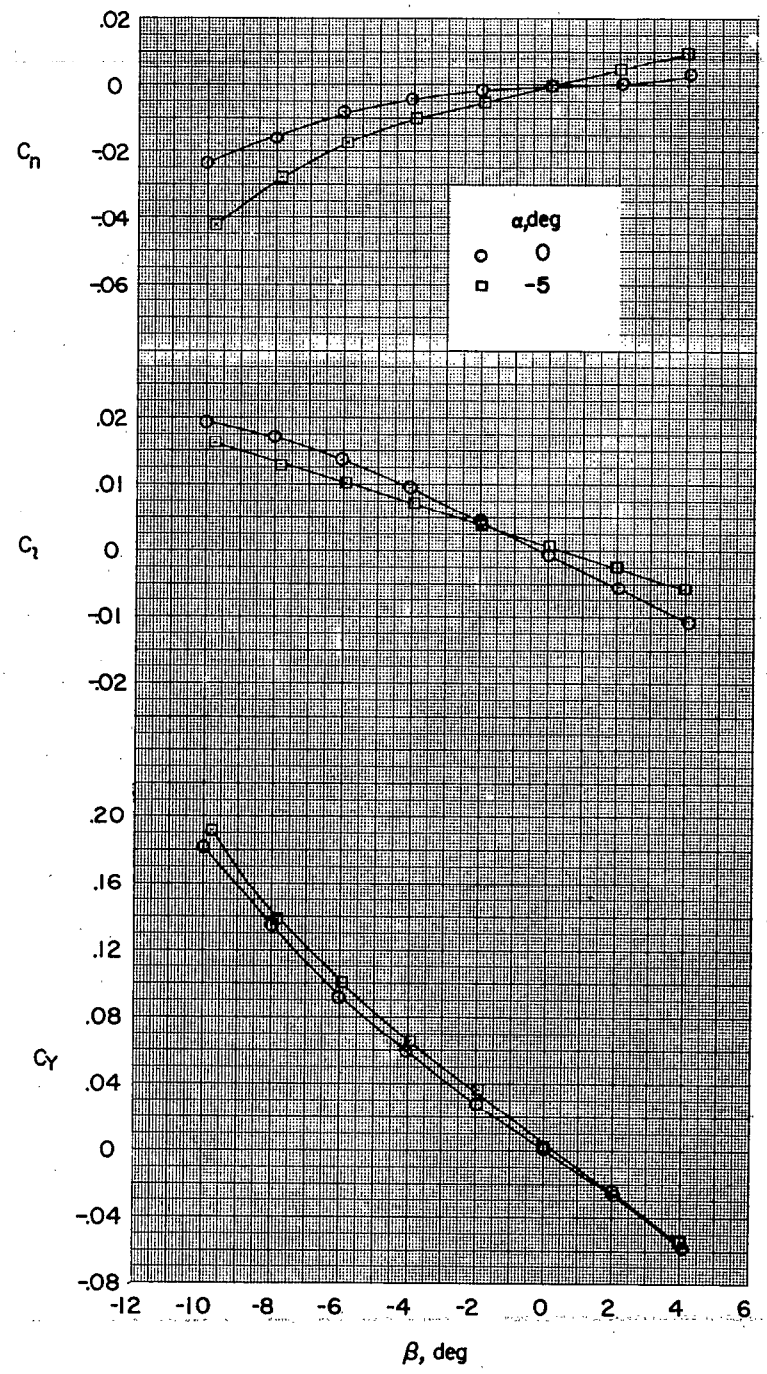

(b) M = 2.01; inlet faired closed.

Figure 16.- Continued.

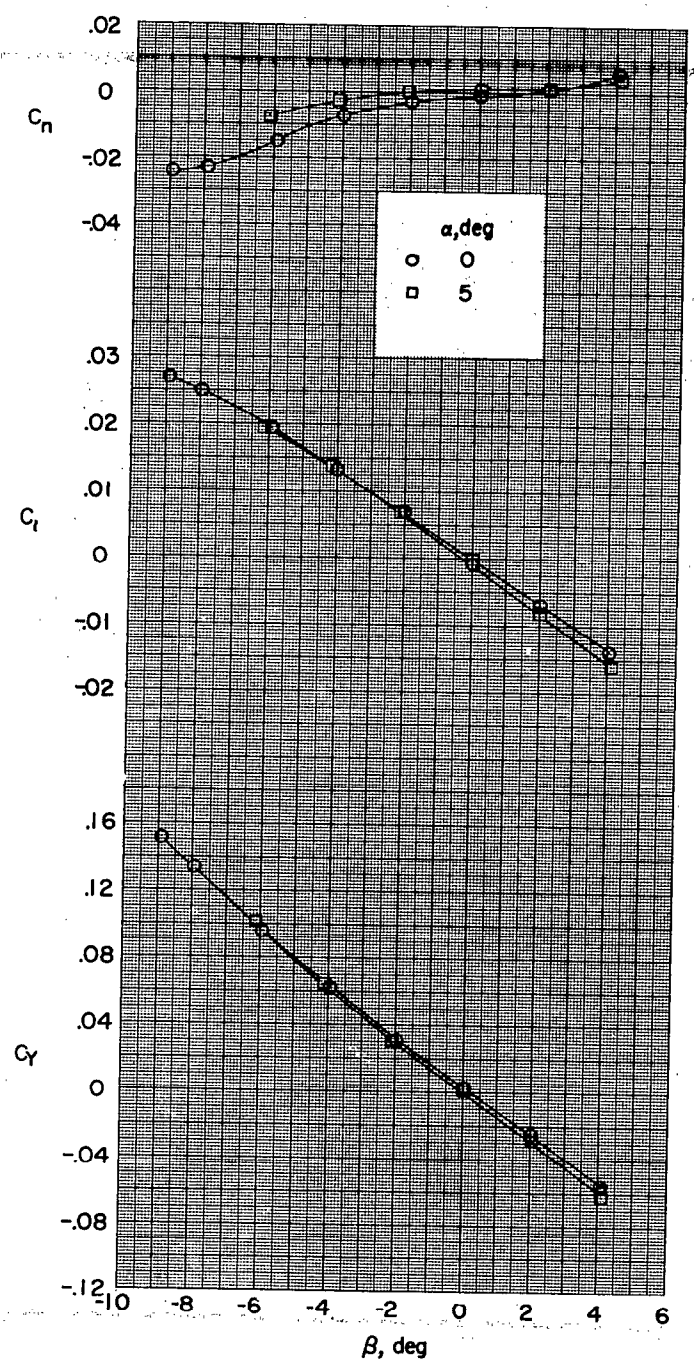

(d) M = 1.41; inlet open.

Figure 16.- Concluded.

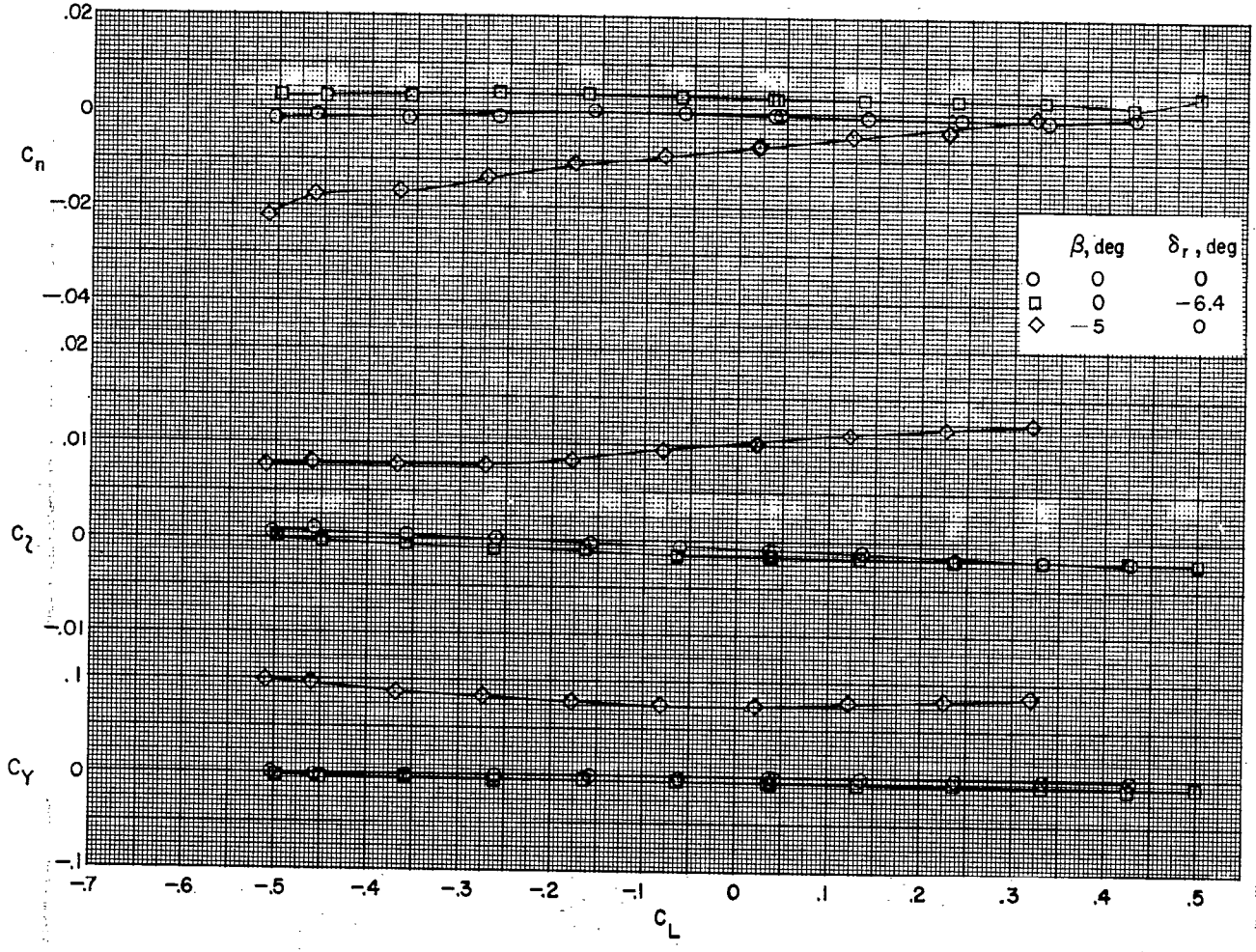

(a) M = 2.01.

Figure 17.- Variation of yawing-moment, rolling-moment, and side-force coefficients with lift coefficient.

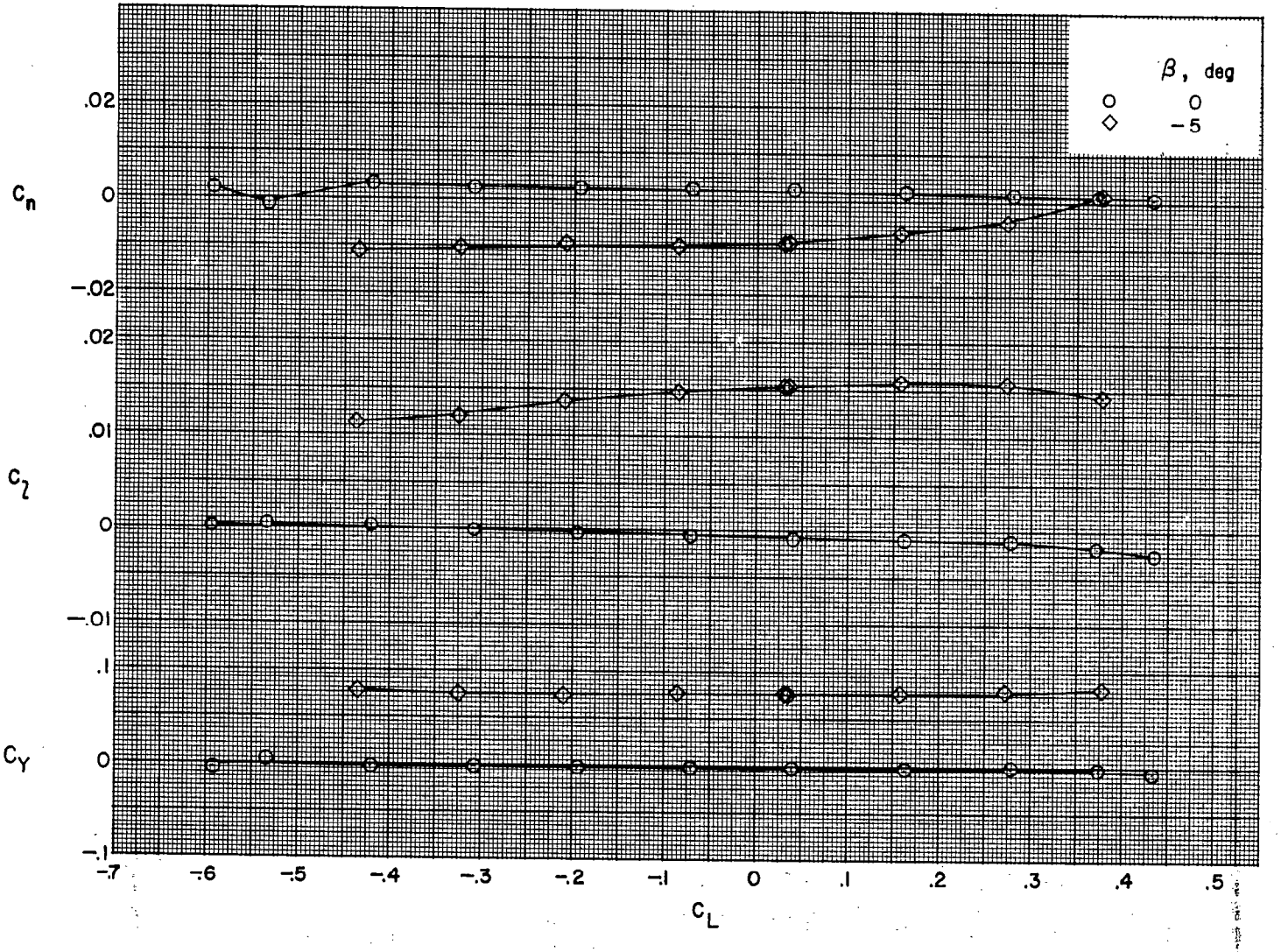

(b) M = 1.61; $\delta_r = 0^\circ$.

Figure 17.- Continued.

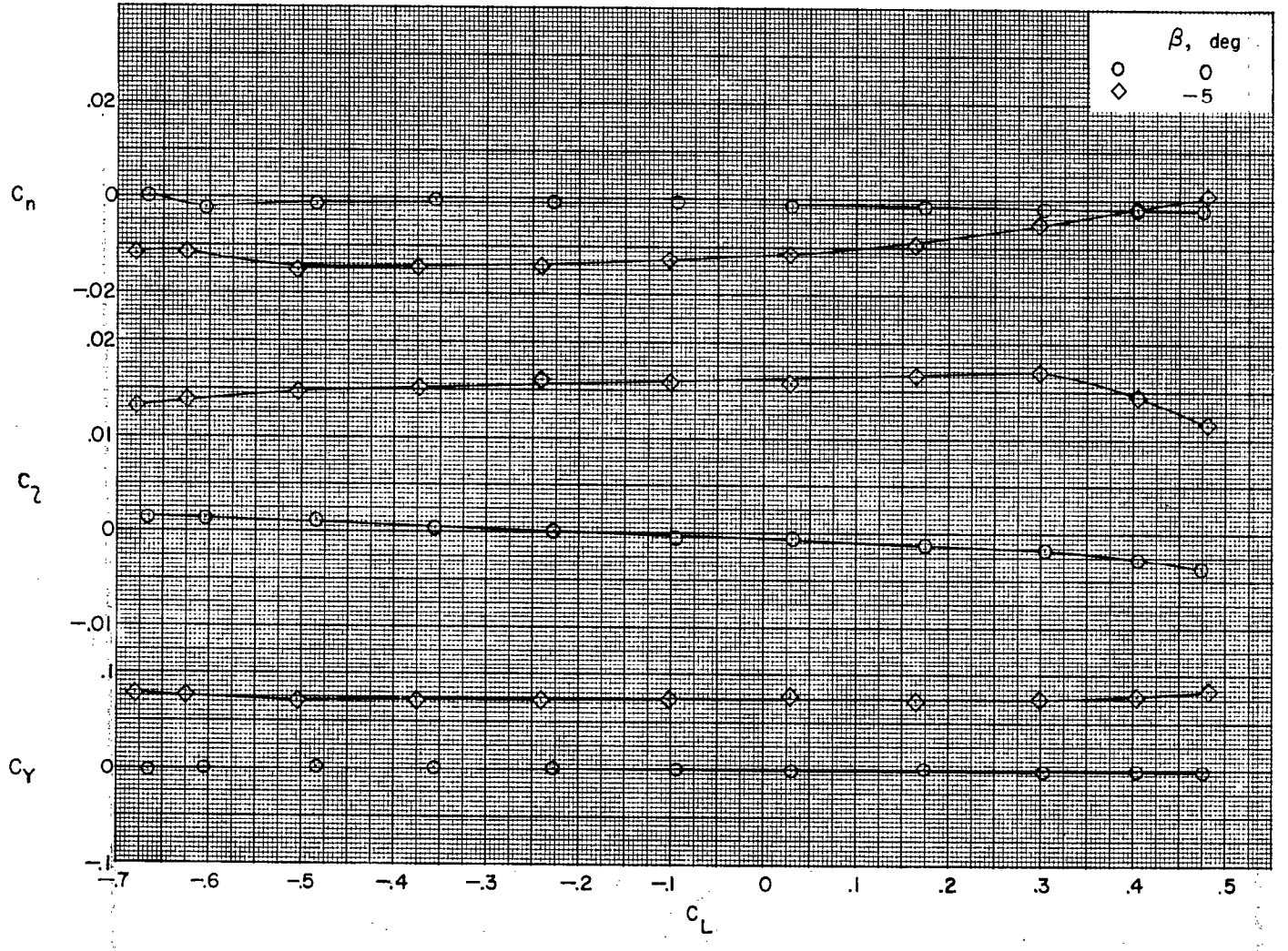

(c) M = 1.41; $\delta_r = 0^\circ$.

Figure 17.- Concluded.

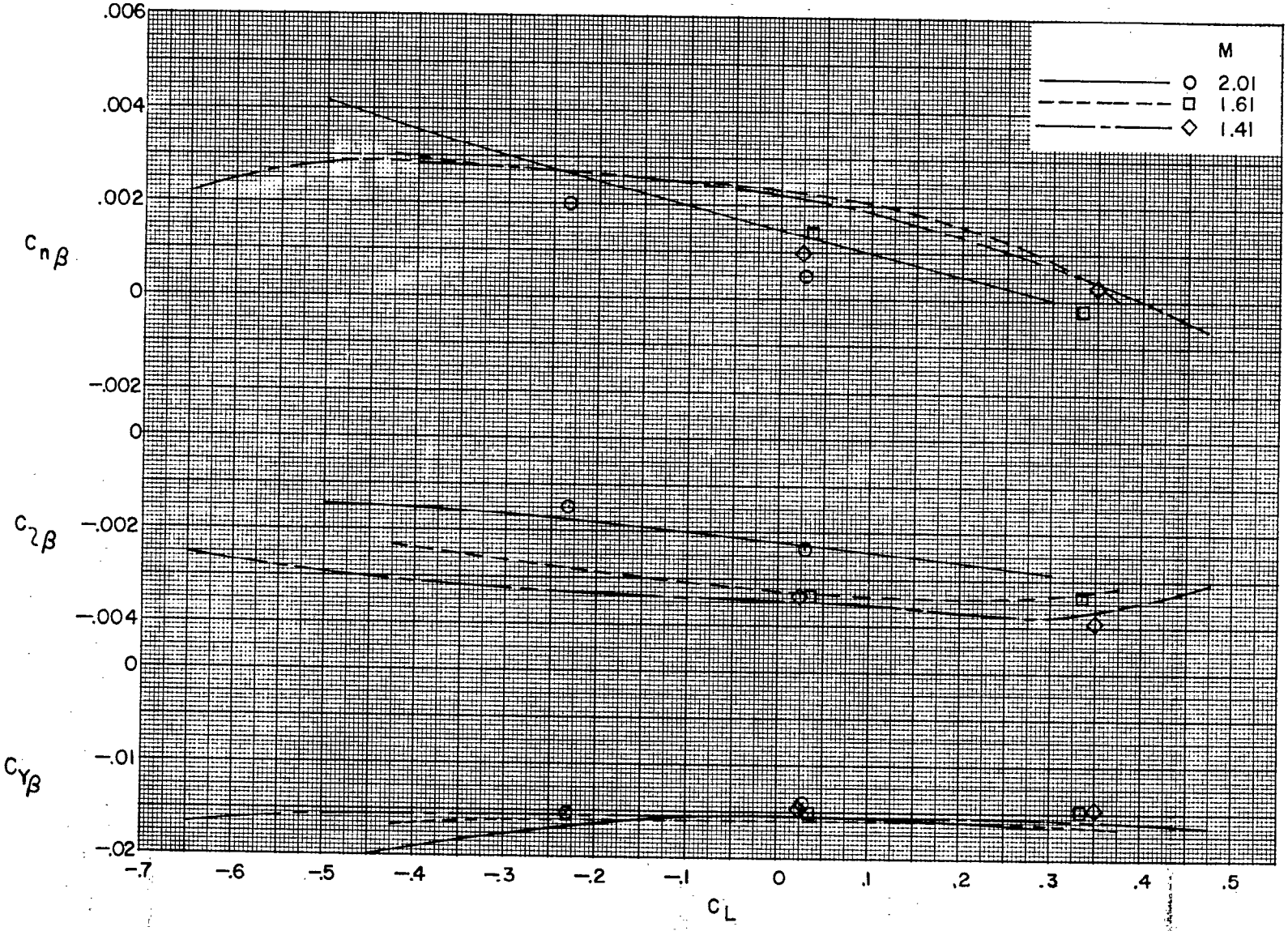

Figure 18.- Variation of sideslip derivatives with lift coefficient. Symbols indicate slopes at $\beta \approx 0^{\circ}$ of results presented in figure 16.

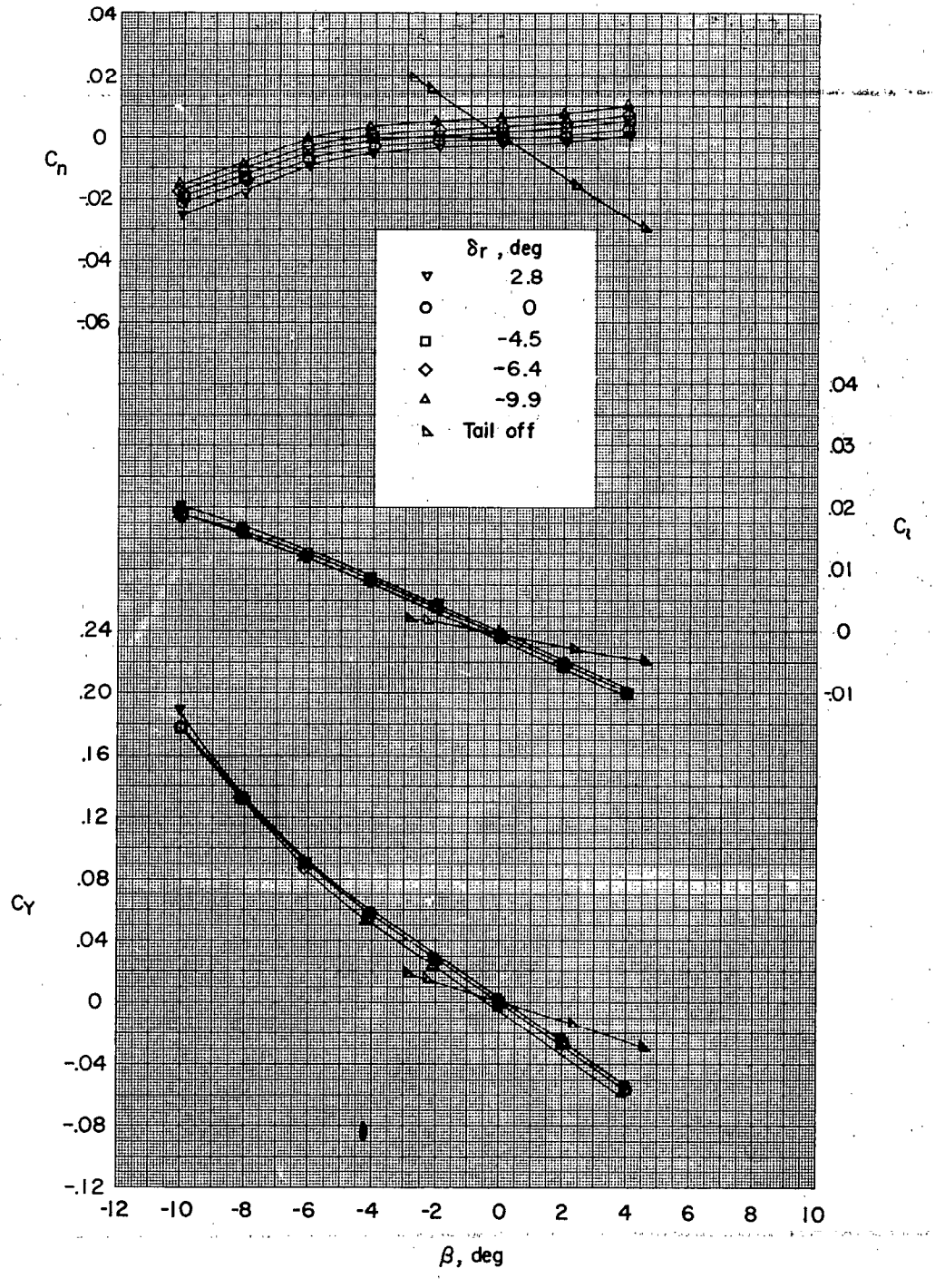

(a) $M = 2.01$; $\alpha = 0^\circ$.

Figure 19.- Effect of rudder deflection on the aerodynamic characteristics in sideslip.

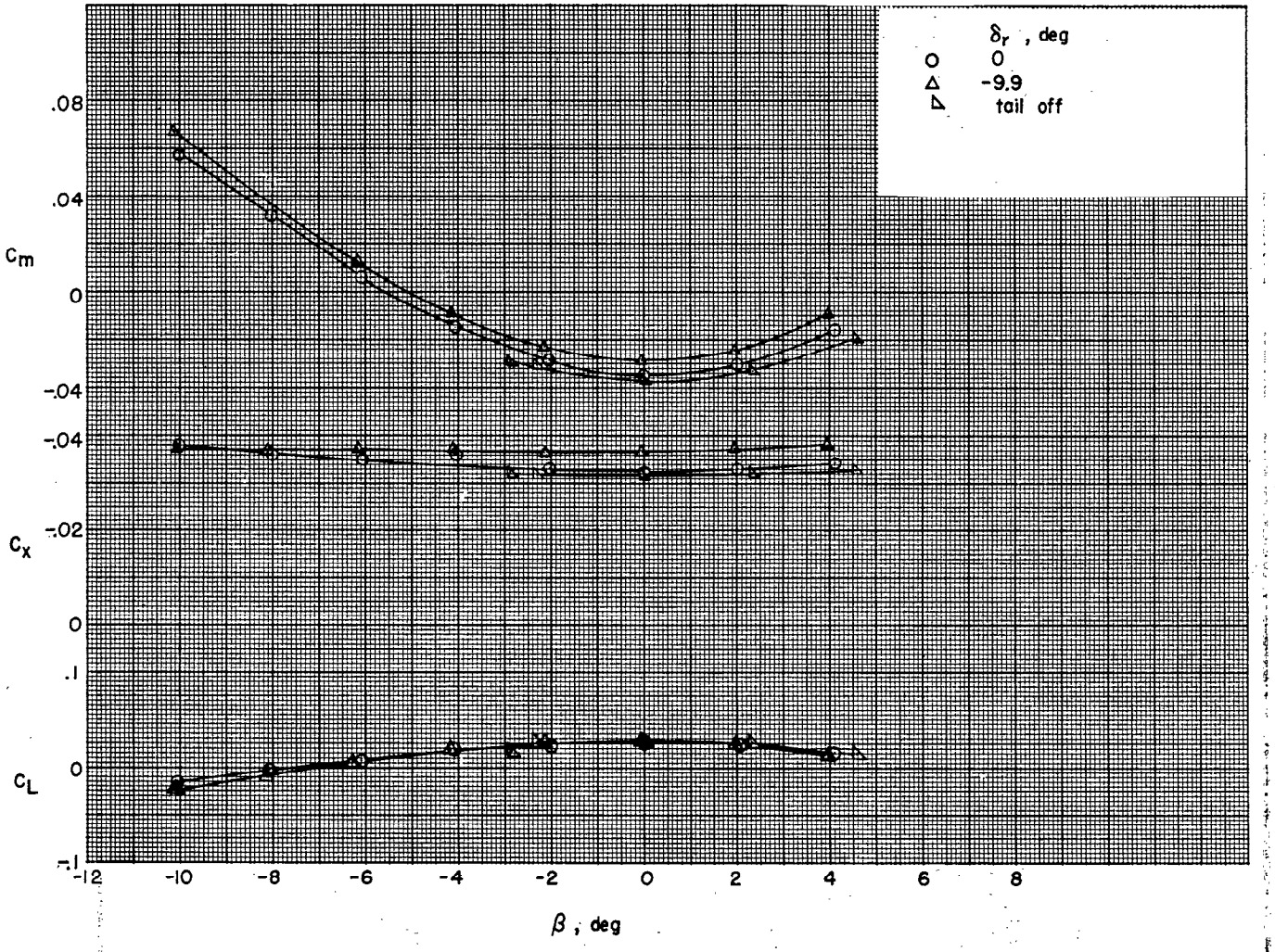

(a) Concluded.

Figure 19.- Continued.

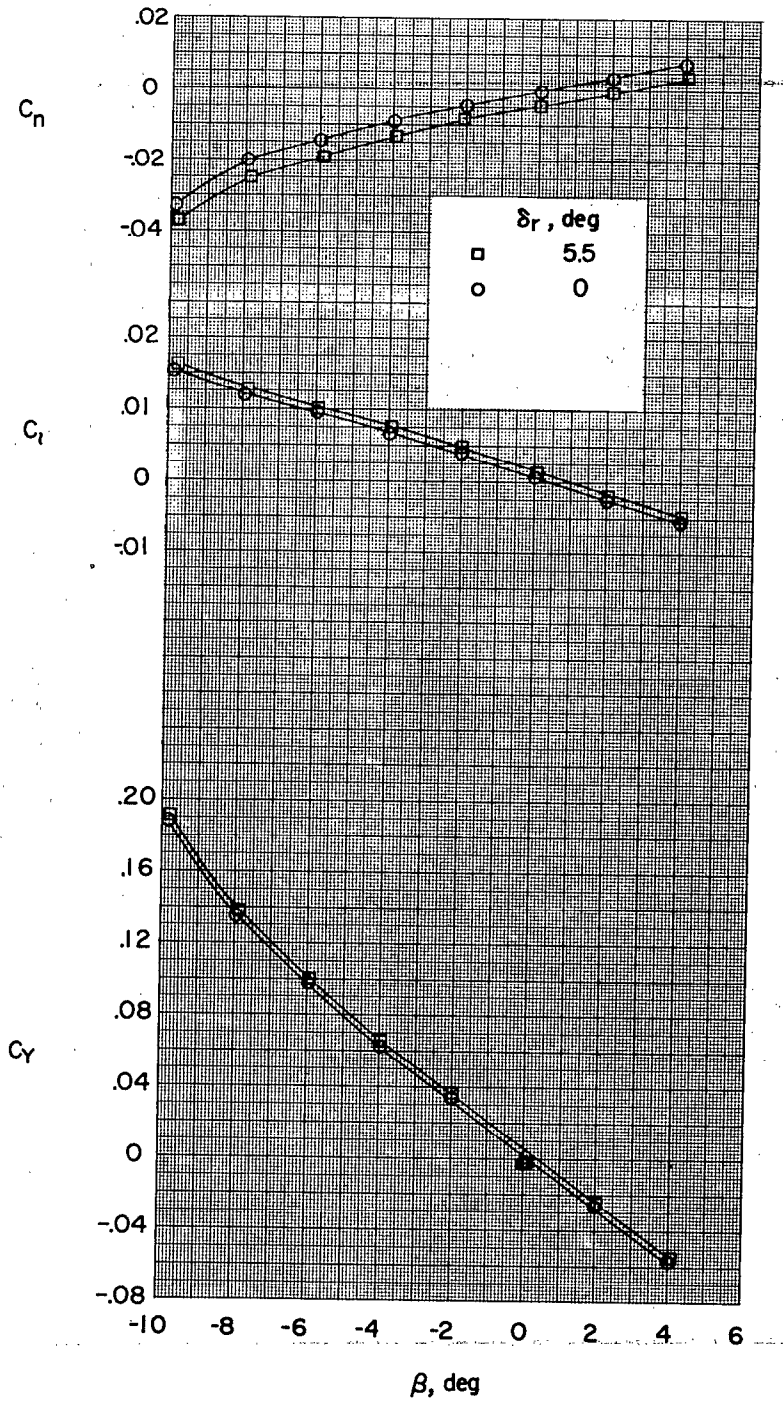

(b) M = 2.01; $\alpha = -5^\circ$.

Figure 19.- Continued.

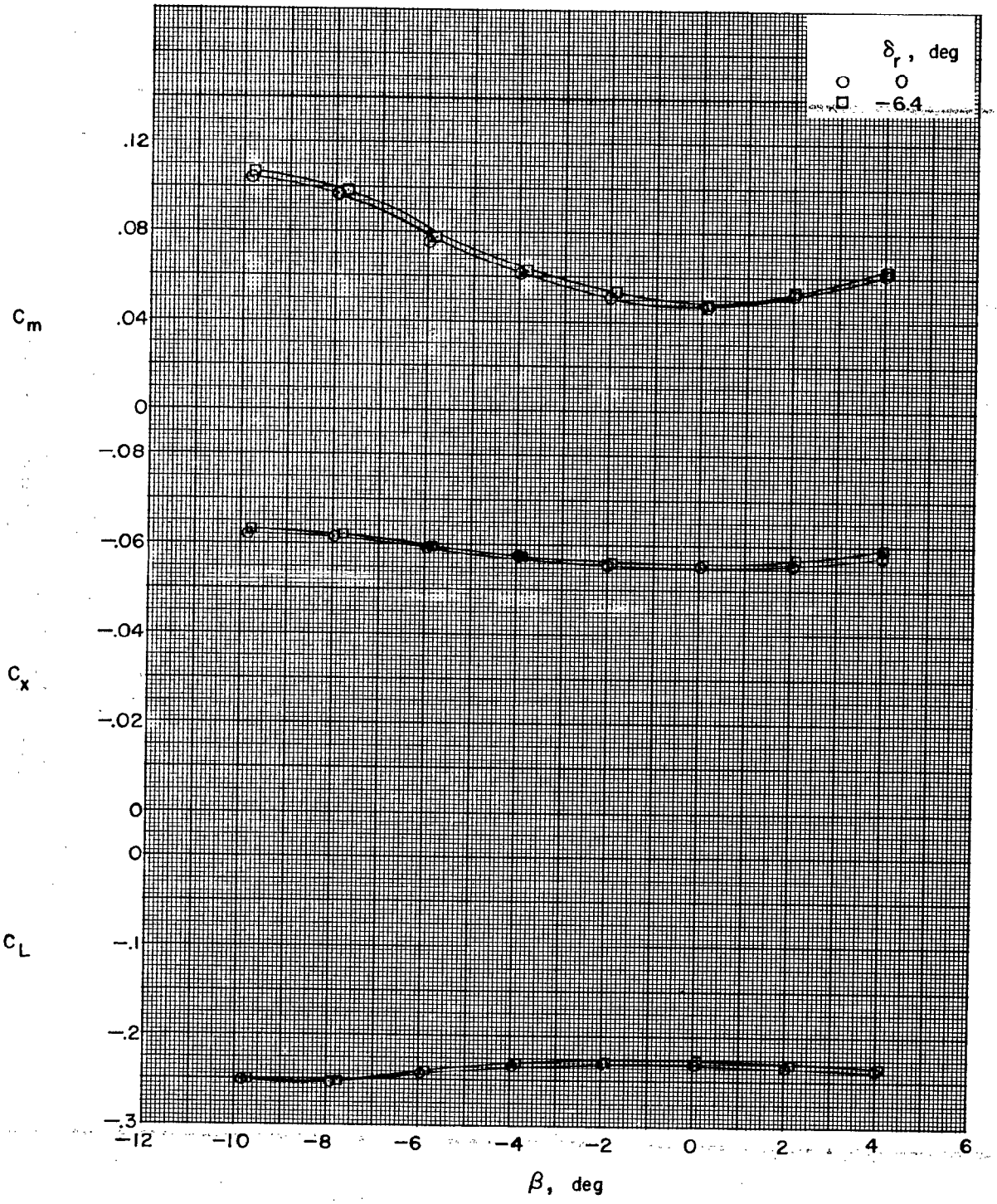

(b) Concluded.

Figure 19.- Continued.

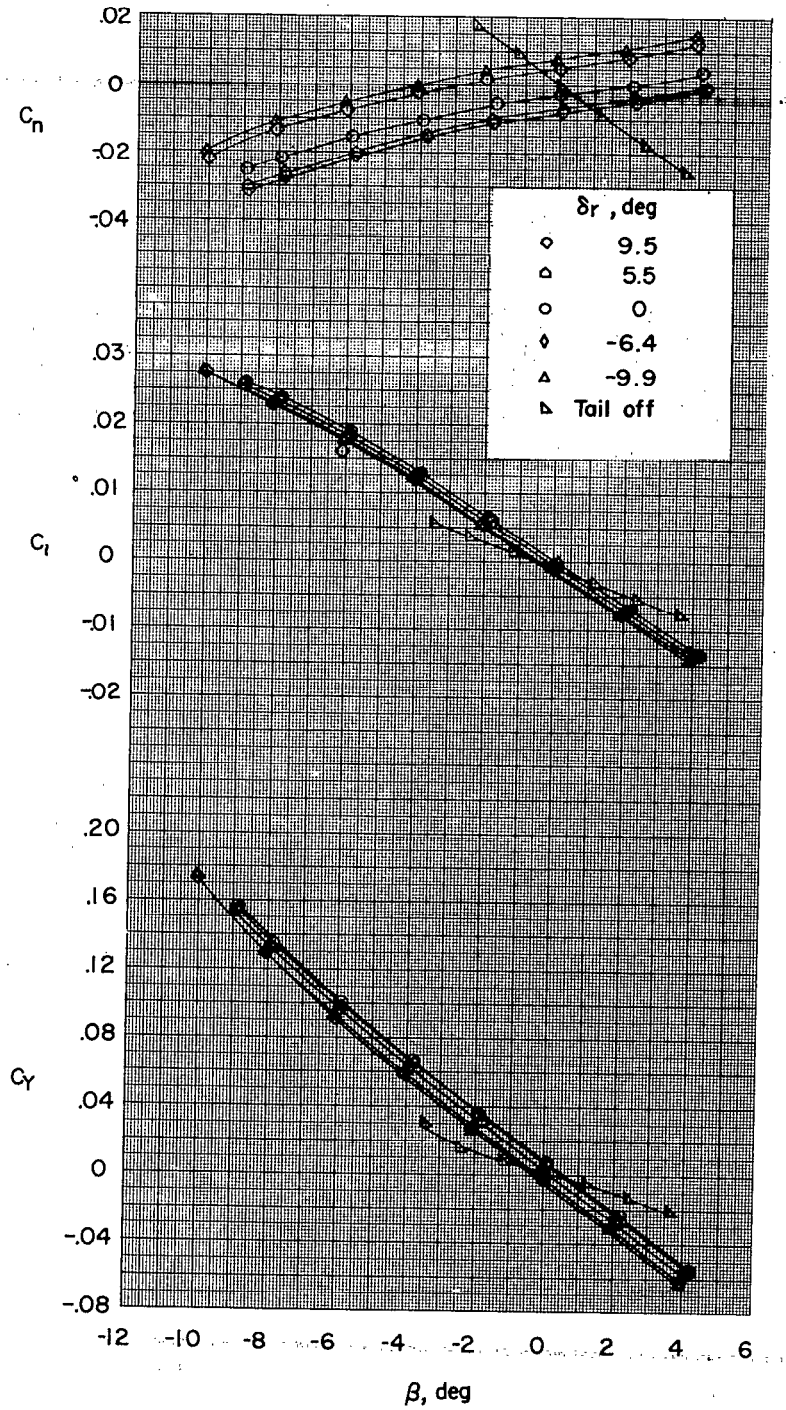

(c) M = 1.61; $\alpha = 0^\circ$.

Figure 19.- Continued.

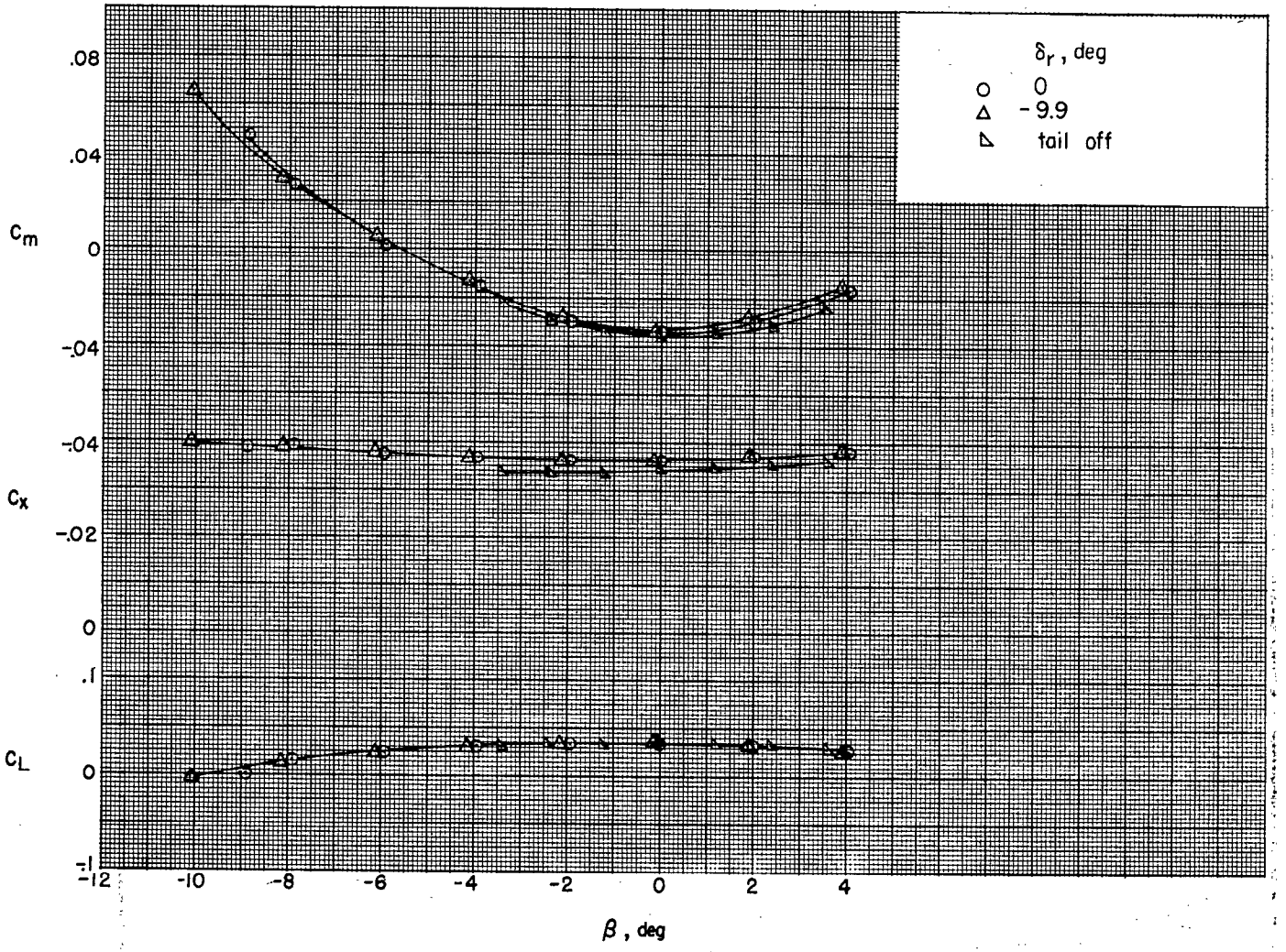

(c) Concluded.

Figure 19.- Continued.

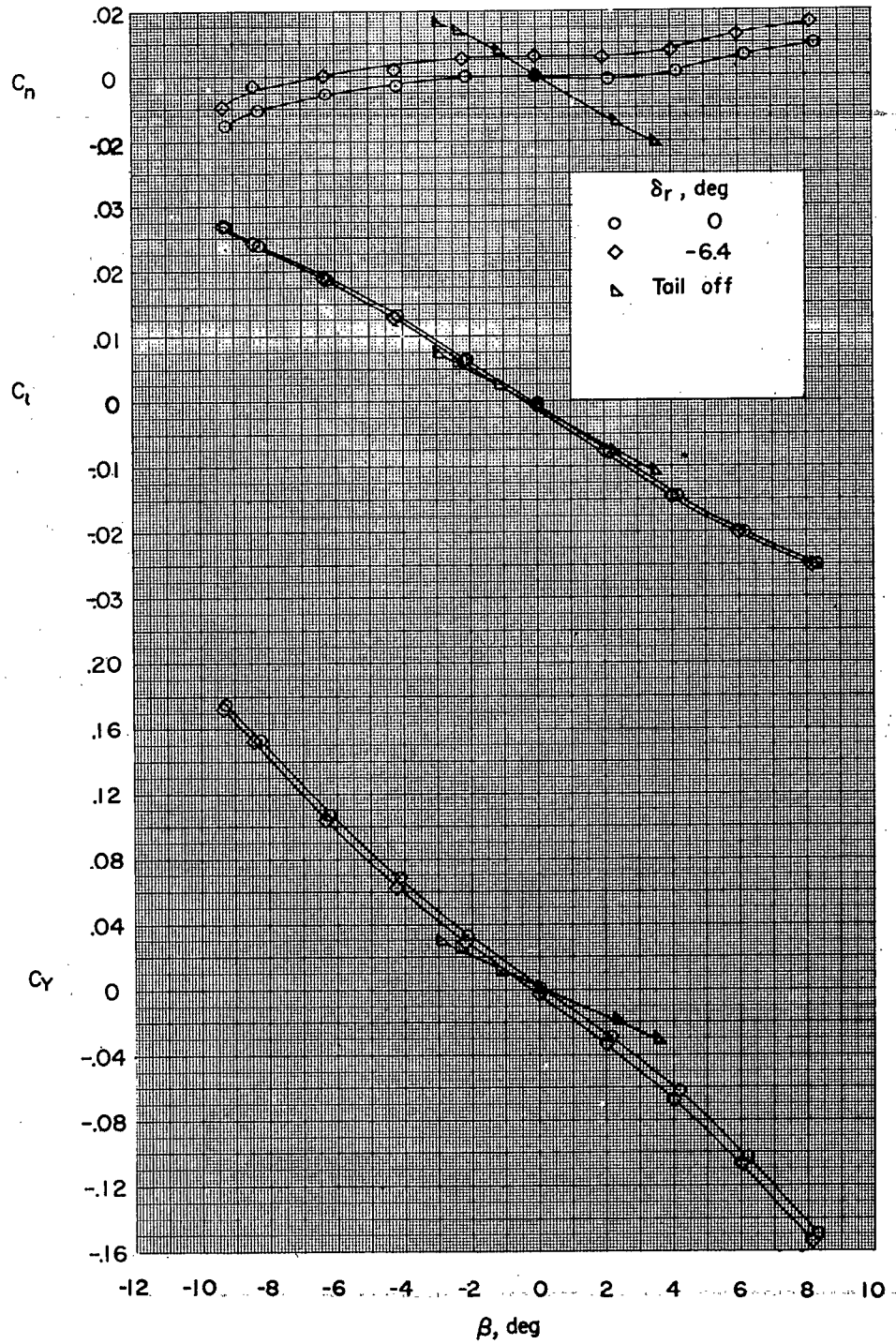

(d) M = 1.61; $\alpha = 5^\circ$.

Figure 19.- Continued.

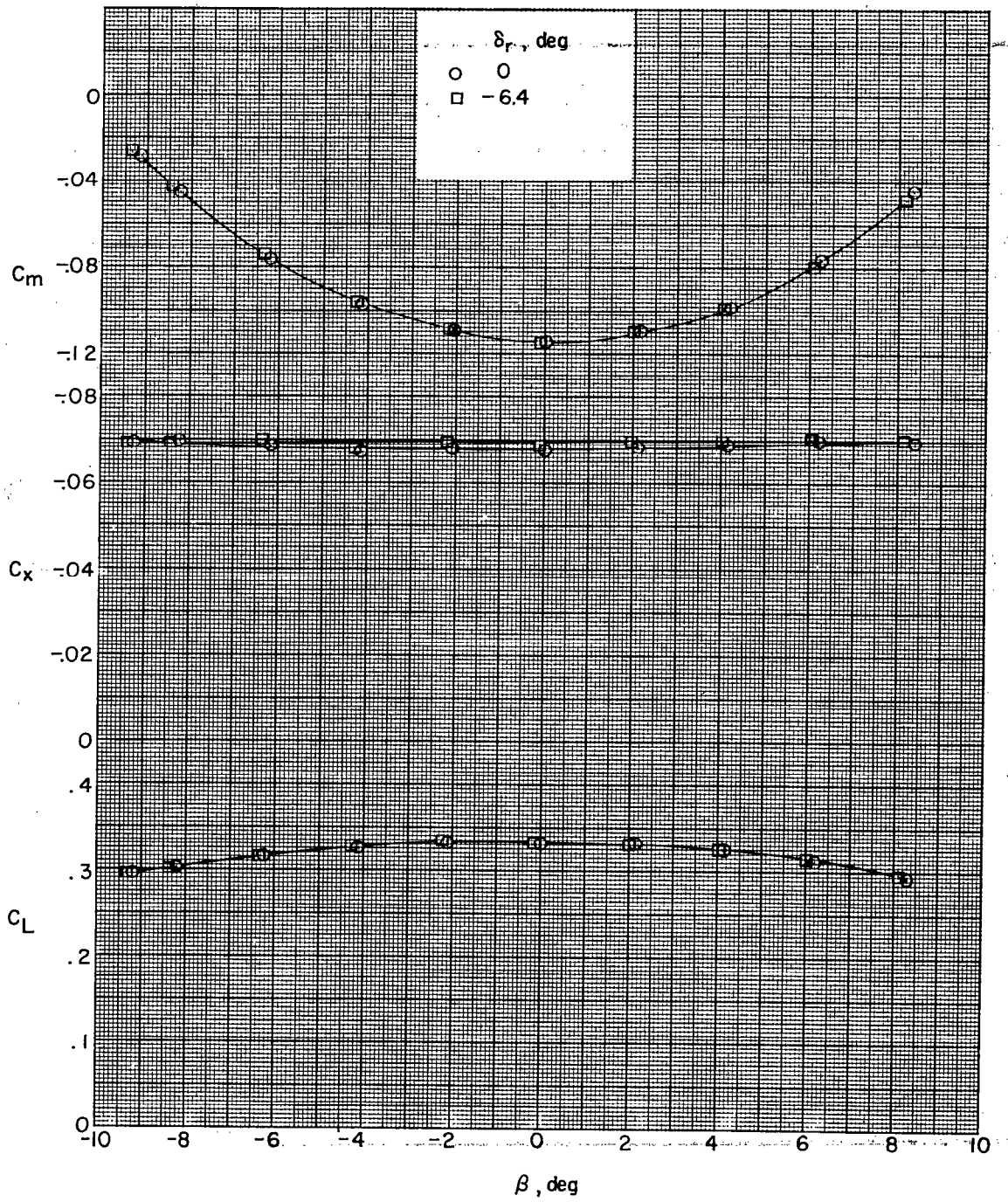

(d) Concluded.

Figure 19.- Continued.

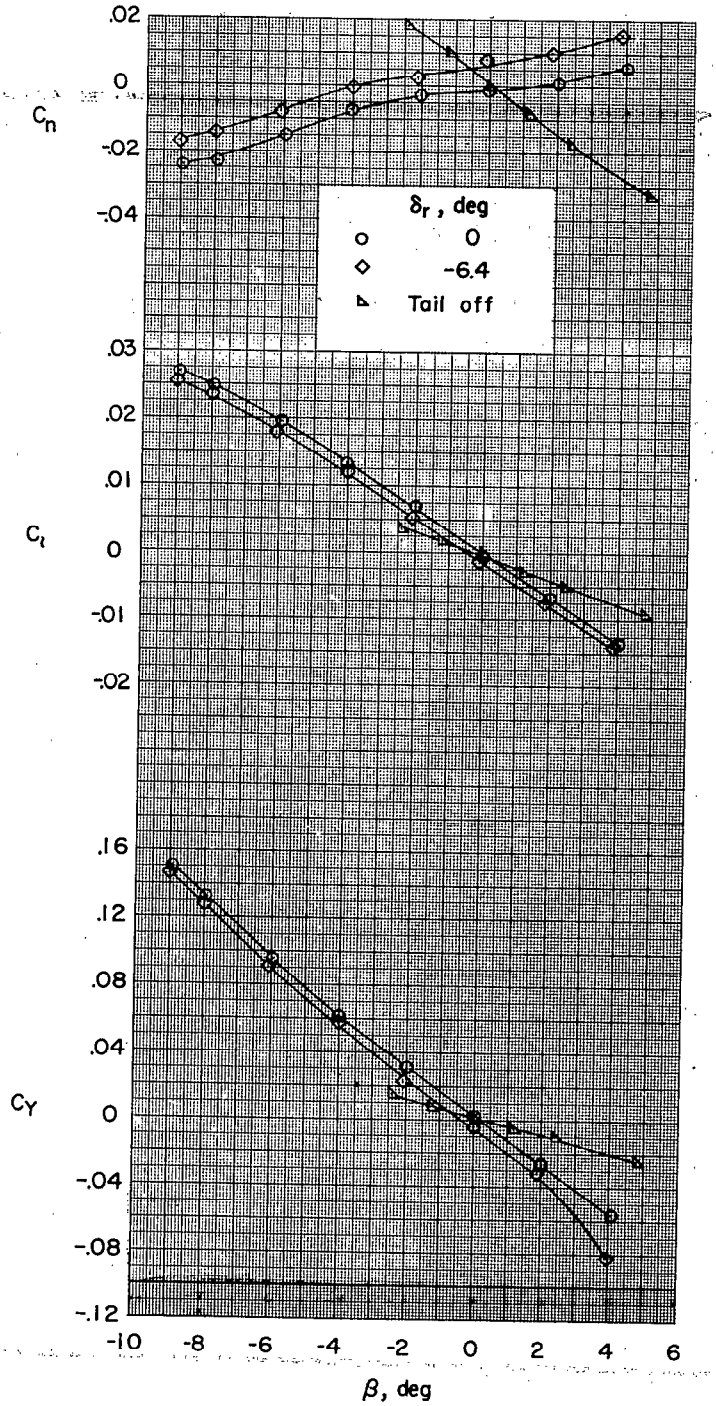

(e) M = 1.41; $\alpha = 0^{\circ}$.

Figure 19.- Continued.

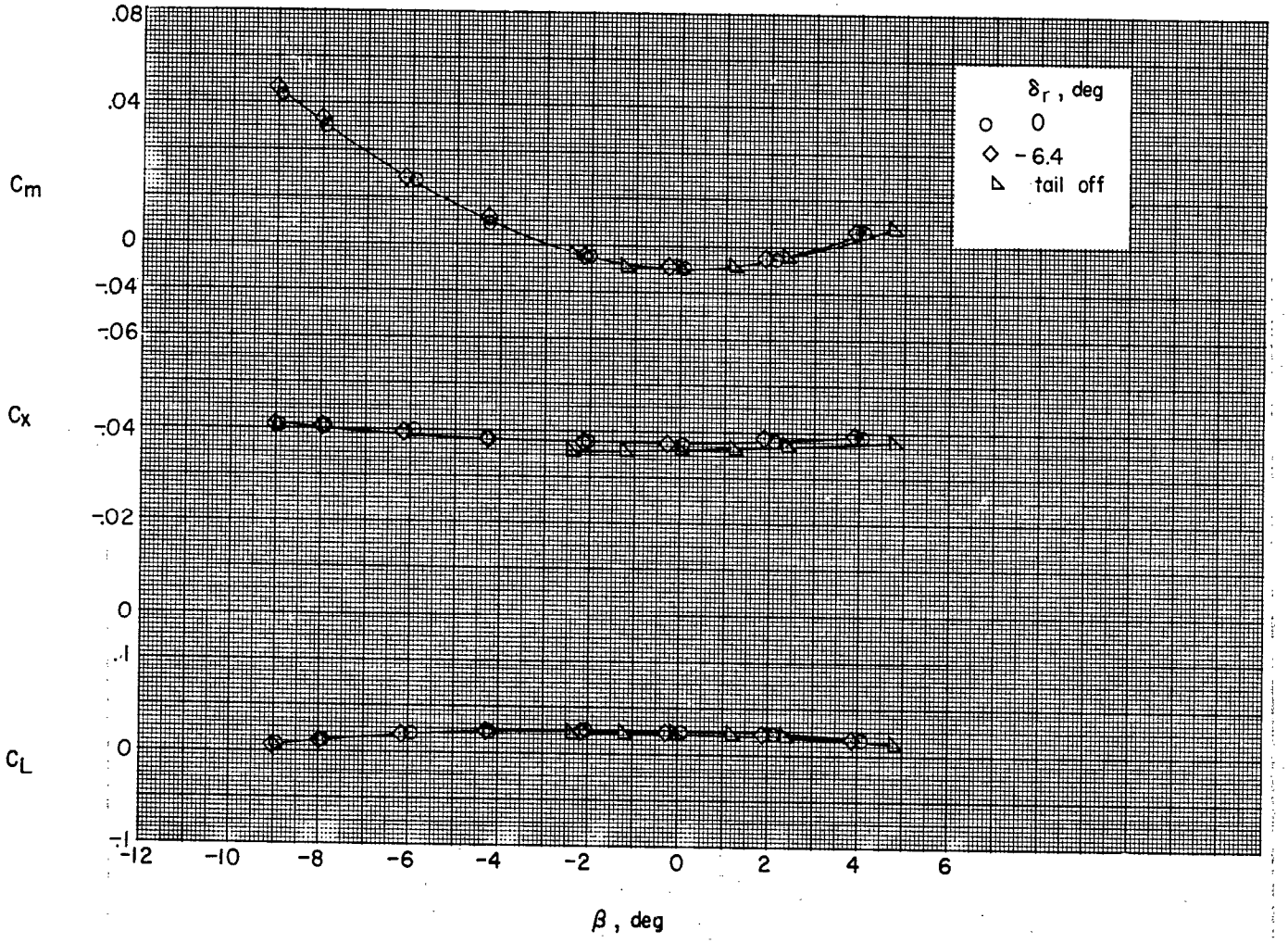

(e) Concluded.

Figure 19.- Concluded.

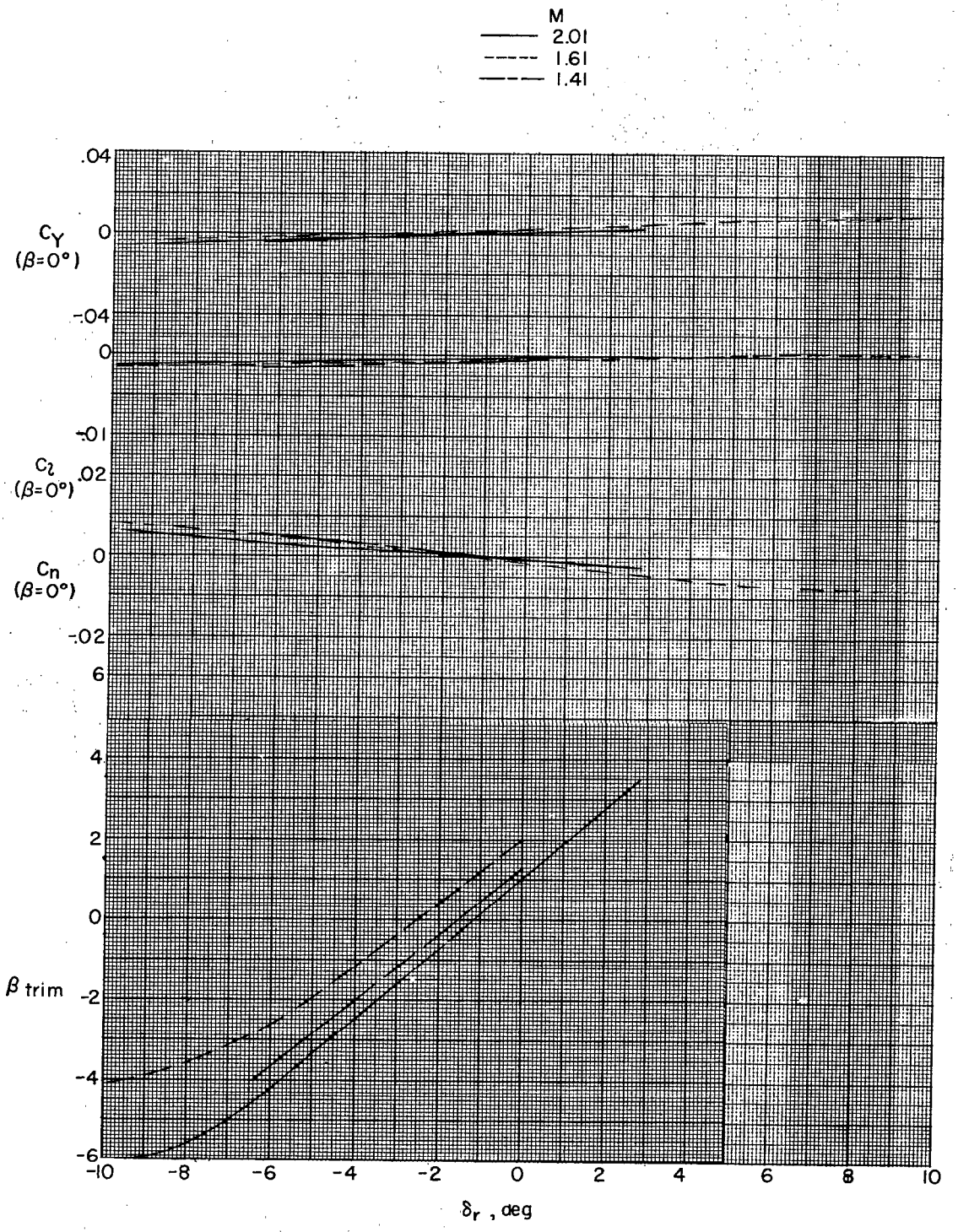

Figure 20.- Directional control characteristics. $\alpha \approx 0^{\circ}$.

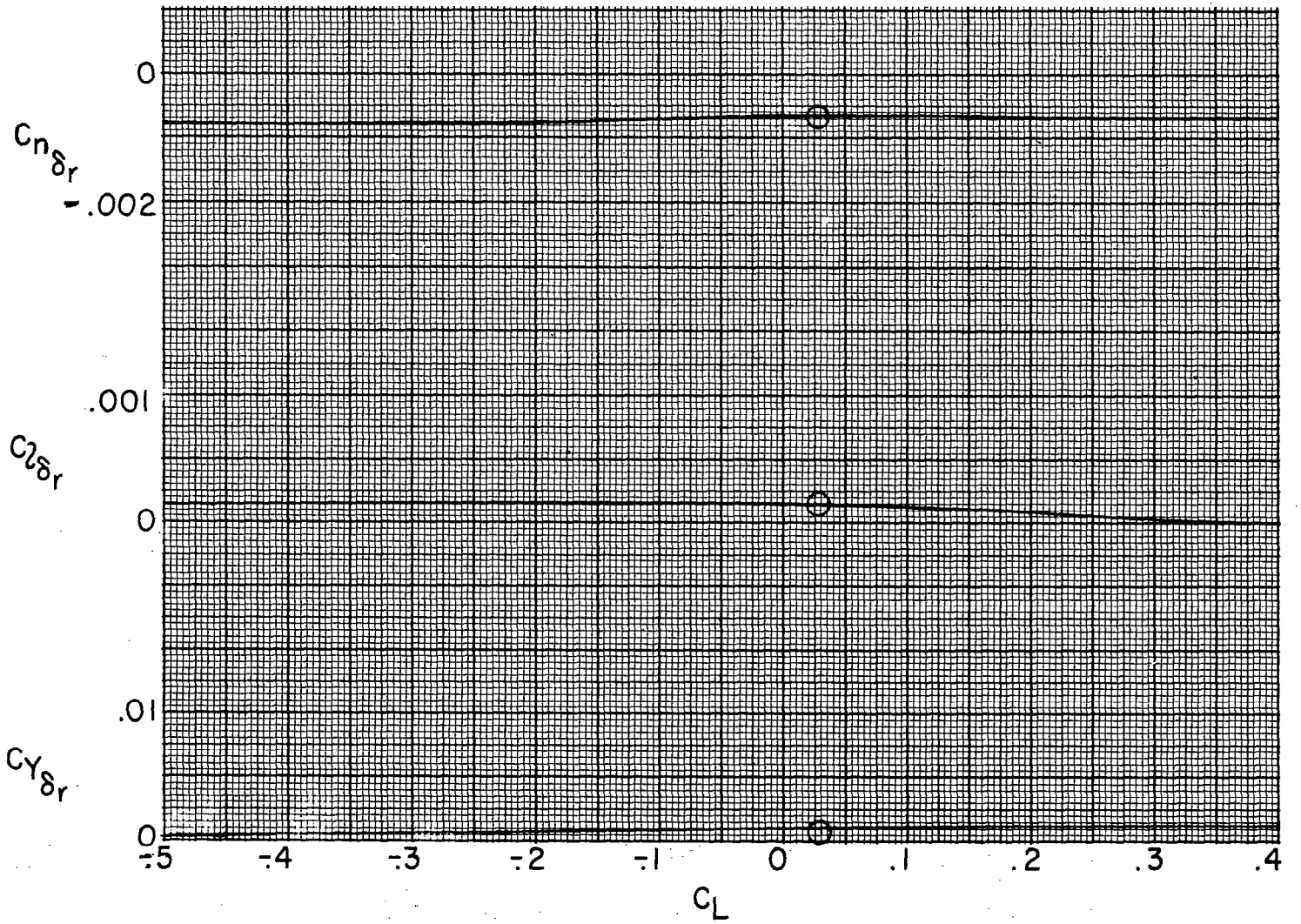

Figure 21.- Variation of rudder characteristics with lift coefficient M = 2.01; $\beta = 0^\circ$. Symbols indicate slopes obtained from results presented in figure 20.

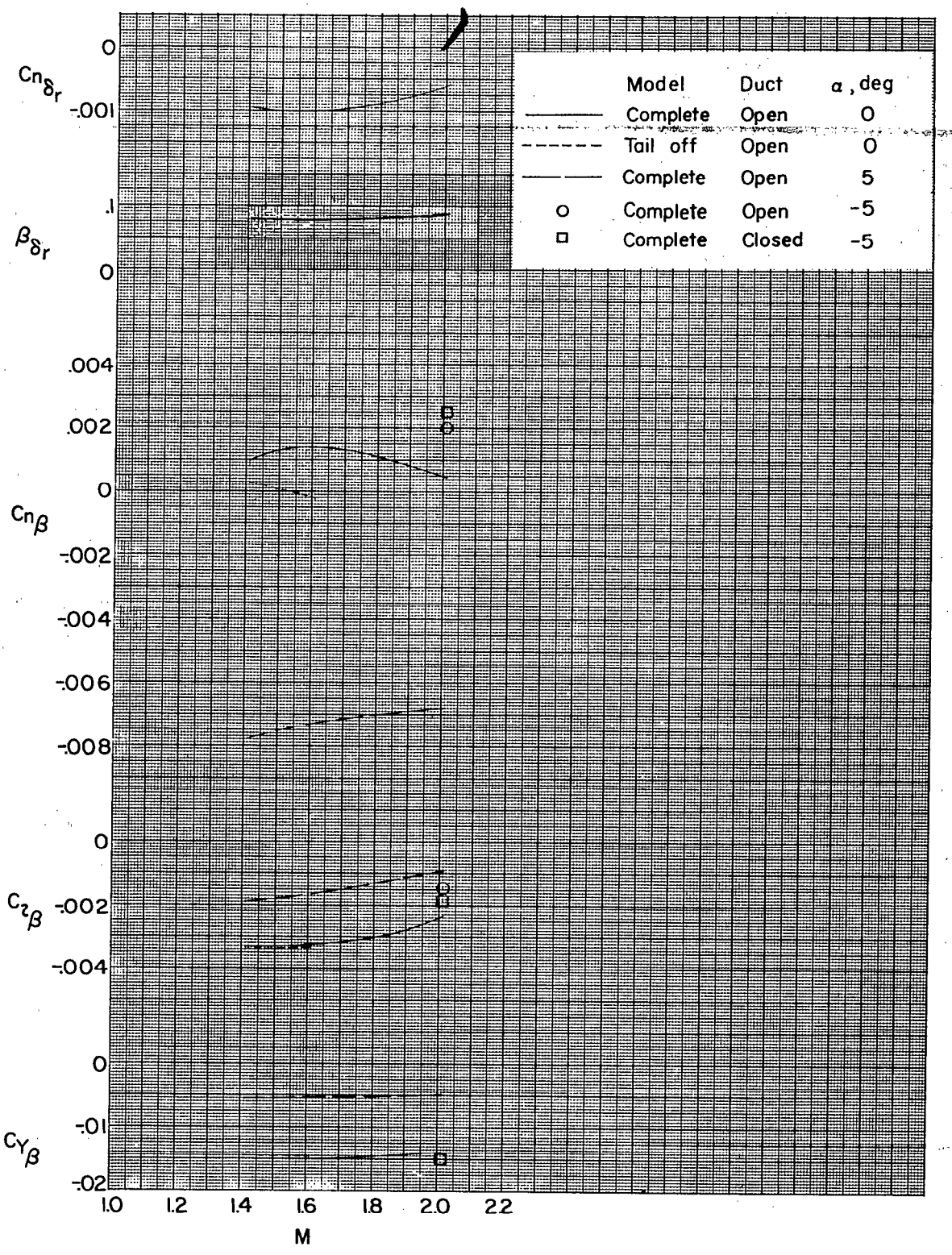

Figure 22.- Summary of directional stability and control characteristics.

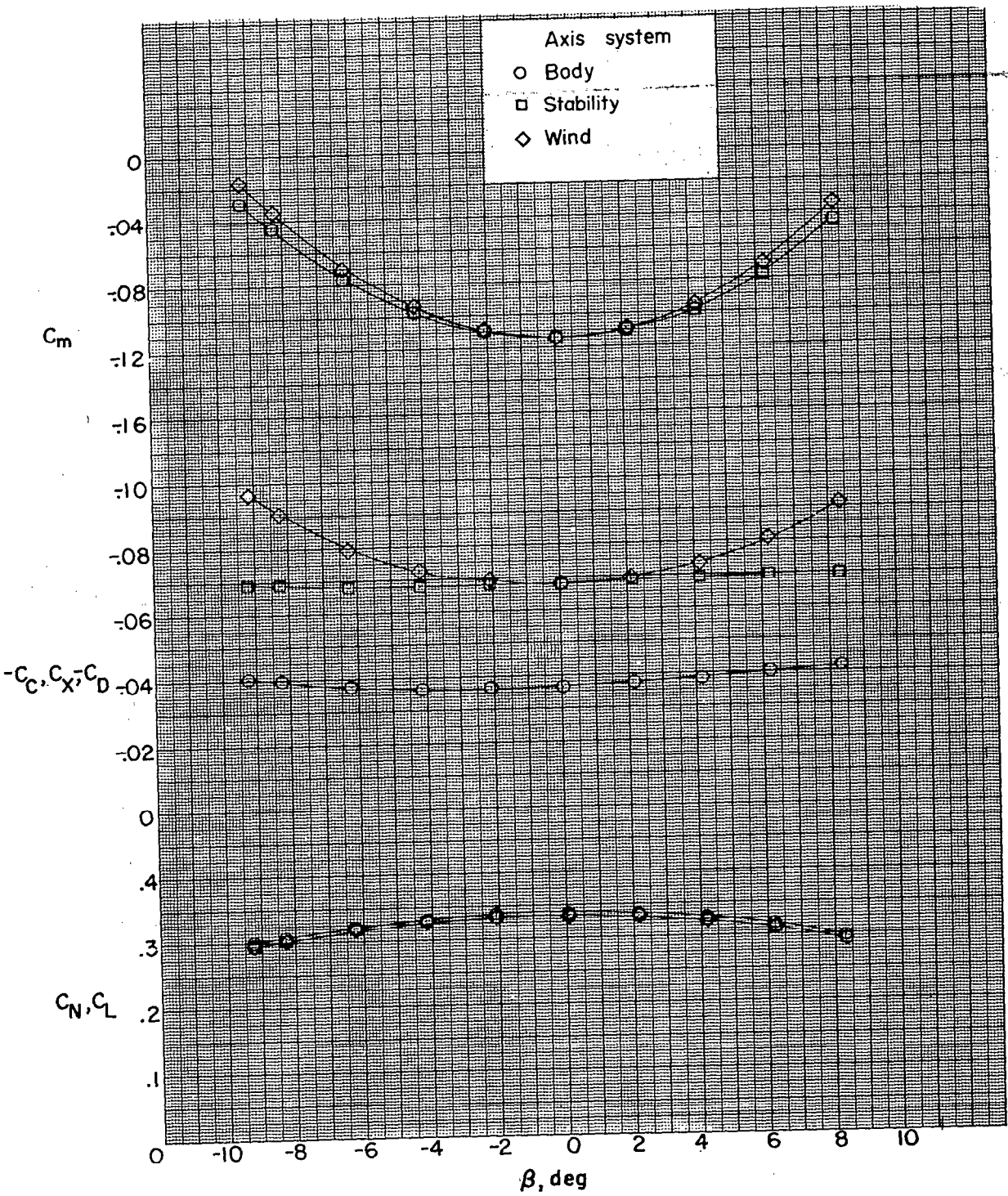

Figure 23.- Aerodynamic characteristics in sideslip for various axis systems. $\alpha \approx 5^{\circ}$; M = 1.61.

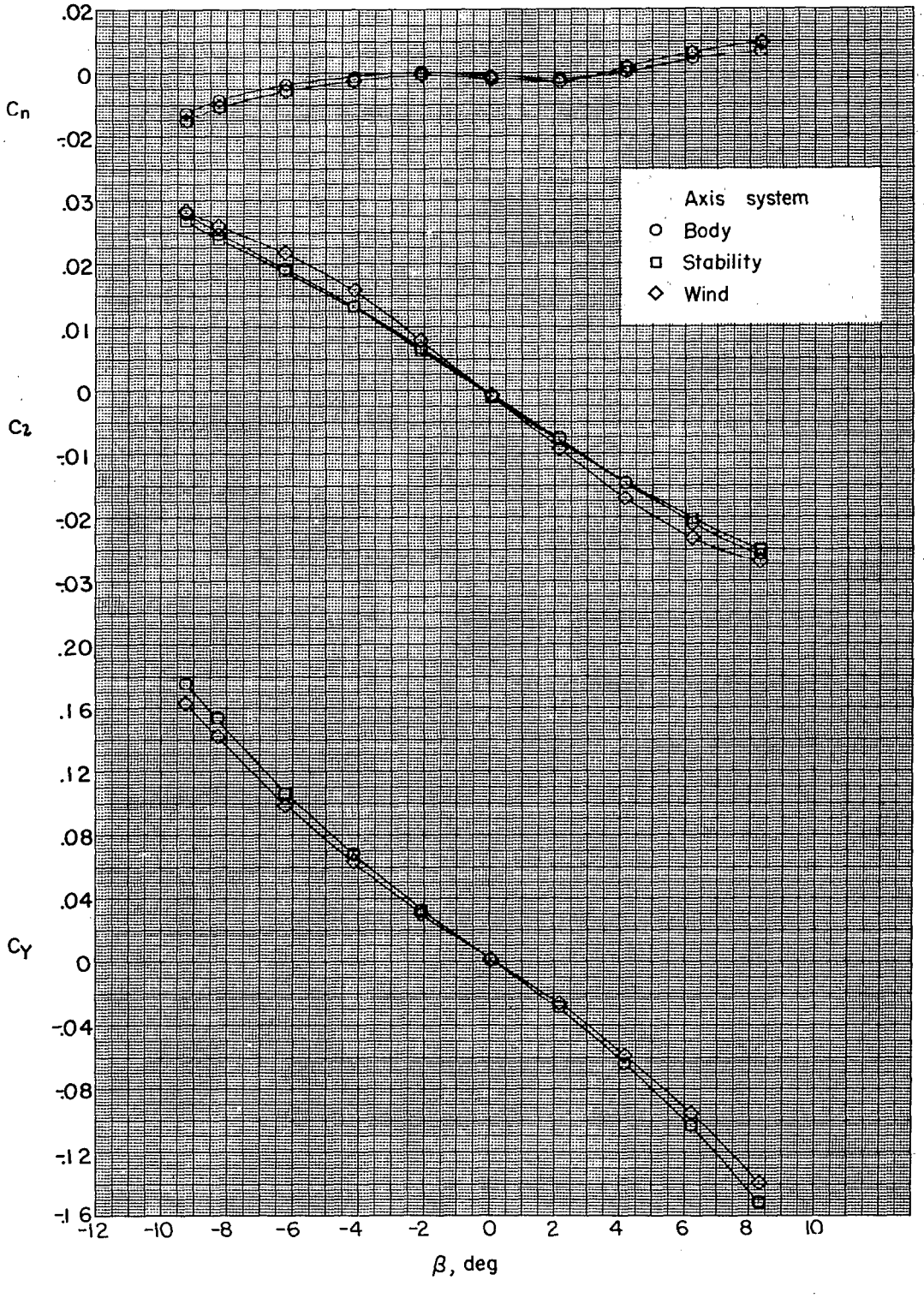

Figure 23.- Concluded.

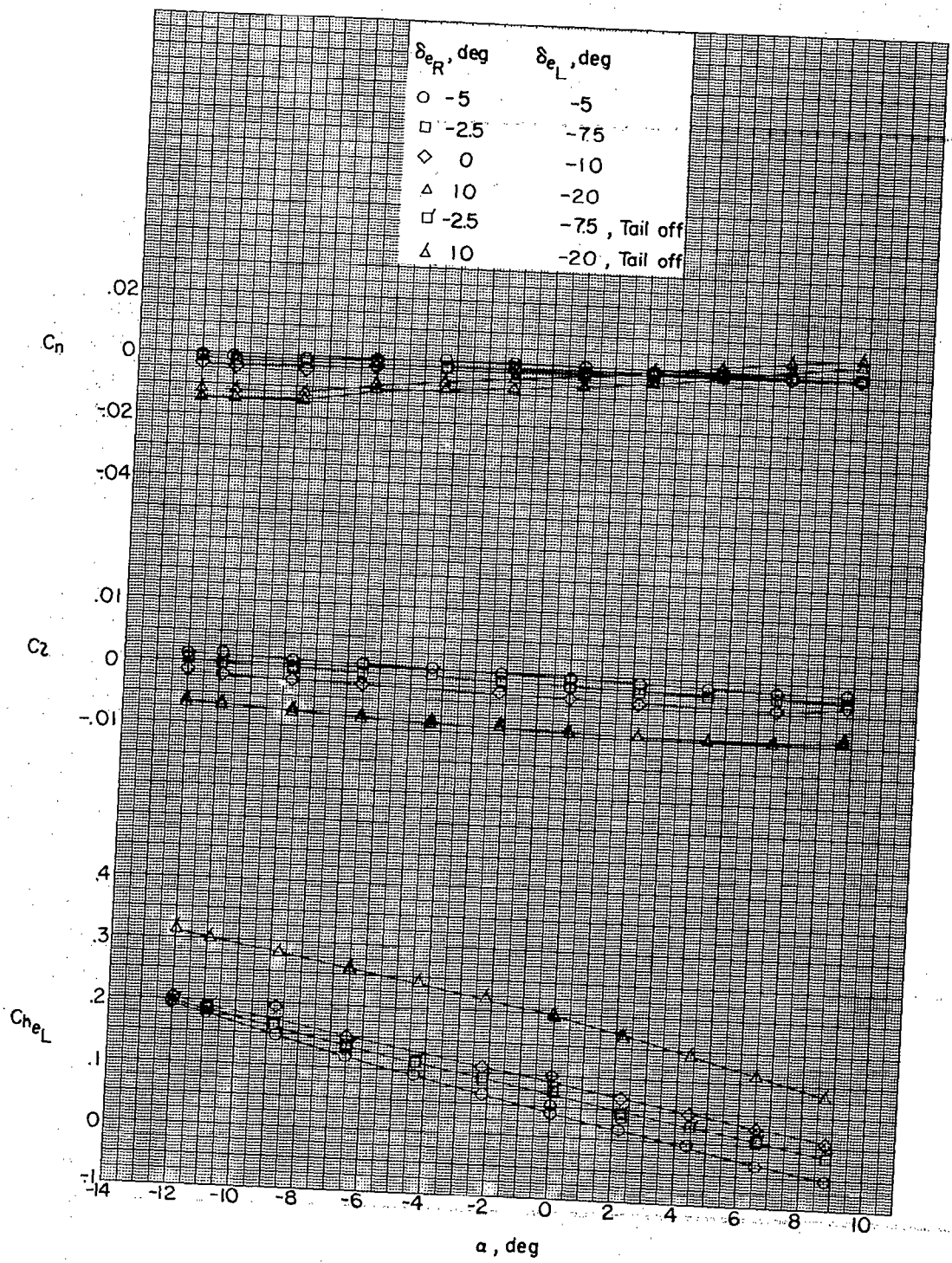

(a) M = 2.01.

Figure 24.- Lateral control characteristics.

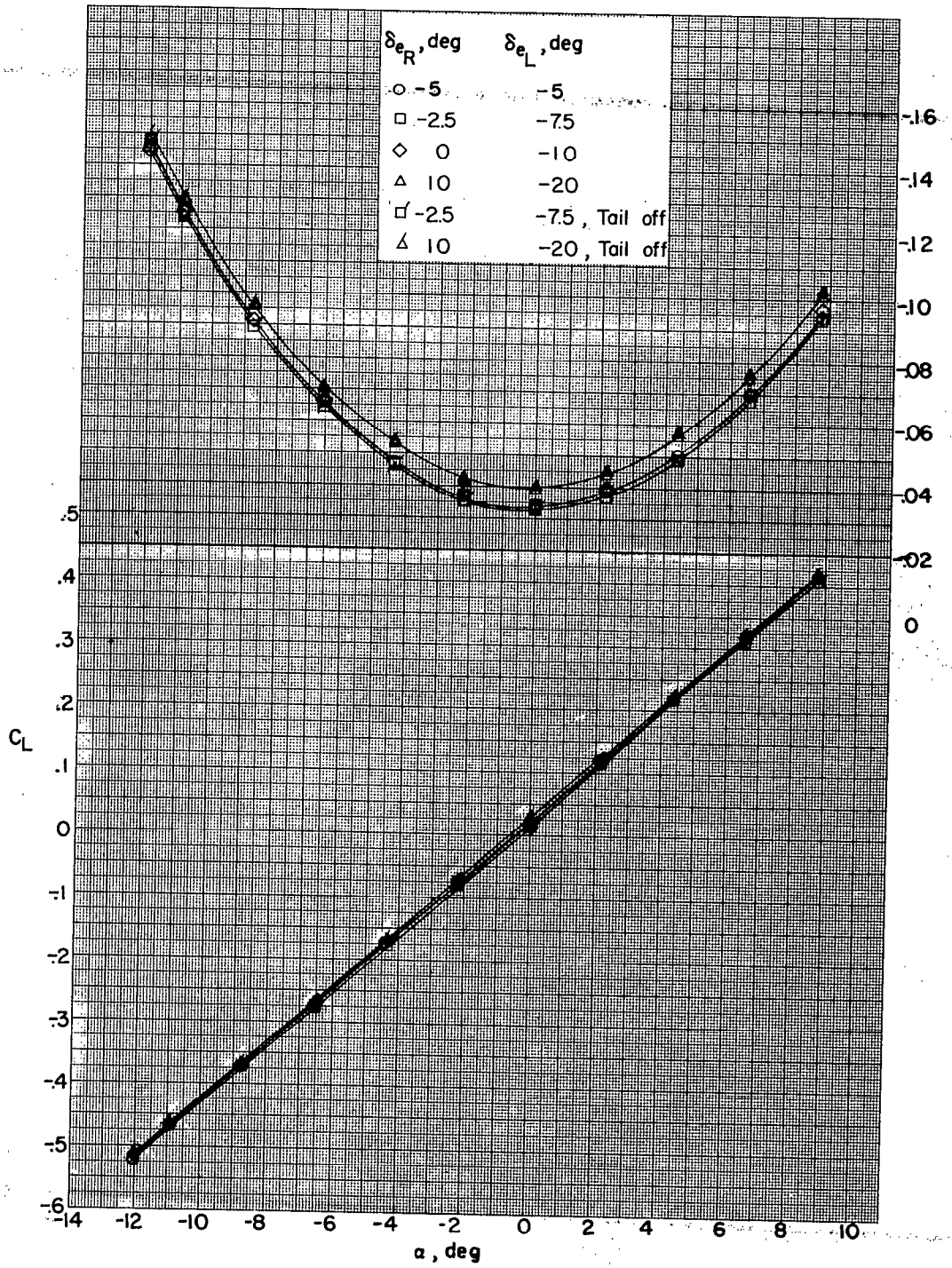

(a) Continued.

Figure 24.- Continued.

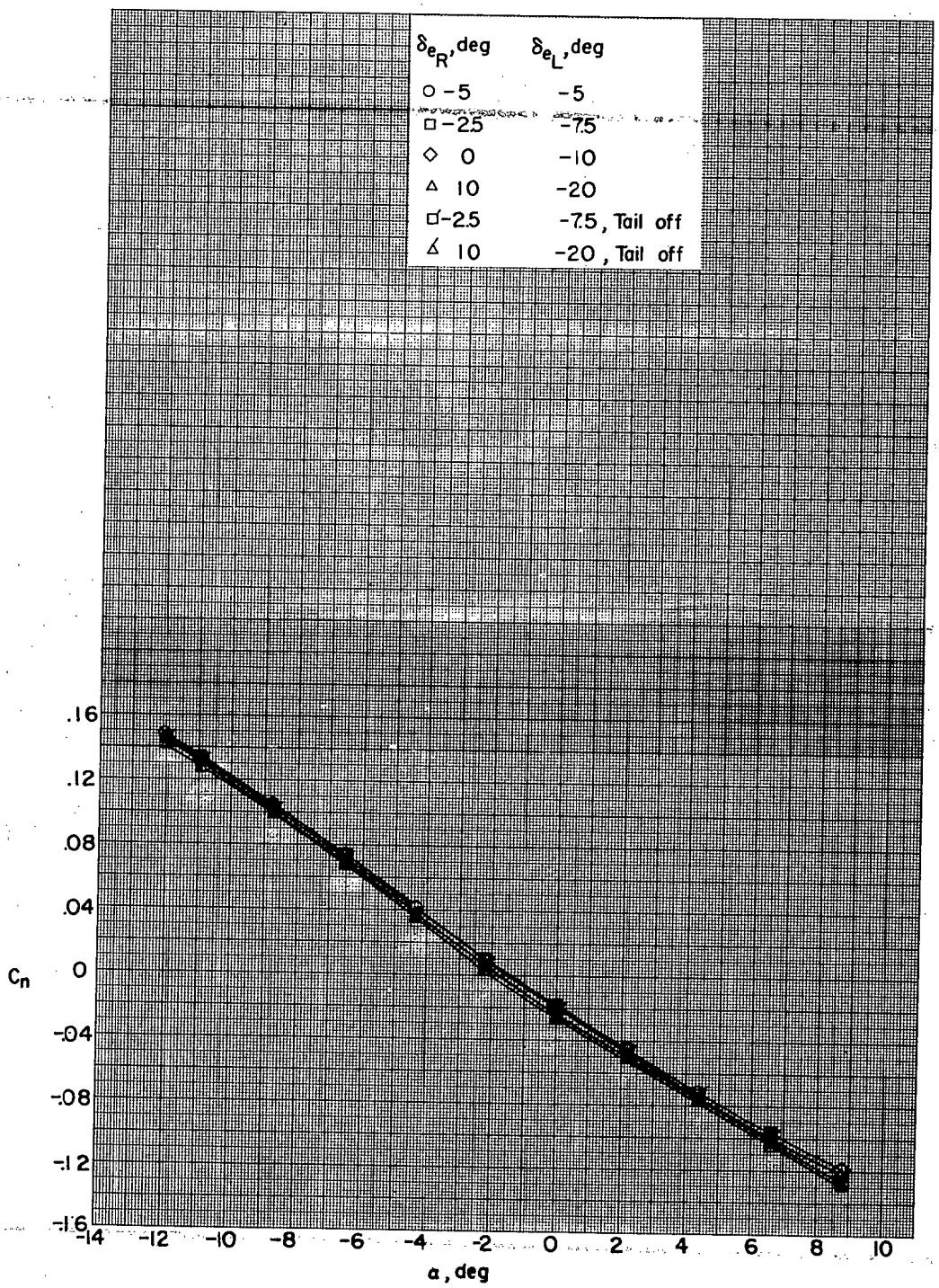

(a) Concluded.

Figure 24.- Continued.

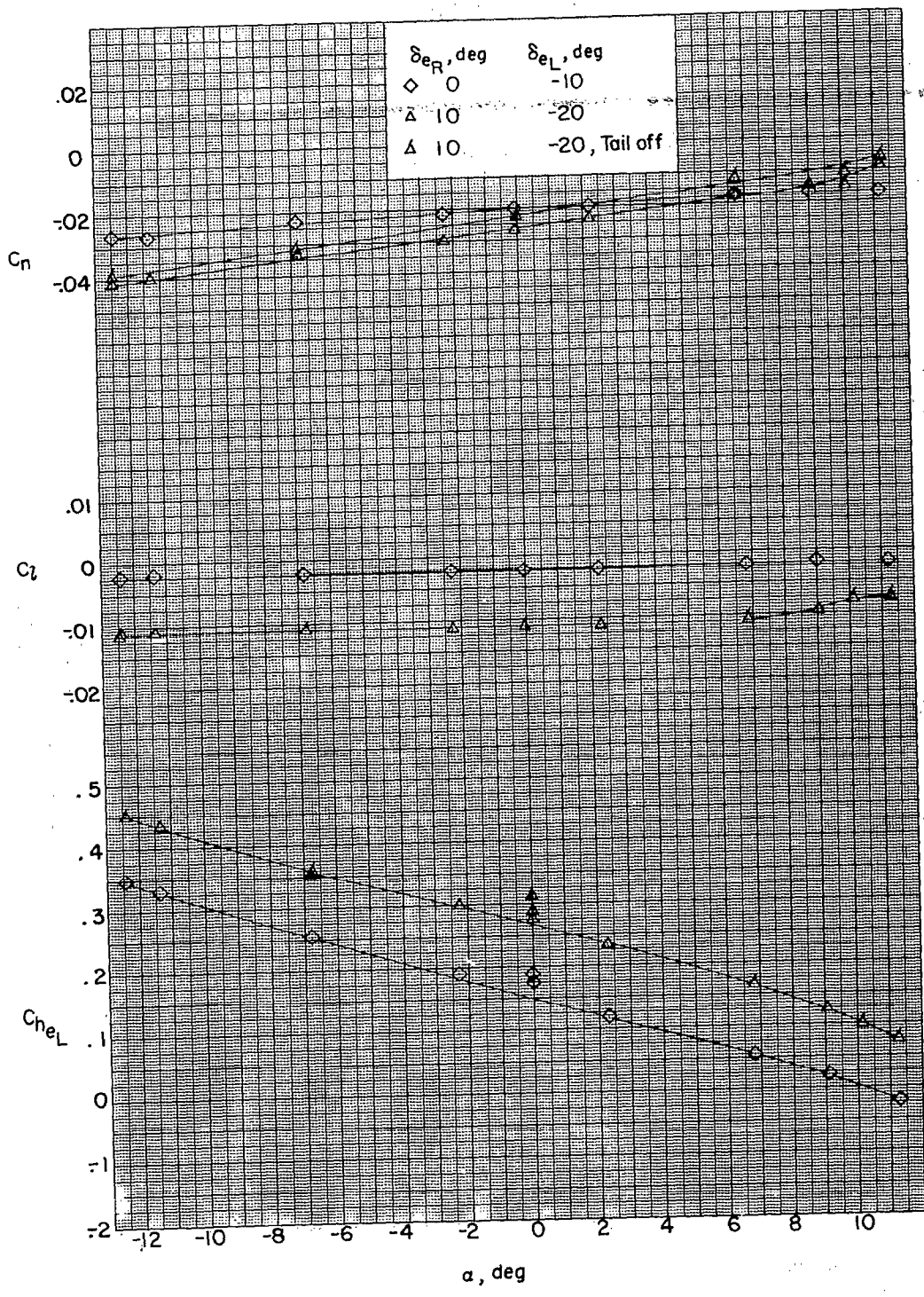

(b) M = 1.61.

Figure 24.- Continued.

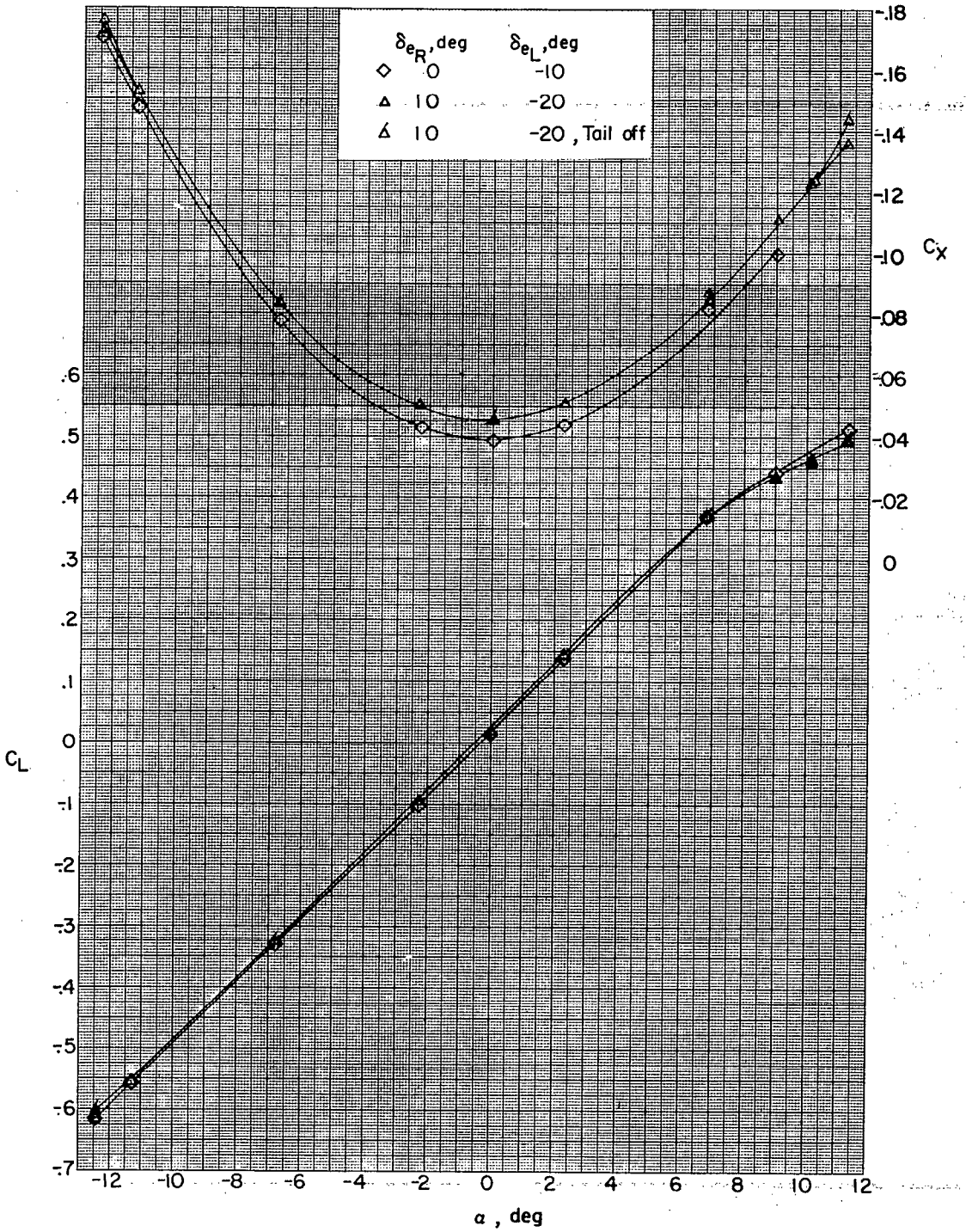

(b) Continued.

Figure 24.- Continued.

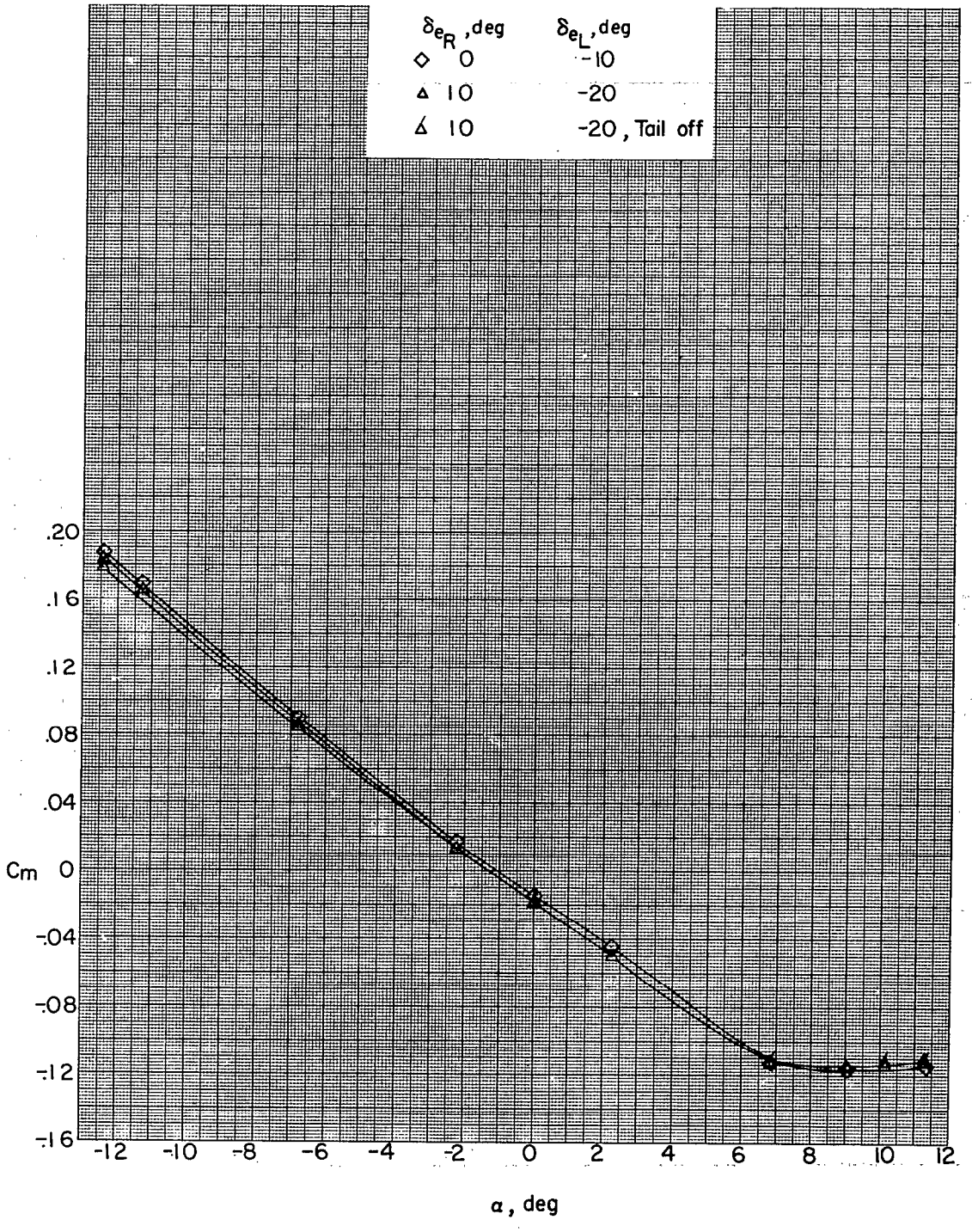

(b) Concluded.

Figure 24.- Continued.

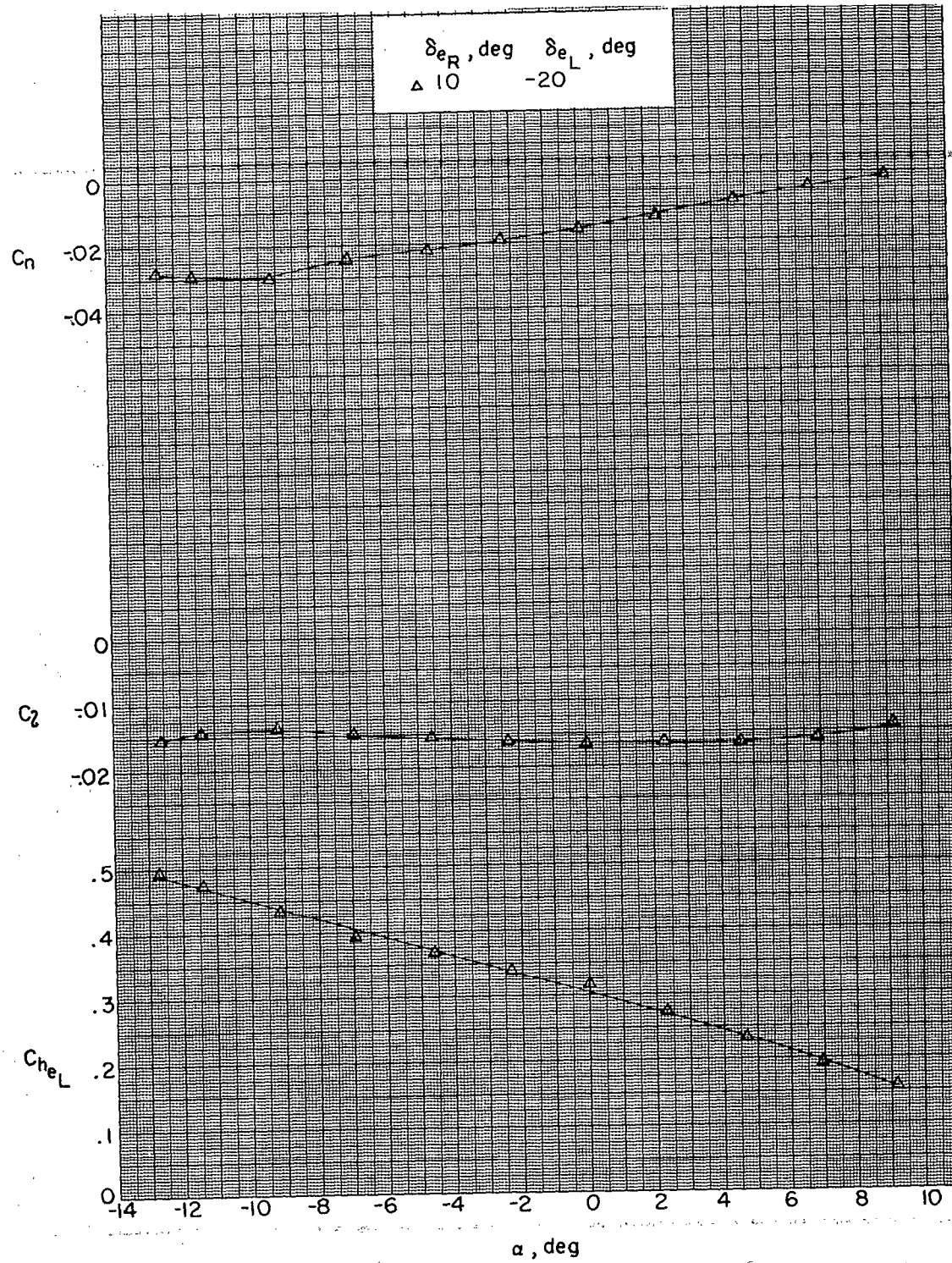

(c) M = 1.41.

Figure 24.- Continued.

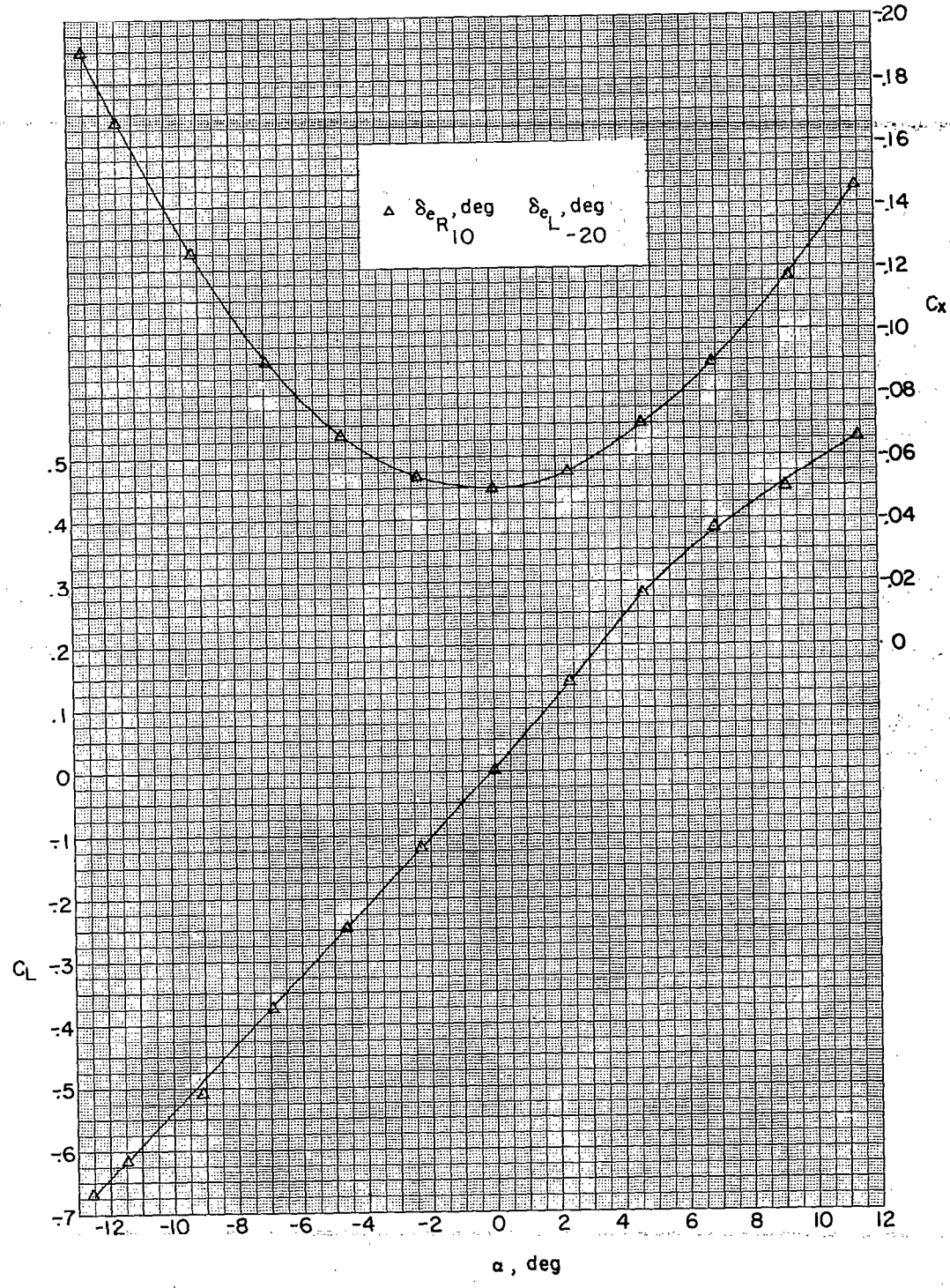

(c) Continued.

Figure 24.- Continued.

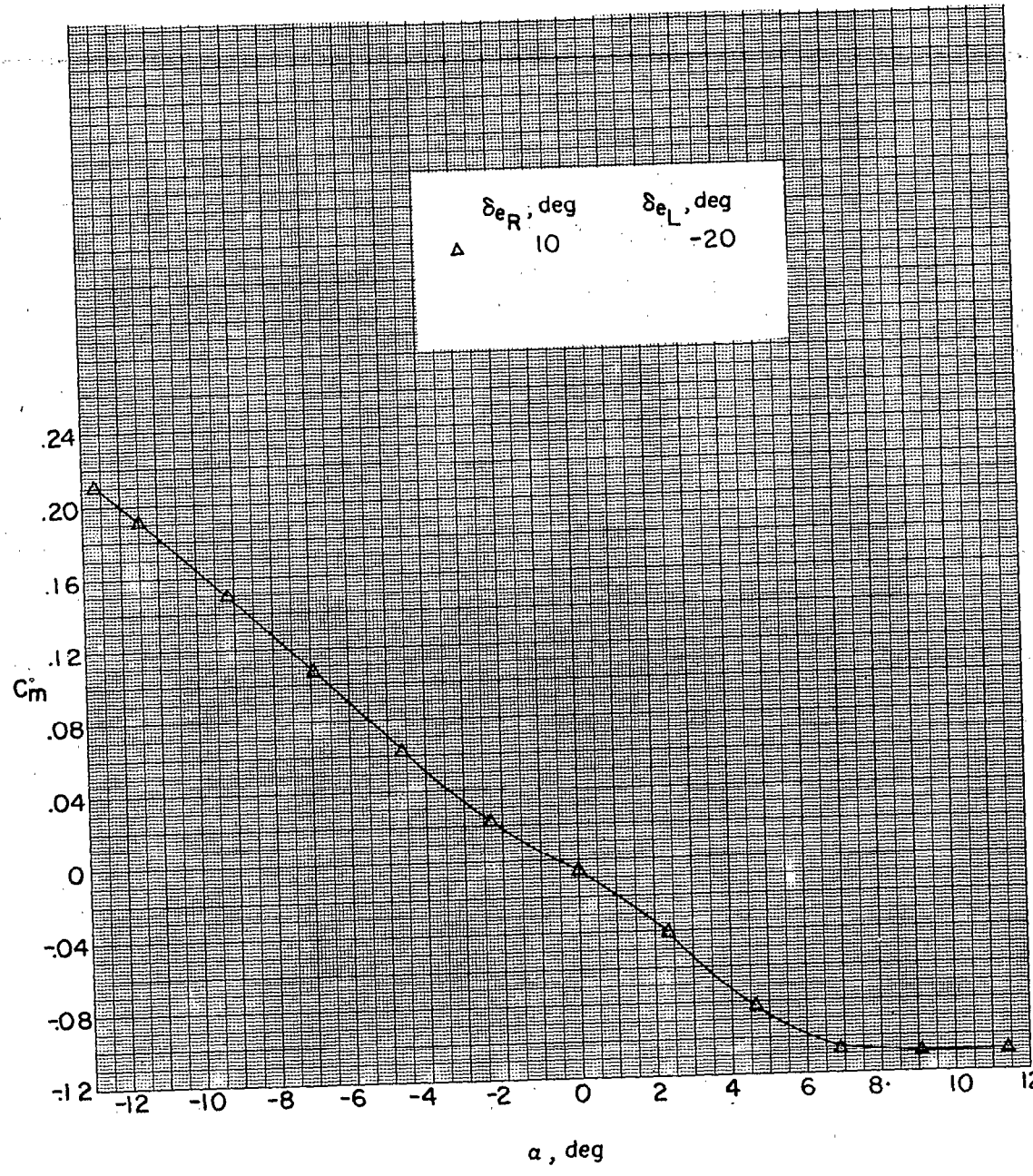

(c) Concluded.

Figure 24.- Concluded.

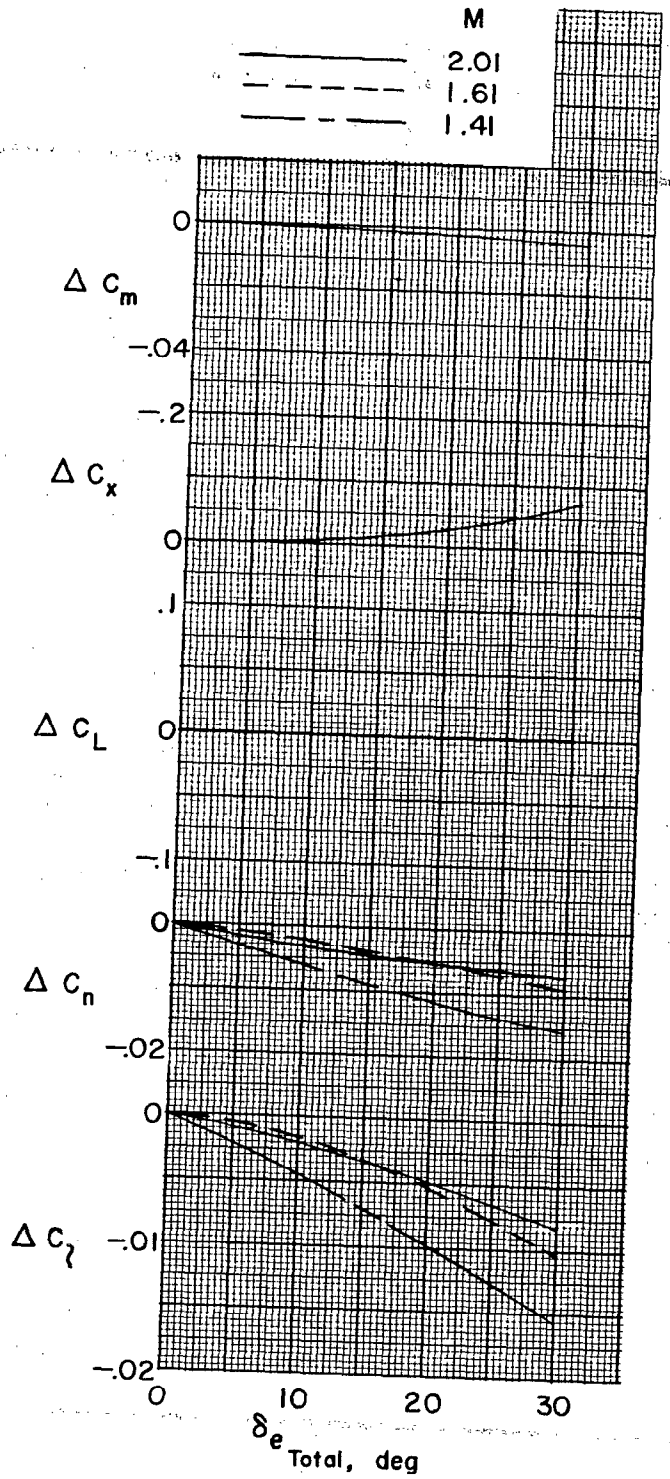

Figure 25.- Incremental aerodynamic characteristics due to differential elevon deflection.